Fakultät für Medizin

Institut für Neurowissenschaften

A Cellular Mechanism of Amyloid β-Induced Neuronal Hyperactivity

Benedikt Hans-Ulrich Zott

Vollständiger Abdruck der von der Fakultät für Medizin der Technischen Universität München zur Erlangung des akademischen Grades eines

Doctor of Philosophy (Ph.D.)

genehmigten Dissertation.

Vorsitzende/r: Prof. Dr. Dr. Stefan Engelhardt

Betreuer/in: apl. Prof. Dr. Helmuth Adelsberger

Prüfer der Dissertation:

1. Prof. Dr. Arthur Konnerth

2. Prof. Dr. Thomas Misgeld

3. Prof. Dr. Christian Alzheimer,
   Friedrich-Alexander-Universität Erlangen-Nürnberg

Die Dissertation wurde am 01.02.2019 bei der Fakultät für Medizin der Technischen Universität München eingereicht und durch die Fakultät für Medizin am 25.03.2019 angenommen.

Acknowledgments

First of all, I would like to thank my supervisors Prof. Dr. Helmuth Adelsberger and Prof. Dr. Arthur Konnerth for their exceptional support, encouragement, and supervision during my PhD work, as well as providing me with the opportunity to work in an invigorating environment and giving me the chance to travel the world promoting my science. Besides my supervisors, I would also like to thank Prof. Thomas Misgeld for joining my thesis committee and providing valuable feedback.

I also want to thank my colleagues Manuel Simon and Dr. Hsing-Jung Chen for their invaluable contribution. Also, I am grateful to my collaborators Loren Looger, Jonathan Marvin, Dominic Walsh and Wei Hong for providing reagents. In the same breath, I would like to thank all those, who make (and keep!) things running in the lab: Christian, Christine, Petra, Andi, Tanja and Rosi.

Special thanks to all my colleagues, past and present, for exciting scientific and non-scientific discussions during mensa-lunches and coffee-breaks: Antje, Arjan, Aurel, Aylin, Bubu, Carsten, Felix, Hongbo, Manuel, Marinus, Peter, Yang and Yonghai.

Last but not least, a huge “Dankeschön” and “Spasiba” to my family and friends and my wonderful wife Marta.

Abstract

Accumulating evidence, both from observations in humans and mouse models, indicates that an early dysfunction in Alzheimer's disease (AD) is the neuronal hyperactivity of certain brain regions. This hyperactivity was shown to be caused by soluble amyloid β (Aβ). Thus, in mouse models of AD, hyperactive neurons are found even prior to the formation of amyloid plaques at times when only the levels of soluble Aβ are increased, while, in wild-type mice, the application of soluble Aβ-dimers can directly trigger hyperactivity. However, the cellular mechanism(s) underlying this hyperactivity remained unknown.

In this study, we used *in vivo* and *in vitro* experiments in various mouse models of AD to investigate this mechanism. We were initially puzzled by the observation that the application of synthetic Aβ dimers can induce activity in hippocampal CA1 neurons *in vivo* but not in *in vitro* hippocampal slices. We then discovered that the ineffectiveness of Aβ in brain slices correlated with the very low levels of spontaneous activity in such *in vitro* preparations. After raising the level of spontaneous neuronal activity of hippocampal slices to that observed *in vivo,* Aβ could activate the neurons in these slices. Conversely, under *in vivo* conditions, Aβ application was ineffective when the neuronal activity was blocked. The activity dependence was also observed in the cortex, where Aβ could activate neurons in layer 5 but not in layer 2/3, indicating that the low levels of baseline activity observed in layer 2/3 were not sufficient to make this brain area susceptible to Aβ. What is the cellular mechanism underlying the baseline activity-dependence of the Aβ-induced hyperactivity? We found compelling evidence *in vivo* and *in vitro* that Aβ blocks the reuptake of synaptically released glutamate. First, Aβ had a similar hyperactivity-inducing effect as the glutamate-uptake blocker TBOA. Second, the application of glutamate receptor antagonists could prevent both the hyperactivity inducing effect of TBOA or Aβ. Third, both the TBOA or Aβ effects were partially saturated in transgenic AD mice. Fourth, electrophysiology experiments revealed that Aβ, just like TBOA, increased the decay time of synaptically evoked NMDA currents but had no effect on the release of glutamate at the presynaptic site. Finally, we confirmed that Aβ derived from the brains of human AD patients also potently induces neuronal hyperactivity. This effect was observed for Aβ-containing full brain extract and isolated Aβ dimers, but remarkably not for Aβ monomers, indicating species specificity of the Aβ-induced effects.

In conclusion, we provide evidence that the Aβ-dependent suppression of the reuptake of the excitatory neurotransmitter glutamate induces hyperactivity in neurons with already high levels of preceding baseline activity**.** These findings provide an explanation for the great susceptibility of highly active brain areas for early circuit dysfunctions in AD. Moreover, the results from this study encourage the search for targeted anti-glutamatergic drugs against AD.

Contents

Glossary

(A)CSF	(artificial) cerebrospinal fluid
(f)MRI	(functional) Magnetic resonance imaging
AD	Alzheimer's disease
AICD	Amyloid precursor protein intracellular cytoplasmic domain
AM	Acetoxymethyl ester
AMPAR	α-amino-3-hydroxy-5-methyl-4-isoxazolepropionic acid receptor
ApoE	Apolipoprotein E
APP	Amyloid Precursor Protein
AUC	Area under the curve
Aβ	Amyloid-β
CA	Cornu ammonis
CHO	Chinese hamster ovary
DMN	Default mode network
EAAT	Excitatory amino acid transporter
EphB2	Ephrin type-B receptor 2
EPSC	Excitatory postsynaptic current
FAD	Familial Alzheimer's Disease
FcγRIIb	Immunoglobulin G fragment crystallizable region γ receptor II-b
GLAST	Glutamate aspartate transporter
GLT-1	Glutamate transporter 1
HMW	High molecular weight
ID	Immunodepleted
iGluR	Ionotropic glutamate receptor
LilrB2	Leukocyte immune receptor B2
LMW	Low molecular weight
LTD	Long-term depression

LTP	Long-term potentiation
MAPT	Microtubule associated protein tau
MCI	Mild cognitive impairment
mGluR	metabotropic glutamate receptor
mOsm	Milliosmolar
mPFC	Medial prefrontal cortex
NFT	Neurofibrillary tangle
NgR1	Nogo-66 receptor 1
NMDAR	N-methyl-D-aspartate receptor
PET	Positron Emission Photography
pH	Potential of Hydrogen
PirB	Paired immunoglobulin-like receptor B2
PPF	Paired pulse facilitation
PPR	Paired pulse ratio
RAGE	Receptor for Advanced Glycation end products
REM	Rapid eye movement
ROI	Region of interest
sAPP	soluble APP
SDS PAGE	Sodium dodecyl sulfate polyacrylamide gel electrophoresis
SEM	Standard error of the mean
SorL1	Sortilin-related receptor L1
TBOA	T*hreo*-β-benzyloxyaspartic acid
TG	Transgenic
WT	Wild-type
A/β-CTF	α/β C-terminal fragment

1 Introduction

The goal of my graduate work was to determine a mechanism of amyloid-β (Aβ)-induced neuronal hyperactivity in Alzheimer's disease (AD). This chapter provides an overview of the AD pathology with a specific focus on Aβ-dependent changes in the brain. I also introduce the theoretical background needed to understand the methodology used in this study. This chapter is partially based on a recent review article (Zott et al 2018).

1.1 Alzheimer's disease

AD is the most prevalent cause of dementia. According to the world health organization, an estimated 47 million patients are suffering from AD worldwide (Prince et al 2015). The pathological changes associated with this debilitating disease were first described in 1907 by the German psychiatrist and pathologist Alois Alzheimer in his essay "A characteristic serious disease of the cerebral cortex" (Alzheimer 1907). In his article, Alois Alzheimer not only outlined the symptoms of his patient, Auguste D., but also provided a detailed description of the pathological changes in her brain, which he had examined post mortem. More than a century after his essay, the three main pathological findings Alois Alzheimer described remain the pathological hallmarks of AD. First, he noted the decreased volume of Auguste D.'s brain as compared to healthy subjects. This cortical atrophy he reported is by now one of the main criteria for the diagnosis of AD and is routinely detected in living patients by magnet resonance imaging (MRI) (Dubois et al 2014). Second, Alois Alzheimer described a "peculiar change of the neurofibrils", which is now usually referred to as neurofibrillary tangles (NFTs) (Serrano-Pozo et al 2011a). Finally, Alzheimer reported "Numerous small miliary foci" in the brain of his patients. These are nowadays called amyloid plaques. In the last decade, the development of novel Positron Emission Tomography (PET)-based imaging

techniques have enabled the detection of plaques (Klunk et al 2004) and tangles (Chien et al 2014, Johnson et al 2016) in living patients. Moreover, they allow for a longitudinal analysis of the pathologies and their propagation in the same cohort of patients (Jack et al 2009, Kadir et al 2012, Kemppainen et al 2014).

It is now clear that these and other pathological changes can occur in the brain decades before they cause any symptoms (Bateman et al 2012, Jack et al 2010). This gap has led researchers and physicians to distinguish between presymptomatic stages, characterized by pathognomonic brain pathology, mild cognitive impairment (MCI), which is now seen as an early precursor of the disease, and Alzheimer's dementia (Jack et al 2011, Sperling et al 2011). Clinically, AD-induced symptoms are primarily severe and specific defects in learning and memory (McKhann et al 2011). More precisely, the memory of recent events is impaired early in AD, while the memory of immediate recall, used for example when memorizing a phone number, and the memory of events that happened long in the past are usually only affected later in the course of the disease (Dubois et al 2014). Procedural memory, that is the memory of specific tasks, is usually preserved until very late stages of the disease. Non-mnemonic symptoms like executive dysfunction, visuospatial impairment, language deficits and behavioral changes typically occur later on (McKhann et al 2011).

1.1.1 The role of Aβ in Alzheimer's disease

Although Alois Alzheimer described the pathological and clinical signs of AD, he could only speculate about the causal relationships between them. Currently, there are many ideas as to what causes AD, the most prominent of which is the amyloid hypothesis (Hardy & Selkoe 2002, Selkoe & Hardy 2016). It states that increased levels of Aβ in the brain are the main cause of AD and subsequently trigger other neuropathological changes. The amyloid hypothesis has repeatedly been criticized, mostly because the number of amyloid plaques in the brain of AD patients is not a good predictor for the severity of disease symptoms.

However, the amyloid hypothesis still provides the most convincing model for pathological changes in the brains of AD patients.

Aβ is cleaved from the Amyloid Precursor Protein (APP), a transmembrane protein which is highly expressed in neurons. The extracellular amino-terminal domain of APP can be cleaved by three different secretases, the α-, β- and γ-secretases. Cleavage by the β- and γ-secretases results in the generation of the amyloidogenic Aβ peptide (O'Brien & Wong 2011), which can aggregate and therefore accumulate in the brain, while cleavage of the α- and γ-secretases will result in secretion of a shorter, non-amyloidogenic peptide, called p3 (Haass et al 1993). The remaining extracellular n-terminal fragments are called soluble APP-α or -β, depending on whether they have been cleaved by α-or β-secretase, while the c-terminal APP intracellular domain (AICD) remains in the cytoplasm (Müller et al 2017) (**Fig. 1**). Because γ-secretase can cleave the protein at different sites, γ-cleavage can result in an Aβ peptide of different lengths, the most abundant of which are 40 and 42 amino acids long (Aβ1-40 and Aβ1-42 respectively)(Klafki et al 1996). This is important because longer Aβ fragments are more prone to aggregate than the shorter variants and an imbalance of the Aβ1-40/Aβ1-42 equilibrium is associated with AD (Bitan et al 2003, Scheuner et al 1996). Apart from this canonical pathway described here, APP can also be cleaved by other enzymes, leading to different peptides and molecules, which will not be discussed here (Müller et al 2017).

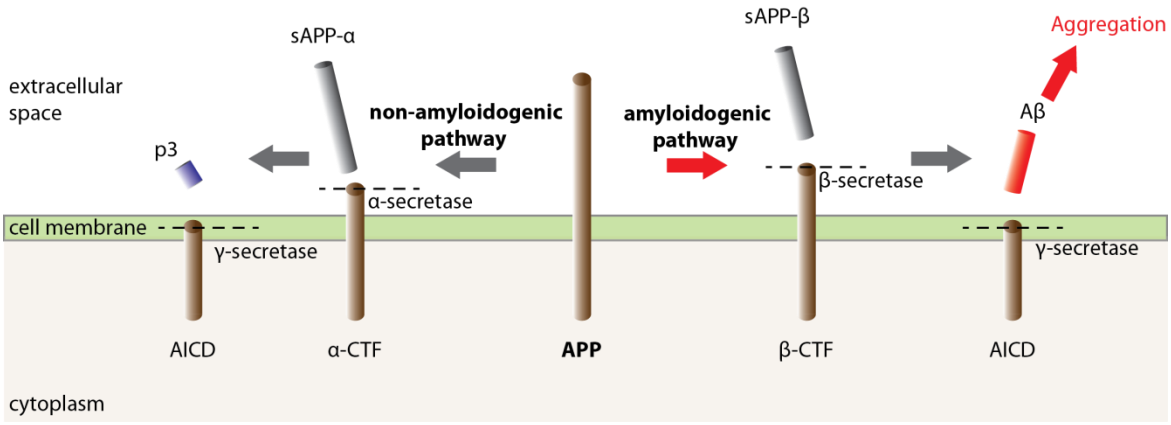

Fig. 1: The canonical pathway of APP processing. APP can be cleaved by α-secretase, inducing the non-amyloidogenic pathway, or by β-secretase, eventually leading to the production of Aβ. Abbreviations: AICD, APP intracellular cytoplasmic domain; APP, Amyloid precursor protein; CTF, C-terminal fragment; sAPP: soluble APP. Based on (O'Brien & Wong 2011)

According to the amyloid hypothesis, either the increased production or the deceased elimination of Aβ causes AD. In consequence, other pathological changes in the brains of AD patients are a result of the ensuing increase in brain Aβ levels (Selkoe & Hardy 2016). Although the hypothesis has been repeatedly criticized, the evidence supporting it is largely overwhelming. A particularly compelling line of evidence emerges from the genetic analysis of patients suffering from familial AD (FAD), which is a rare (~5% of all AD cases) but especially aggressive form of the disease associated with an early onset and a quick loss of cognitive function (Tanzi 2012). FAD patients carry mutations in either the APP gene itself or, more commonly, presenilin (PS) 1 or 2. At first, the fact that most FAD mutations are not located on the APP gene was puzzling. However, almost all of the PS mutations, just like the APP mutations were reported to increase the ratio of Aβ1-42 to Aβ1-40 (Scheuner et al 1996), thus providing a direct association to Aβ pathology. This link was strengthened when it was discovered that PS1 is the active site of the γ-secretase protein complex and, in effect, directly involved in APP processing (De Strooper et al 1998, Wolfe et al 1999). Further genetic evidence comes from patients with Down syndrome, which is caused by a triplication of chromosome 21. Since the APP is located on this chromosome, an extra copy is expected

to result in increased Aβ levels. Indeed, virtually all patients with Down syndrome show amyloid pathology over the age of 40 (Head et al 2012). In line with this, patients with a triplication of only parts of chromosome 21 that do not contain APP did not have AD-like pathology (Prasher et al 2004). Finally, a protective APP mutation that decreases the risk of developing AD was detected in parts of the Icelandic population (Jonsson et al 2012). While carriers of FAD mutations represent only a small fraction of AD patients, variants or mutations in other genes, most notably ApoE and Trem2, are associated with a much larger number of AD cases (Karch & Goate 2015). Even though these genes, unlike the FAD mutations, are not directly involved in APP processing, recent studies in mice have also linked most of them to the Aβ pathway. ApoE ε4, the most important genetic risk factor for AD, has been linked to a decreased amyloid clearance from the brain (Castellano et al 2011) and mutations in Trem2 most likely interfere with plaque phagocytosis (Ulrich et al 2014).

One finding, which has puzzled researchers in the past, is the observation that the amount of amyloid plaques in the brain does not predict disease severity and dementia in AD patients, while the number of NFTs does (Arriagada et al 1992). For a long time, this was a major argument against the amyloid hypothesis and pointed towards NFTs as the main culprit in AD. These tangles are formed by intracellular aggregation of tau, which is a protein associated with stabilizing microtubules predominantly in the axon (Bancher et al 1989). In AD, tau gets hyper-phosphorylated and aggregates into paired helical filaments and NFTs, but the causal relationship between phosphorylation and aggregation is not entirely clear (Goedert et al 2017) . In contrast to the abundance of NFTs in AD brains, mutations in the tau-coding microtubule-associated protein tau (MAPT) gene do not result in an AD-like phenotype, but typically lead to other diseases such as frontotemporal dementia (Goedert et al 2017). This observation virtually rules out tau as the cause of AD. Also, in patients with familial AD, tau deposition starts approximately 10 years after the first detection of anomalies in the Aβ metabolism (Bateman et al 2012), suggesting that tau in fact lies

downstream of Aβ. In line with these findings, studies in mice have supported the notion of tau as an effector of Aβ pathology. Thus, mice that carry mutations in both the APP and MAPT genes show higher densities of NFT tangles than mice with only MAPT mutations (Hurtado et al 2010). Also, injection of Aβ drastically increased NFTs in mice expressing a mutated form of human tau (Götz et al 2001). Intriguingly, a complete knockout of the MAPT gene rescued Aβ-dependent neuronal dysfunction and memory impairment (Roberson et al 2007) suggesting that tau is necessary for Aβ-dependent neurotoxicity. Together, these findings suggest that Aβ is the main cause for AD and that tau might mediate the toxic effects of the Aβ pathology (Bloom 2014). Moreover, Aβ is present in many different forms and the fact that the plaque number is not a good predictor of symptoms does not rule out a correlation between other forms of Aβ and the severity of the disease.

1.1.2 Soluble Aβ as the main mediator of Aβ toxicity in the brain

As Aβ is very prone to aggregate, in the brains of AD patients there is a constantly changing mix of differently sized Aβ clusters (Benilova et al 2012) (**Fig. 2**). Once monomers get released into the extracellular space, they quickly aggregate to form clusters of different sizes ranging from 4 to more than 100 kDa (Rushworth & Hooper 2011). These aggregates can be roughly divided into two groups, namely soluble and insoluble forms. Per definition, soluble aggregates stay dissolved in the supernatant after ultracentrifugation, while the insoluble forms can be pelleted (Selkoe 2008). Thus, monomers, dimers, oligomers and protofibrils, also sometimes called high molecular weight (HMW) oligomers, are seen as soluble aggregates. Aβ fibrils and plaques, on the other hand, are insoluble (**Fig. 2**). In light of the vast number of different Aβ species, it is important to ask, whether these forms are equally toxic or whether some species are responsible for most of the detrimental effects observed in AD patients.

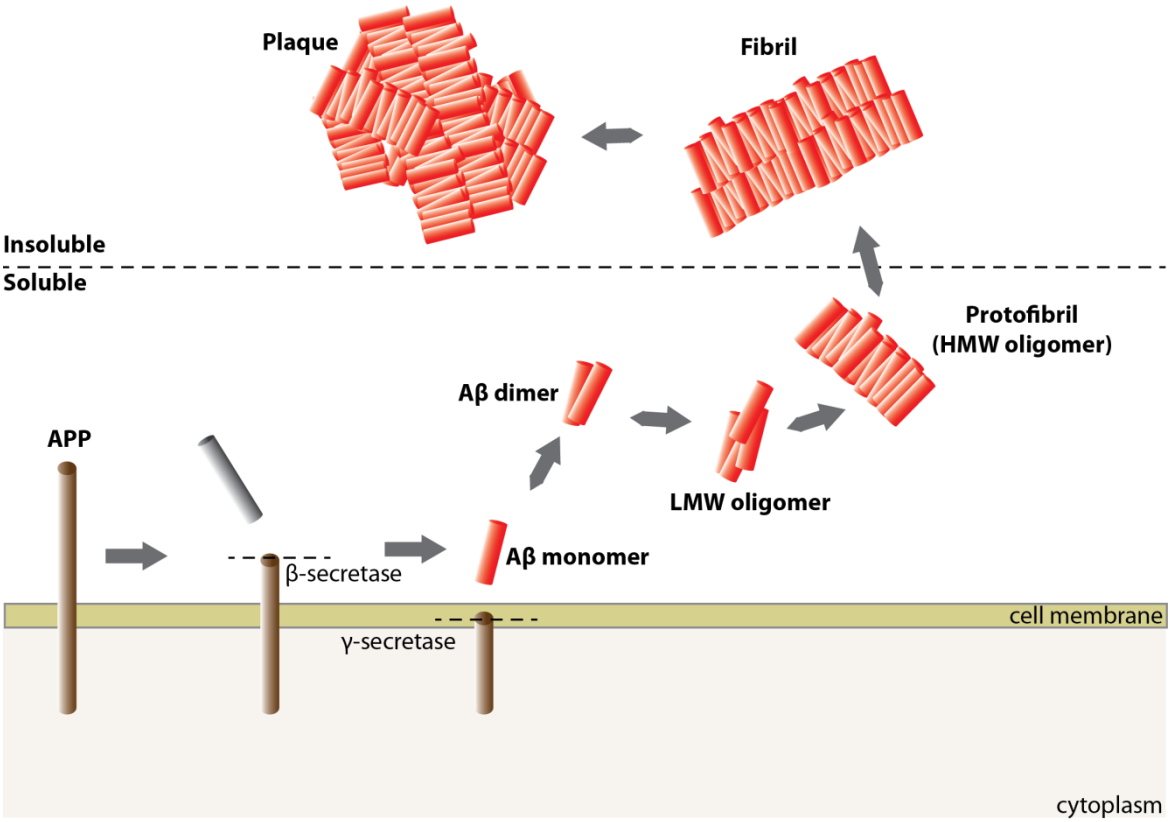

Fig. 2: Aβ aggregation. After the subsequent cleavage by β- and γ-secretase, Aβ monomers aggregate in the extracellular space. They form dimers, oligomers, fibrils and eventually plaques. Abbreviations: APP, Amyloid precursor protein; HMW, High molecular weight; LMW, low molecular weight.

Which Aβ species are most toxic?

Since amyloid plaques were the most striking changes in the brain of AD patients, they have long been deemed to be responsible for the better part of the Aβ-induced toxicity. This hypothesis was supported by pathological studies which reported that neuritic destruction (Spires et al 2005, Tsai et al 2004) and glial activation (Mehlhorn et al 2000, Serrano-Pozo et al 2011b) were particularly pronounced in the vicinity of amyloid plaques. However, this model was in stark contrast with clinical findings. Amyloid plaques can be found in patients that show no sign of memory impairment (Erten-Lyons et al 2009) and neuronal death can occur in brain regions without amyloid plaques. Additionally, as mentioned above, there is no correlation between amyloid plaque load and memory impairment (Arriagada et al 1992). How are these findings still compatible with the amyloid hypothesis? Accumulating evidence

indicates that the main culprits in AD are in fact soluble Aβ species and not amyloid plaques. In consequence, the observed pathology around plaques can likely be explained by increased levels of soluble Aβ in their vicinity rather than by a toxic effect of the plaques themselves (Hefendehl et al 2016, Koffie et al 2009). A rapidly growing body of evidence supports the notion that soluble oligomers are, in fact, causing most of the pathological and functional changes in AD. Thus, mice with amyloid plaques fail to show memory deficits in developmental phases, in which soluble Aβ is very low (Lesné et al 2008). Also, acutely decreasing soluble amyloid with inhibitors of γ-secretase rescued functional deficits in a mouse model of AD without changing the amount of plaques (Busche et al 2012). Moreover, a large number of studies have since reported that the application of soluble forms of Aβ in healthy mice can cause many of the structural and functional changes observed in mouse models of AD and AD patients[1]. Studying the effects of soluble Aβ by application in healthy humans is obviously impossible for ethical reasons.

The application of Aβ in wild-type mice is usually performed either *in vitro* or by the direct injection into the hippocampus or the cerebrospinal fluid (CSF) (Selkoe 2008). It is important to note that there are several ways to obtain soluble Aβ. First, amyloid can be synthetically produced, most commonly as monomers or as covalently linked dimers (Shankar et al 2008). In order to obtain larger assemblies, the monomers can be incubated before the application to form oligomers or fibrils (Stine et al 2011). Alternatively, low molecular weight (LMW) oligomers, such as dimers and trimers with varying lengths can be generated by cultured Chinese hamster ovary (CHO) cells that express a mutation determinant for FAD (Podlisny et al 1995). The third source of Aβ is brain extract from mouse models of AD (Meyer-Luehmann et al 2006) or the post-mortem brains of AD patients (McLean et al 1999, Meyer-Luehmann et al 2006, Shankar et al 2008). In these preparations,

[1] A detailed description of the Aβ-induced structural and functional pathology can be found in chapter 1.1.3.

Aβ is extracted by homogenization and centrifugation of the post mortem brain tissue. All of these ways to gain or synthesize Aβ have their advantages and disadvantages. Synthetically produced Aβ monomers or cross-linked dimers are a very specific form of Aβ that can be used in huge quantities, but may not recapitulate the full complexity of what is happening in the brain of AD patients. Aβ prepared from the brains of patients suffering from sporadic AD is relevant for pathology, but it is difficult to attribute dysfunctions to certain forms of Aβ. Aβ from cell cultures lies somewhat in the middle with more physiological Aβ levels and lengths than synthetic Aβ but less pathological relevance to sporadic AD than human Aβ. In consequence, it is important to use Aβ from all these preparations to get a full understanding of Aβ toxicity.

The emerging picture from Aβ application studies is that the majority of the Aβ-induced toxic effects are mediated by only a small fraction of Aβ oligomers (Hong et al 2018, Yang et al 2016). More precisely, an inverse relationship between assembly size and toxicity has recently been hypothesized (Sengupta et al 2016). Thus, dimers and LMW oligomers, which can only be found in AD brains at low concentrations, are critically responsible for the most part of the Aβ-dependent pathology, while the more abundant HMW and plaque-associated oligomers as well as insoluble forms of Aβ are less active. In fact, large assemblies such as HMW oligomers or plaques could not induce deficits in synaptic plasticity, while oligo- and dimer enriched solutions could (Shankar et al 2008). Moreover, it was recently reported that the HMW aggregates contained smaller oligomers, which were toxic when they were dissociated from the HMW oligomers (Yang et al 2016). Furthermore, the group of Karen Ashe proposed two classes of oligomers in the brain based on different antibody affinity, the highly toxic type 1 or Aβ*56, which impaired memory in a mouse model, and the inert type 2 oligomers (Lesné et al 2006, Liu et al 2015), which were larger and did not change memory performance.

In the continuum of Aβ species (**Fig. 2**), monomers and dimers both seem to play distinct roles. Monomers, on the one hand, have widely been reported to have very little toxicity (Li et al 2009, Shankar et al 2008, Walsh et al 2002). They occur in the brains of healthy patients (Shoji & Kanai 2001) and might even be neuroprotective (Giuffrida et al 2009). Dimers, on the other hand, were in a lot of cases sufficient to trigger many of the changes in AD, and are arguably the most toxic form of Aβ (Busche et al 2012, Li et al 2009, Shankar et al 2008, Walsh et al 2002). Remarkably, the transgenic expression of covalently linked Aβ dimers in mouse models led to synaptic deficits and memory loss in the absence of plaque formation, neuro-inflammation or tau hyper-phosphorylation (Müller-Schiffmann et al 2016). In the past, there has been surprisingly little hard evidence for the existence of Aβ dimers in AD patients. The most widely used tool to separate Aβ according to the size of different assemblies is polyacrylamide gel electrophoresis (PAGE) using sodium dodecyl sulfate (SDS) as a detergent (SGS-PAGE). When performing SDS-PAGE on Aβ obtained from human samples, but also from supernatant of Aβ-producing Chinese hamster ovary (CHO) -cells, two bands are particularly prominent - the 4 kilo Dalton (kDa)-band which contains Aβ monomers and a band close to 7-8 kDa which likely contains dimers, but whose exact origin remained enigmatic (Klyubin et al 2008, Klyubin et al 2005, Welzel et al 2014). What is more, the use of SDS-PAGE to study Aβ aggregates has recently come under attack because it is prone to induce artificial oligomers that have not been present in the original sample, so it was controversial, whether the 7 kDa band was an artefact (Benilova et al 2012, Pujol-Pina et al 2015, Watt et al 2013). To overcome these limitations, various groups adopted the technology of size exclusion chromatography (SEC) to separate the Aβ oligomers according to their molecular weight without the use of denaturing agents such as SDS (Cleary et al 2004, Esparza et al 2016, Yang et al 2017). Using this technique, the group of Dominic Walsh demonstrated that the 7 kDa fraction of Aβ exists and indeed contains amyloid dimers, which, surprisingly, are covalently crosslinked (Dominic Walsh, personal communication).

Together with the recent indication of crosslinked Aβ dimers by antibodies in the brains of AD patients (Vázquez de la Torre et al 2018), there is now substantial evidence that Aβ dimers indeed play a large role in AD pathology.

In light of the great toxicity of Aβ dimers, I have chosen to focus my study on investigating the effects of Aβ dimer application in the brain of wild-type mice. For most parts of my experiments, I used synthetic crosslinked dimers (Shankar et al 2008). To validate that Aβ derived from the brain of AD patients had the same effects as synthetic Aβ, I repeated key experiments with dimers which had been extracted from patients with sporadic AD. Furthermore, I tested the action of human monomers and human brain extract containing a mix of soluble Aβ species.

1.1.3 Aβ-induced structural and functional pathology

AD is a very complex disease which affects many cell types in the whole brain (De Strooper & Karran 2016). Since the scope of my PhD work was to determine the mechanism of Aβ-induced neuronal hyperactivity, only the neuronal pathology will be discussed here, while other cell types will be omitted. This chapter summarizes the structural changes, i.e. neuronal cell loss and synaptic atrophy, as well as the functional neuronal changes which are a consequence of impaired neuronal signaling. Also, all of these pathological changes will be put in relation to Aβ and, more specifically, soluble Aβ species.

Neuronal death

Later disease stages of AD are characterized by marked brain atrophy, which is the macroscopic reflection of neuronal cell death. This atrophy was already described by Alois Alzheimer (Alzheimer 1907, Alzheimer et al 1995) and can by now be readily detected with noninvasive methods such as MRI (Dickerson et al 2009, Jack et al 1999). Atrophy and cell death are most prominent in the medial temporal lobe which includes the hippocampal

formation and can be used as a diagnostic tool (Dickerson et al 2011). It has been repeatedly reported that Aβ can induce cell death, most likely by inducing oxidative stress (Jang & Surh 2002, Kadowaki et al 2004, Xie et al 2013). However, significant neuronal cell death can surprisingly hardly be found in mouse models of β-amyloidosis (Jankowsky & Zheng 2017). A possible explanation for these observations might be that Aβ is not toxic enough to cause neurodegeneration within the relatively short lifespan of mice. In mouse models that develop tau tangles, neuronal death is prominent even in relatively young animals (Ramsden et al 2005, Santacruz et al 2005, Spires et al 2006).

Loss of synapses

Another structural impairment that is typically observed in AD patients is synapse loss. Post-mortem studies in AD patients have reported a decreased number of synapses, especially in the hippocampus. Remarkably, synapse loss was the strongest pathological correlate of memory impairment and is a better predictor of disability than plaques, tangles or neuronal cell death (DeKosky et al 1996, Masliah et al 1994, Terry et al 1991). In consequence, the quantification of synapse loss *in vivo* would be a valuable staging tool for AD patients. Recently, a radio ligand for the quantification of synapse density in PET studies was developed and could possibly lead to a diagnostic breakthrough in AD (Finnema et al 2016).

Unlike neuronal death, the loss of synapses can be readily reproduced in mouse models of β-amyloidosis (Jacobsen et al 2006, Malthankar-Phatak et al 2012). The loss of synaptic spines is a very early sign of AD and can occur even before the formation of Aβ plaques at times, when only soluble Aβ is increased (Hsieh et al 2006, Jacobsen et al 2006). In line with this, the application of soluble Aβ oligomers in wild-type mice triggered substantial synapse loss in the hippocampus which was dependent on an activation of the complement system (Hong et al 2016, Shankar et al 2007). Together, this data indicates that spine loss is a direct consequence of increased levels of soluble Aβ.

Impaired synaptic plasticity as a cellular basis for memory deficits

The most extensively studied functional impairment in AD is impaired synaptic plasticity. In the hippocampus, long-term potentiation (LTP) and long-term depression (LTD) are widely accepted as a cellular model for learning and memory. The concept of LTP and LTD is based on the observation that stimulating a synapse repeatedly changes its strength for a long time-period (Bliss & Lømo 1973) . This change in transmission strength is recorded as a potentiation (LTP) or depression (LTD) of the response of the postsynaptic neuron to a defined presynaptic stimulus. It is now clear that, in certain neurons, LTP and LTD rely on the activation of postsynaptic N-methyl D-aspartate receptors (NMDARs) and are mostly based on changes in the postsynaptic cell, such as an altered number of glutamate receptors (Nicoll 2017). Studies in mouse models of AD have provided mixed results, but the majority reports an impairment of LTP and an enhancement of LTD compared to wild-type mice (Marchetti & Marie 2011). Studies in wild-type mice after the intraventricular application of Aβ *in vivo* or the superfusion of brain slices with Aβ-containing CSF, have reported more constant results. These studies have almost unanimously reported the Aβ-dependent impairment of LTP after the application of Aβ from different sources, including synthetic preparations, cell culture, AD mouse and AD human brain extracts (Barry et al 2011, Klyubin et al 2008, Shankar et al 2008). However, it is important to note that very small concentrations of Aβ can in fact enhance LTP (Puzzo et al 2008). In addition to the electrophysiological findings, Aβ was reported to prevent the growth of the postsynaptic spine after LTP induction (Wei et al 2010). Conversely to the findings in LTP, different preparations of soluble Aβ can also potently enhance LTD (Li et al 2009). In AD, impairments of synaptic plasticity might be connected to memory loss. Thus, in mouse models of AD or after the injection of Aβ directly into the hippocampus, impairments of synaptic plasticity were reported to be paralleled by a disruption of memory performance in a water maze task (Chapman et al 1999, Nalbantoglu et al 1997, Stéphan et al 2001).

It is not entirely clear what the mechanisms of the observed Aβ-dependent impairments of synaptic plasticity are. However, a direct or indirect interaction of Aβ with the NMDA receptor seems to be very likely (Malinow 2012)[2].

Neuronal hyperactivity

Due to the loss of synapses and the impairment in LTP, which were often referred to as a "synaptic failure" (Selkoe 2002), it was expected that neurons in the brain are less active in AD. As a consequence, it came as a surprise when many groups reported neuronal hyperactivity in the brains of different AD mouse models (Busche et al 2012, Busche et al 2008, Busche & Konnerth 2015, Keskin et al 2017, Liebscher et al 2016, Rudinskiy et al 2012, Scala et al 2015, Siskova et al 2014, Xu et al 2015) (**Fig. 3 A, B**). These findings are backed up by *in vitro* studies indicating neuronal hyperactivity after Aβ application in slices (Kurudenkandy et al 2014) or cell cultures (Alberdi et al 2010, Brorson et al 1995). Neuronal hyperactivity in AD can disrupt the normal function of cortical and hippocampal circuits. Thus, hyperactive neurons in the visual cortex displayed impaired response properties to certain stimuli which was correlated to behavioral impairments (Grienberger et al 2012). In the hippocampus, hyperactivity can impair the function of so-called place cells (Koh et al 2010, Wilson et al 2005), neurons that are essential for processing spatial information and encoding a map of the environment (Brun et al 2002, Moser et al 2008). In addition to these findings, AD mice have repeatedly been reported to be prone to developing spontaneous epileptiform activity as well as nonconvulsive seizures (Palop et al 2007, Palop & Mucke 2016, Verret et al 2012) (**Fig. 3 C, D**). Contrary to hyperactive neurons, some cells in AD mice are also hypoactive or can be functionally silent (Busche et al 2012, Busche et al 2008). Remarkably, this hypoactivity develops at much later ages than hyperactivity and could thus be the consequence of a compensatory mechanism to prevent excessive activity (Busche & Konnerth 2015). However, the picture could be more complex. Thus, the recently discovered

[2] Aβ interactions with neuronal and non-neuronal proteins will be discussed in chapter 1.1.4.

amyloid fragment amyloid-eta can directly decrease neuronal firing rates in mice (Willem et al 2015).

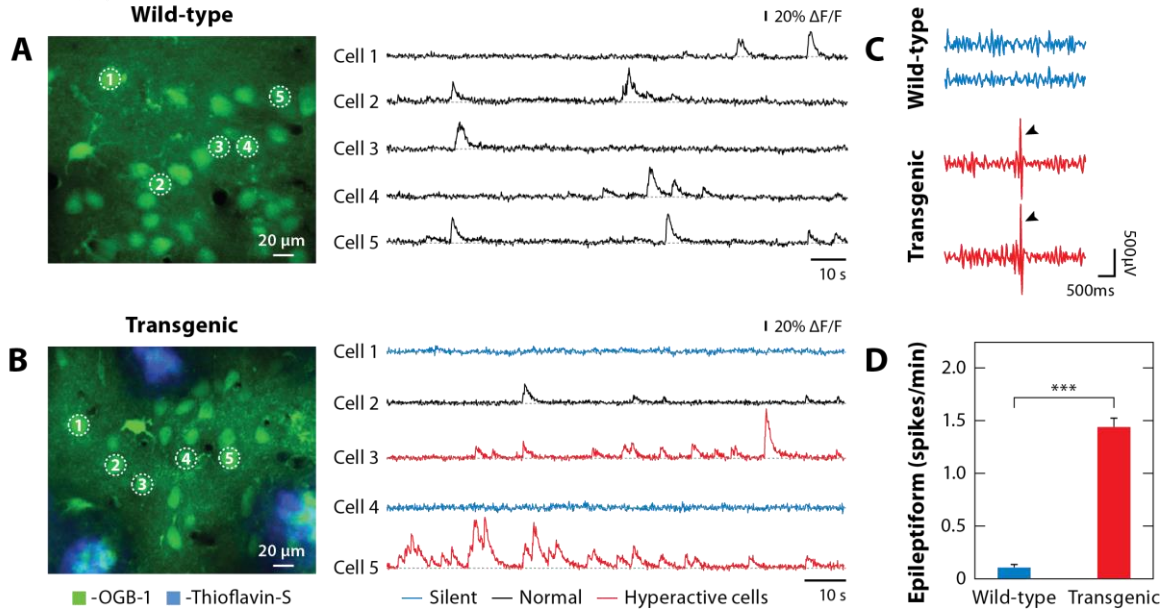

Fig. 3: Neuronal hyperactivity in mouse models of AD *in vivo*. *A* and *B)* Left: A representative two-photon image from layer-2/3 neurons was recorded in the frontal cortex in a wild-type mouse (*A*) and an APP23×PS45 transgenic mouse (*B*). Neurons are characterized by high brightness in the green channel (OGB-1), while Aβ plaques are indicated by blue fluorescence after Thioflavin-S staining. Right: Ca^{2+}- traces from the neurons cycled in the left panel. The Ca^{2+}- traces are color coded according to the activity status of the respective neuron (silent, blue; normal, black; hyperactive, red). *C)* Electroencephalogram recordings from a wild-type mouse (top, blue) and a mouse model of AD (bottom, red). The arrowheads indicate epileptiform spikes. *D)* Frequency of spikes in wild-type and transgenic mice; summary bar graph from panel *C* (***, $P < 0.001$). Panels *A* and *B* adapted from (Busche et al 2008), panels *C* and *D* adapted from (Verret et al 2012). The whole figure was modified from (Zott et al 2018).

The observed hyperactivity in mouse models of AD is largely backed up by studies in patients with early stages of AD. It is not feasible to study neuronal activity on a single-cell level in humans. However, it is possible to estimate gross changes of the activity status of brain regions by measuring changes in the level of blood oxygenation (Logothetis et al 2001) in functional MRI (fMRI). In these experiments, the brain activity while performing a certain task is compared with control conditions at rest and allows to detect activity changes with a reasonable temporal (several seconds) and spatial (sub-mm^3) resolution (Chen & Glover 2015). Some of the most striking functional impairments in AD can be found in the so-called

default mode network (DMN). It includes a number of brain regions, which are usually active at rest and deactivate when the subject shifts their attention to the outside, for example in learning tasks (Buckner et al 2008, Raichle et al 2001). In AD patients, this deactivation breaks down (**Fig. 4 A, B**), indication that the DMN stays active at all times (Lustig et al 2003, Sperling et al 2009).

Another brain region which was found to be hyperactive in patients with early or presymptomatic stages of AD is the hippocampus. Hippocampal hyperactivation during memory tasks was observed in subjects with normal memory performance that had either an increased genetic risk of developing AD (Bookheimer et al 2000), were carriers of FAD mutations (Quiroz et al 2010) or already had some Aβ deposits in the brain (Mormino et al 2012). Moreover, MCI patients also exhibited hippocampal hyperactivity (Dickerson et al 2005, Huijbers et al 2015). With disease progression, however, the trend was reported to reverse and late-stage AD patients are usually characterized by a marked hypoactivity of the hippocampus (Dickerson et al 2005, Pariente et al 2005) (**Fig. 4 C**). This finding was recently supported by longitudinal studies which reported an increase of neuronal activity at early stages and a successive decrease over time (Huijbers et al 2015, O'Brien et al 2010). In these subjects, there was a strong correlation between high activity levels of the hippocampus at baseline and the speed of memory loss. Even though it is not clear what induces the change from hyperactivity to hypoactivation, it is natural to speculate that the emergence of first hyperactive cells and then additionally hypoactive cells in mouse models of AD (Busche et al 2008) is the cellular basis for the observed “inverse U-shaped trend” (Sperling et al 2010) of hippocampal activity in AD patients.

One pressing question in light of these findings is whether the observed hyperactivity is the result of a compensatory mechanism and is thus beneficial to maintain a sufficient level of memory performance at the beginning of the disease. Two lines of evidence make

this possibility rather unlikely and indicate that neuronal hyperactivity is instead a pathogenic contributor to the disease process (Stargardt et al 2015). First, under experimental conditions, the levels of neuronal activity predict subsequent Aβ deposition with higher firing rates promoting Aβ release from neurons (Cirrito et al 2005, Dolev et al 2013, Yuan & Grutzendler 2016). Also, a recent longitudinal study in MCI patients reported that the level of hippocampal activity predicted the speed of Aβ deposition over the following years (Leal et al 2017) (**Fig. 4 D**). Second, pharmacologically restoring normal levels of hippocampal activity by reducing neuronal firing was reported to rescue memory performance in MCI patients (Bakker et al 2015, Bakker et al 2012). This was achieved by administration of the antiepileptic drug levetiracetam[3].

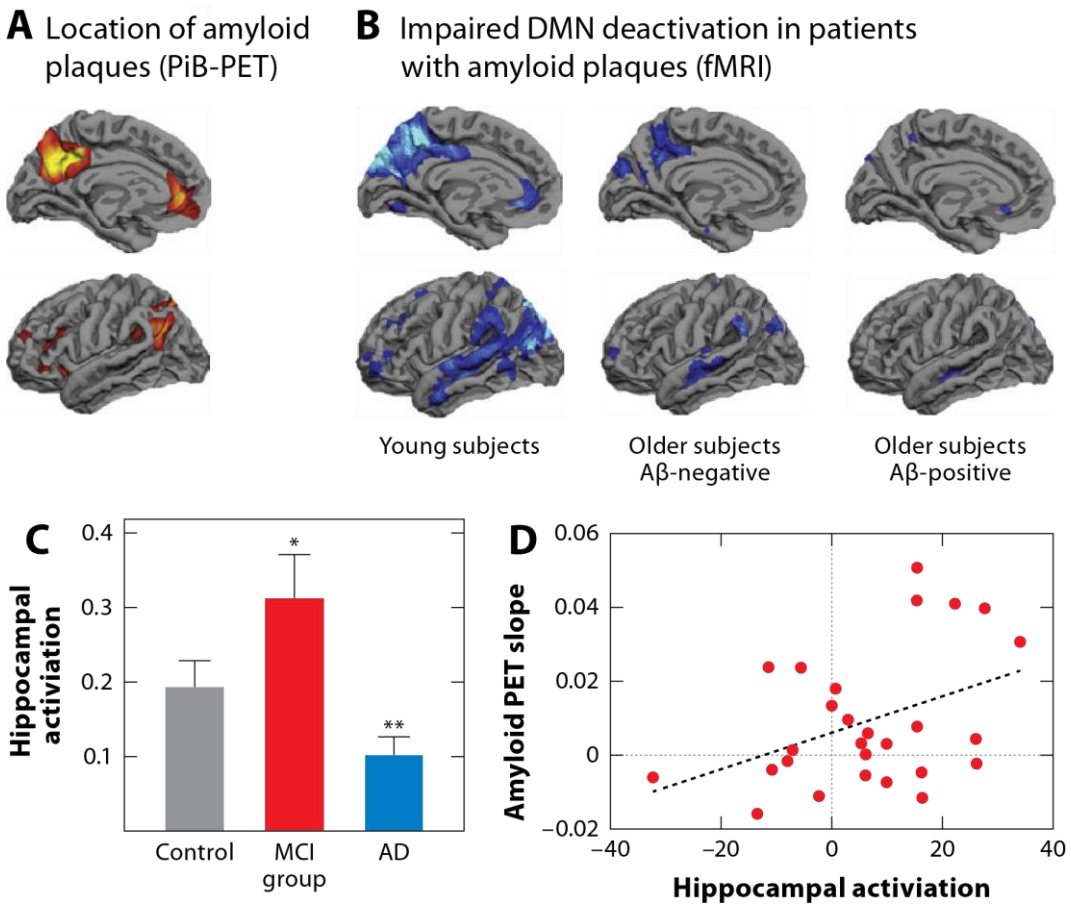

[3] A detailed discussion of the possible use of levetiracetam as a disease-modifying drug in AD patients can be found in chapter 4.5.

Fig. 4: AD-dependent disruptions of neuronal circuits in humans. *A)* Cortical hotspots of amyloid plaque deposition (red-yellow). *B)* fMRI recordings indicate cortical areas with task-specific deactivations (blue). Summary data of young (left), older Aβ-negative (middle), and older Aβ-positive subjects (right). *C)* Task-associated activation is increased in the hippocampus of MCI patients compared with healthy controls or AD patients. (∗, $P < 0.03$; ∗∗, $P < 0.005$). *D)* Regression-analysis of the dependence of the speed of amyloid accumulation (slope) on the level of hippocampal activation at baseline. Hippocampal activation was determined using fMRI and amyloid levels were detected using PET imaging. Panel *A* and *B* adapted from (Sperling et al 2009). Panel *C* adapted from (Dickerson et al 2005). Panel *D* adapted from (Leal et al 2017). The whole figure was modified from (Zott et al 2018).

There is now ample *in vivo* evidence that neuronal hyperactivity is causally related to Aβ and most likely mediated by soluble Aβ oligomers such as dimers. First, hyperactivity can be observed in young AD mice before plaques are formed. Second, there is a strong correlation between the levels of soluble Aβ and the number of hyperactive neurons in the cortex of AD mice (Keskin et al 2017). Third, removal of soluble Aβ by inhibitors of γ-secretase potently abolished hyperactivity in the hippocampus (Busche et al 2012). Strikingly, this decrease in hyperactivity could be achieved with the acute administration of a single dose of a γ-secretase-inhibitor, which is unlikely to change the number and size of plaques in the brain. In line with this, reducing the levels of soluble Aβ by the chronic treatment of AD mice with a BACE inhibitor rescued the cortical activity phenotype (Keskin et al 2017). Fourth, in later disease stages, hyperactive neurons are exclusively found in the direct vicinity of amyloid plaques (Busche et al 2008). This association can be explained by the observation that the levels soluble Aβ are especially high in the direct neighborhood of plaques (Hefendehl et al 2016, Koffie et al 2009). Finally, the acute application of soluble Aβ dimers could trigger neuronal hyperactivity, both in wild-type mice (Busche et al 2012) and in AD mice, in which the neuronal activity had previously restored by BACE inhibition (Keskin et al 2017).

What is the mechanism of the Aβ-induced neuronal hyperactivity? Previous work from the Konnerth laboratory has demonstrated that the neuronal hyperactivity is driven by synaptic inputs rather than a release from Ca^{2+} stores or a tendency towards

hyperexcitability (Busche et al 2008, Busche & Konnerth 2016). More specifically, an impaired balance of neuronal excitation and inhibition (E/I balance) with a relative decrease in GABAergic inhibition leads to a shift of the E/I balance towards excitation. This leads to an increase in neuronal activity and the emergence of hyperactive neurons. In consequence, enhancing synaptic inhibition by agonists of GABA receptors (Busche et al 2008) completely abolished neuronal hyperactivity and, remarkably, restored memory function in a mouse model of AD. However, the exact mechanism of the Aβ-dependent disruption of the E/I balance remained unknown.

Accumulating evidence indicates that Aβ induces neuronal hyperactivity but also that neuronal hyperactivity influences the amount of Aβ production. Thus, high levels of activity can lead to elevated extracellular concentrations of Aβ or an altered balance of Aβ40/Aβ42 (Cirrito et al 2005, Dolev et al 2013, Kamenetz et al 2003, Wei et al 2010). In line with these findings, chronic sensory activation of certain cortical areas increased the subsequent plaque deposition in those regions (Bero et al 2011, Yuan & Grutzendler 2016). Conversely, decreasing neuronal activity by chronic sensory deprivation (Bero et al 2011) or by chemogenetic inhibition *in vivo* (Yuan & Grutzendler 2016) led to a markedly decreased amyloid burden in the same cortical areas. It is not entirely clear, what the molecular mechanism behind this activity-dependent increase in Aβ production is. One study reported an activity-dependent change in the conformation of the catalytic site of γ-secretase to be responsible for an activity-dependent shift of the Aβ 40/Aβ42 balance (Dolev et al 2013). Also, RNA levels of APP are higher in layer than in other cortical layers (Bahmanyar et al 1987), which could be due to the exceptionally high baseline activity levels of layer 5 pyramidal neurons (Tischbirek et al 2015).

In summary, a prominent feature of AD both in mouse models of AD and humans at early stages of the disease is neuronal hyperactivity. The basis of this hyperactivity is a

soluble Aβ oligomer-induced impairment of E/I balance which is shifted towards excitation. However, the underlying cellular mechanism remained elusive.

Impaired sleep-related slow oscillations

In addition to functional impairments on the synaptic and cellular level, AD is also characterized by disruptions of large-scale network activity. Of particular interest is the prominent loss of sleep slow oscillations which can be observed both in mouse models of AD and human patients (Busche et al 2015b, Mander et al 2015). Sleep and especially sleep slow oscillations are vital for the maintenance of long-term memory. There is now ample evidence that particularly during non-REM (rapid eye movement) sleep, recently acquired information is transmitted from the short-term memory in the hippocampus to storage sites for long-term memory located in the neocortex (Diekelmann & Born 2010). The physiological correlate of this transfer is so-called replay, which means that neuronal activity patterns present during learning in the awake state are repeated in a compressed manner during sleep (Peigneux et al 2004, Wilson & McNaughton 1994). Replay occurs preferably during deep sleep stages, characterized in the electroencephalogram by the occurrence of slow waves, which carry faster rhythms such as sleep spindles and ripples (Staresina et al 2015, Steriade 2006, Steriade et al 1993). Even in healthy subjects, impairment of these sleep rhythms can lead to impaired memory performance (Clemens et al 2005, Helfrich et al 2018) and enhancing slow oscillations improves memory recall (Marshall et al 2006, Ngo et al 2013).

Sleep disturbances are an early symptom in many AD patients (Hita-Yanez et al 2012, Spira et al 2013, Sprecher et al 2017) and correlate with memory performance (Ficca et al 2000, Westerberg et al 2010). Even though sleep disturbances are a symptom of many diseases (Foley et al 2004), the strong impairment of sleep slow oscillations is specific for AD. Since memory loss is one of the most debilitating symptoms of AD, a loss of slow oscillations

could be one of the mechanisms responsible for this impairment. Indeed, a recent study elegantly described the relationship between Aβ, slow oscillations and memory performance (Mander et al 2015). In this study, the authors suggest that the amount of Aβ in certain brain areas can predict the level of slow oscillation deficiency and the worsening of memory performance (**Fig. 5**).

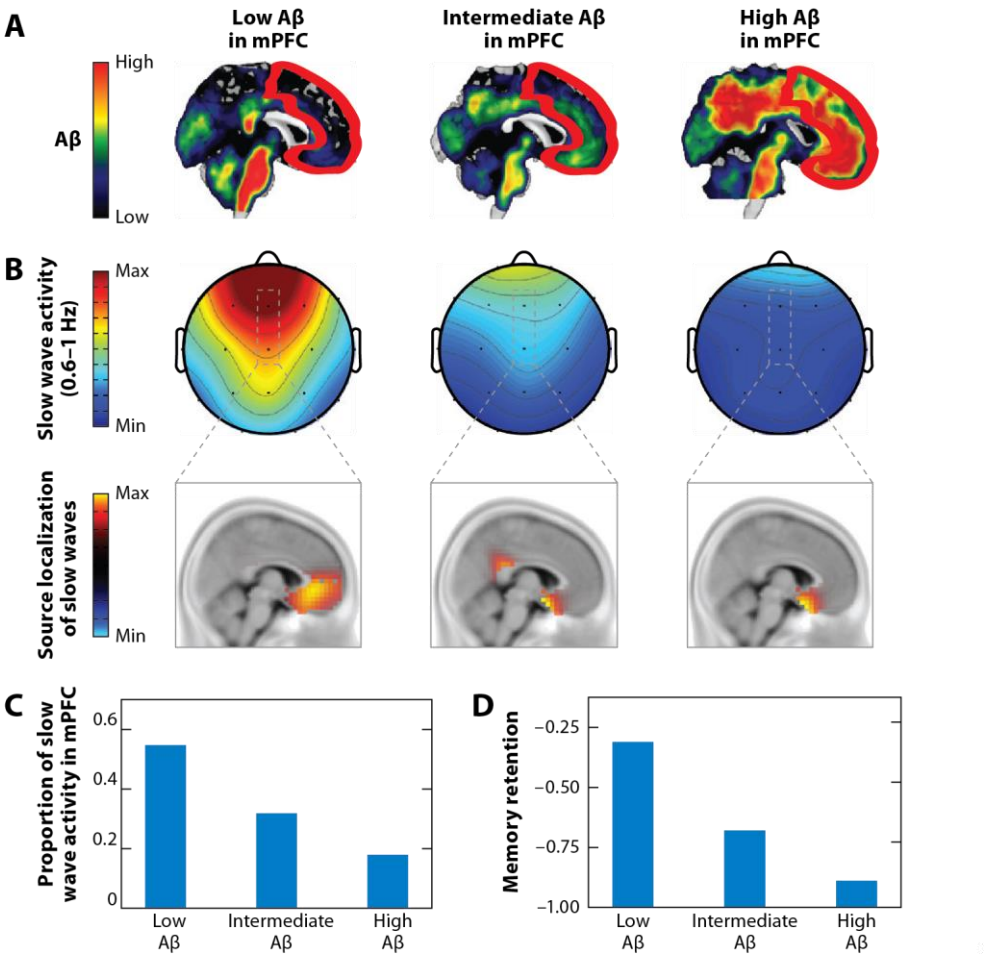

Fig. 5: Impaired memory performance is associated with high amyloid plaque load and impaired slow wave activity during sleep. A) PET-imaging of the amyloid plaque load in three example subjects without cognitive impairments and low (left), intermediate (middle) and high (right) levels of Aβ in the medial prefrontal cortex (mPFC, outlined in red). B) Top: EEG-based power spectrum (top) and source localization (bottom) of the sleep slow wave activity for the three subjects. C) Relative levels of sleep slow wave activity for the subjects sorted according to their level of brain Aβ. D) Memory performance of the three subjects. Modified from (Mander et al 2015) and reproduced from (Zott et al 2018).

As with the other impairments described here, there is now strong evidence from mouse studies indicating that soluble Aβ is both sufficient and necessary for the disruption of slow oscillations. In mouse models of AD, studies using calcium (Ca^{2+}) imaging demonstrated a clear impairment of the coherence of slow waves over all cortical areas (Busche et al 2015b, Keskin et al 2017). This desynchronization could be rescued by the removal of soluble Aβ by BACE inhibition and reoccurred in the same mice after Aβ application (Keskin et al 2017). Conversely, the application of soluble Aβ in wild-type-mice readily induced this desynchronization (Busche et al 2015b) (**Fig. 6 A**). Just like the neuronal hyperactivity, desynchronization of slow waves was a product of a shift of the E/I balance towards excitation. Thus, enhancing GABAergic tone with benzodiazepines such as midazolam restored the coherence of the slow oscillations in AD mice (Busche et al 2015b) (**Fig. 6 B, C**). This intervention also rescued the behavioral phenotype in those mice (**Fig. 6 D**). However, at this point it is still unknown whether the impairment of slow oscillations is a direct consequence of the neuronal hyperactivity and whether the same Aβ-dependent mechanisms induce neuronal hyperactivity and the impairment of slow oscillations.

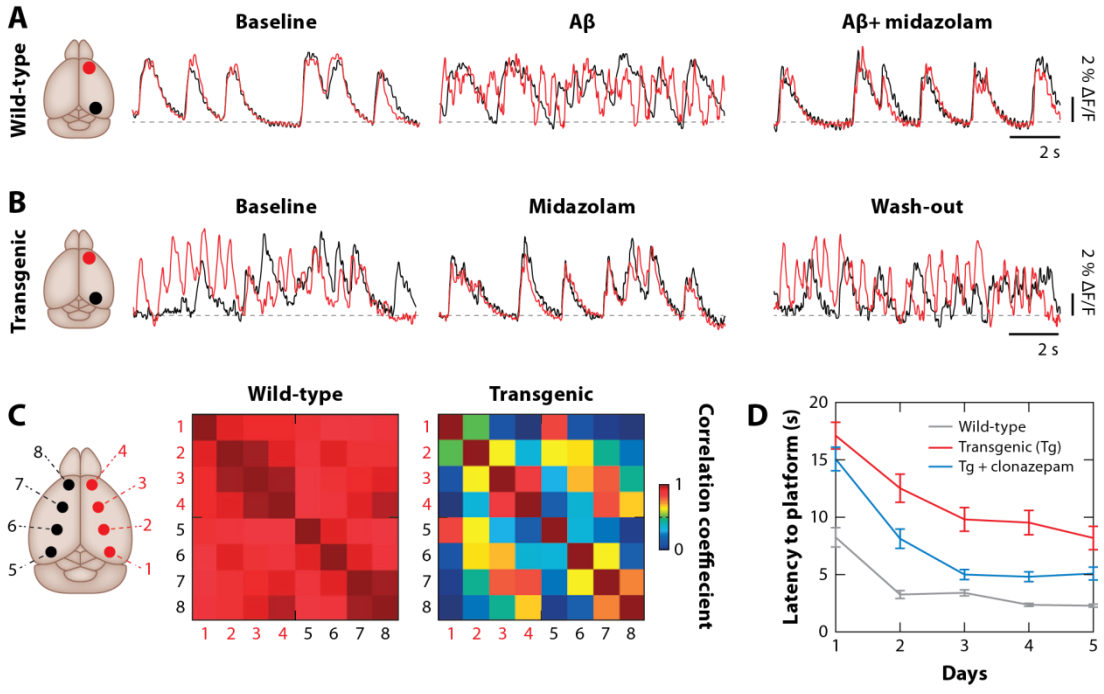

Fig. 6: Aβ-induced disruption of cortical slow oscillations *in vivo*. *A)* Wide-field fluorescence imaging of Ca^{2+}-activity in the frontal (red) and occipital (black) cortices of a wild-type mouse under baseline (left), Aβ application (middle) and Aβ and midazolam co-application (right) conditions. *B)* Same as *A*, but in an APP23 x PS45 transgenic muse under baseline (left), midazolam application (middle) and washout (right) conditions. *C)* Color-coded cortical cross-correlation matrices for the eight recording sites indicated in the left panel indicate a high coherence of slow oscillations in wildtype mice (left) and low correlations in transgenic mice (right). *D)* Memory performance of wildtype (grey), transgenic (red) and transgenic clonazepam-treated (blue) mice in a five-day discriminatory water maze task. Adapted from (Busche et al 2015b) and reproduced from (Zott et al 2018).

1.1.4 Do specific Aβ receptors exist?

While it is widely accepted that Aβ triggers an extensive range of changes in the brain (described in the previous chapter), the exact mechanisms for many of these changes remain elusive. It is most likely that the functional and structural changes observed in AD are mediated by a direct or indirect interaction of Aβ with one or more receptors. In fact, a huge number of possible Aβ receptors have been identified. The literature dedicated to this topic is vast and highly controversial (Jarosz-Griffiths et al 2016). Hence I will only give a brief overview over the most important possible interaction partners of Aβ.

One widely accepted fact is that Aβ can bind to neurons and astrocytes (Hong et al 2014, Lacor et al 2007) and especially to synapses (Lacor et al 2004). In consequence, it is important to ask exactly which part of the neuron Aβ binds to. Since Aβ is generally located in the extracellular space, the possible binding partners include membrane proteins, the extracellular matrix and membrane lipids.

Proteins as suggested Aβ receptor candidates

Three classes of membrane proteins evolve as possible Aβ receptors. The first group comprises proteins involved in the Aβ homeostasis and trafficking. A second class includes receptors on immune cells, which are implicated in synaptic pruning and could induce neuronal cell death. The third class of receptors is located mainly on neurons and involved in the Aβ-dependent impairment of synaptic transmission.

One of the early candidates implicated in AD was the receptor for advanced glycation end products (RAGE), (Yan et al 1996). RAGE is an endothelial receptor and is thought to mediate the uptake of Aβ into the brain across the blood-brain barrier (Deane et al 2003). In consequence, the disease progression in AD-mice overexpressing RAGE was accelerated and, conversely, RAGE-KO mice were protected from AD-dependent changes (Arancio et al 2004). Another receptor, which is involved in intracellular Aβ trafficking, is the Sortilin-related receptor L1 (SorL1), which was reported to be involved in transporting APP through the cell as it gets cleaved. More specifically, SorL1 seems to inhibit BACE-cleavage and the release of Aβ into the extracellular space and is thus protective against AD (Andersen et al 2005, Offe et al 2006, Spoelgen et al 2006). Recently, SorL1 has repeatedly been implicated as a risk gene for AD (Cuccaro et al 2016, Lambert et al 2013). Structurally very similar to SorL1 is sortilin, which was recently reported to be important for Aβ clearance from the extracellular space (Carlo et al 2013). Also involved in the regulation of Aβ processing is the Nogo-66 receptor 1 (NgR1), which reportedly modulates the processing of APP by α- and β-secretases (Park et al 2006a). Generally speaking, exogenously increasing NgR1 reduced Aβ levels and toxicity, while its deletion worsened AD pathology in the brains of a mouse model of AD (Park et al 2006a, Park et al 2006b).

Receptors of the second group are expressed on immune cells of the brain. One candidate protein implicated in Aβ toxicity is the immune-receptor IgG Fcγ receptor II-b (FcγRIIb), which is expressed on B-cells, neutrophils and macrophages. The levels of FcγRIIb were reported to be increased in AD patients and knockout or inhibition of this receptor alleviated many Aβ-induced deficits *in vitro* and improved memory performance in a mouse model of AD (Kam et al 2013). Also expressed on immune cells is the LilrB2-receptor and its murine homolog, the paired immunoglobulin-like type 2 receptor B (PirB). This receptor can bind Aβ oligomers (Kim et al 2013). Additionally, it has been reported that deletion of the LilrB2-receptor eliminated Aβ-induced neurotoxicity and rescued LTP levels in a mouse

model of AD (Kim et al 2013). Recently, the receptor crystal structure has been solved and a possible binding pocket for Aβ oligomers has been identified (Cao et al 2018). Finally, the excessive pruning of synapses which is a hallmark of early AD was reported to be mediated by a complement-dependent activation of microglia (Hong et al 2016). Although not classically considered as a receptor for Aβ, there is some evidence for a direct binding of Aβ to certain complement factors (Rogers et al 1992).

The neuronal surface proteins that soluble Aβ binds to are generally regulators of neuronal excitability. One of these receptors which has been implicated in Aβ toxicity early on is the α-7 subtype of the nicotinic acetylcholine receptors (nAchRα7) which reportedly binds Aβ with a very high affinity (Wang et al 2000). Furthermore, nAchRα7 were reported to be increased in a mouse model of AD and this increase was associated with worse memory performance (Dineley et al 2001). One of the receptors most frequently indicated in AD is the NMDAR. An Aβ-dependent impairment of this receptor, which is highly important for memory formation, could possibly explain the Aβ-induced impairments of LTP and LTD (Malinow 2012)[4]. At the moment, however, it is unclear, whether Aβ can directly interact with the NMDAR. Thus, Aβ binds to glutamatergic synapses containing NMDARs, but not to GABAergic synapses (Lacor et al 2007). One of the most robust finding was that blocking the NMDAR or its NR2B subunit prevented the Aβ-dependent effect on synaptic plasticity (Hu et al 2009, Rammes et al 2011, Rönicke et al 2011) as well as the Aβ-induced structural impairments (Hsieh et al 2006, Shankar et al 2007, Wei et al 2010). However, the interaction between Aβ and the NMDAR is probably indirect (De Felice et al 2007, Malinow 2012). This indirect interaction could, for example, be mediated by the ephrin type B receptor 2 (EphB2). Unlike for NMDA, a direct binding of Aβ to EphB2 has been reported (Cissé et al 2010) . The function of this receptor tyrosine kinase is to regulate NMDAR-levels on the neuronal surface. Thus, AD is associated with decreased levels of both NMDARs (Ikonomovic et al

[4] For a summary of Aβ-dependent LTP and LTD impairments, see chapter 1.1.3

1999) and EphB2 (Simon et al 2009). Also, restoring EphB2 levels reversed LTP deficits and memory impairment in a mouse model of AD (Cissé et al 2010). An indirect Aβ-dependent involvement of postsynaptic NMDARs could also be caused by an Aβ-induced inhibition of glutamate uptake, as was reported by the Selkoe lab (Li et al 2009, Li et al 2011). The authors of these studies reported that Aβ application impaired synaptic plasticity via an excessive activation of NR2B-containing receptors and that the mechanism of this impairment most likely involved an impaired uptake of synaptically released glutamate[5]. One of the best-characterized receptors for Aβ is the prion protein (PrP^c). It can bind Aβ oligomers in mice and humans (Dohler et al 2014, Laurén et al 2009) and the knock-out of PrP^c as well as the application of anti-PrP^c antibodies prevented some of the Aβ induced pathology. Thus, PrP^c is required to mediate the Aβ-induced effects on neuronal plasticity, synapse loss and behavior in a mouse model of AD (Barry et al 2011, Gimbel et al 2010, Kudo et al 2012, Laurén et al 2009, Resenberger et al 2011). However, there is also evidence that PrP^c is in some cases not required for Aβ-induced neuronal dysfunction (Cissé et al 2011, Kessels et al 2010). Another question is how PrP^c binding can be translated into an intracellular signal, since PrP^c is not a transmembrane protein, but rather linked to the outside of the cell membrane with a lipid anchor. A possible mediator of PrP^c-binding could be mGluR5 (Um et al 2013). When activated by Aβ-bound PrP^c, mGluR5 was reported to activate, among others, Fyn-Kinase, which might further downstream effects such as NMDAR-internalization and the loss of dendritic spines (Um et al 2012). The involvement of mGluR5 in AD is of particular interest, since it opens a path for pharmacological manipulations. Thus, the chronic inhibition of mGluR5 alleviated memory symptoms and pathology in a mouse model of AD (Hamilton et al 2016).

[5] The Aβ-dependent impairment of glutamate uptake is discussed in more detail in chapter 4.2.

Aβ can interact with various membrane components

Regardless of the binding of membrane proteins, Aβ could also directly interact with membrane lipids. In fact, there is some evidence that Aβ binds to gangliosides on the plasma membrane (Hong et al 2014, Yanagisawa et al 1995) and cholesterol (Avdulov et al 1997). A few studies have also suggested that membrane-associated Aβ has a high propensity to aggregate (Bokvist et al 2004, Nagarathinam et al 2013). The membrane-associated Aβ aggregates preferentially form in the vicinity of synapses (Renner et al 2010), where they can interfere with the function of membrane proteins without necessarily binding to them. Thus, a recent study reported that Aβ restricts the lateral mobility of postsynaptic mGluR5 (Renner et al 2010). Finally, the interaction of Aβ with the plasma membrane could lead to the formation of Ca^{2+}-permeable pores in the membrane (Lashuel et al 2002, Quist et al 2005), a process which was reported to be dependent on cholesterol (Di Scala et al 2014). However, compelling *in vivo* evidence for this hypothesis is not available yet.

In summary, a plethora of receptors have been implicated in AD. The sheer number of possible targets makes it rather unlikely that there is only one dedicated Aβ receptor. More likely, Aβ pathology is conveyed by the binding of Aβ to a number of different mediators. Moreover, it is important to keep in mind that there is not just one species of Aβ in the brain. Aβ of different aggregate sizes or conformations could theoretically bind to different receptors. Remarkably, what little is known about the relationship of aggregate size with receptor affinity is in line with the observed toxic effects of Aβ. For example, Aβ receptors such as the PrP^c binds Aβ oligomers with a much higher affinity than monomers or fibrils (Um et al 2012) and FcγRIIb predominantly binds Aβ oligomers (Cao et al 2018). However, further research is needed to determine the interactions of Aβ with membrane proteins and lipids.

1.2 Recording neuronal function and dysfunction on the single cell level *in vivo*

The goal of my thesis was to study the mechanism of Aβ-induced neuronal dysfunction based on previous observations that the direct application of Aβ is sufficient to trigger neuronal hyperactivity *in vivo* (Busche et al 2012). In order to investigate Aβ-induced neuronal dysfunction, it is necessary to record neuronal activity with high temporal and sub-cellular spatial resolution. The method of choice to achieve this is *in vivo* two-photon Ca^{2+}-imaging. Here, I will introduce the necessary methodological knowledge for the later chapters.

1.2.1 Two-photon calcium imaging of neurons

Before the widespread adoption of two-photon imaging, the preferred method to simultaneously record neuronal action potentials was based on extracellular electrophysiology using tetrodes (Gray et al 1995). This method provides an excellent temporal resolution and can be applied in freely moving animals, but the recordings do not contain any anatomical information about the network the neuronal activity is recorded from. Moreover, tetrode recordings are biased to only detect active cells (Shoham et al 2006). In consequence, the invention of two-photon fluorescence imaging (Denk et al 1990, Helmchen & Denk 2005) together with the development of methods to detect neuronal Ca^{2+} signals in living brain tissue (Stosiek et al 2003) was a major breakthrough in neuroscience. Applying these techniques not only allowed neuroscientists to simultaneously probe the neuronal activity of many neurons, including silent ones, in real time. It also enabled them, for the first time, to do so with exact knowledge of the anatomy of the neuronal network they were recording from.

Calcium imaging in neurons

Since two-photon imaging relies on light microscopy, it is vital to translate neuronal activity into detectable light signals. This is usually achieved by fluorescent indicators. During an

action potential, the neuronal membrane depolarizes and this change in membrane potential can be visualized by fluorescent voltage-sensitive dyes. Unfortunately, the limited signal-to-noise ratio and the extremely rapid time-course of the voltage signal of these dyes does not yet allow for a wide-spread application of this technique. However, recent advancements might make a use in the future more feasible (Gong et al 2015). The depolarization of the neuronal cell membrane is associated with the influx of cations, most notably sodium (Na^+) and Ca^{2+} into the neuron. While fluorescent Na^+-imaging is possible but not widely used due to methodological limitations (Schreiner & Rose 2012), fluorescent Ca^{2+}-indicators dominate the field and are the most extensively used tool to visualize neuronal activity *in vitro* and *in vivo* (Grienberger & Konnerth 2012, Yang & Yuste 2017). Imaging concentration changes of Ca^{2+} is in many ways an optimal way to record neuronal activity. The intracellular Ca^{2+} concentration is only 50-100 nM at rest and can increase massively during action potential activity, which allows for high signal-to noise ratios (Berridge et al 2000). Moreover, the action-potential induced fluorescence changes reported by Ca^{2+}-indicators have decay times in the range of tens to hundreds of milliseconds, depending on the indicator and the cellular compartment (Cornelisse et al 2007, Helmchen et al 1996). Thus, in contrast to measurements of membrane voltage changes, Ca^{2+} imaging of neuronal activity can be performed at reasonably slow sampling rates of 10-40 Hz. In the soma of neurons, action potentials trigger a rapid influx of Ca^{2+} through voltage-gated Ca^{2+} channels, followed by a slower extrusion of Ca^{2+} from the cytoplasm into the extracellular space or into intracellular stores such as the endoplasmic reticulum (Grienberger & Konnerth 2012). These changes of intracellular Ca^{2+} are then detected as conspicuous changes in the fluorescence of the indicator with sharp rise-times and slow decay times (Rochefort et al 2008, Stosiek et al 2003, Yuste et al 2011).

One widely used technique to deliver Ca^{2+}-indicators into the brain tissue is the use of genetically encoded indicators, which can be stably expressed in transgenic mouse lines or

after the injection of a virus carrying the DNA coding for the construct. The advantage of the genetically encoded Ca^{2+}-indicators (GECIs) is that it is possible to specifically target subpopulations of cells and that they allow for long-term imaging over weeks or months (Tian et al 2012). Accordingly, viral or transgenic expression of GECIs is the method of choice to perform chronic Ca^{2+}-imaging experiments. However, viral injection of GECIs is cumbersome and does not allow for acute experiments. Moreover, even though rapid technological advancements in the field have led to a huge improvement of the indicator proteins (Chen et al 2013, Dana et al 2018), GECIs still have issues with nonlinearity. Because, unlike organic Ca^{2+}-indicators, GECIs have more than one (typically four) binding sites for Ca^{2+}, there is no strong linear correlation between increases in Ca^{2+} and the fluorescence changes of the indicator (Rose et al 2014). In consequence, the preferred method to perform acute experiments in neurons and astrocytes in a given brain region, is the use of organic Ca^{2+}-indicators (Tischbirek et al 2015, Tischbirek et al 2017). These dyes are highly versatile and can simply be injected into the brain by pressure-injection from a glass pipette (Kerr & Denk 2008, Stosiek et al 2003). In order to homogeneously label virtually all neurons in a certain brain area, acetoxymethyl (AM) ester-bound organic Ca^{2+}-indicators are injected into the brain tissue (Stosiek et al 2003, Tsien 1981). As long as the indicator is bound to the AM ester, it can readily diffuse through cell membranes, but once it has diffused into the cytoplasm, the lipophilic ester is cleaved by endogenous esterases, trapping the indicator in the cell. Since the goal of my thesis was to determine the acute action of Aβ on neuronal activity, I chose to use an organic Ca^{2+}-indicator based approach for my experiments.

The basics of two-photon microscopy

One of the major restrictions of light microscopy is the limited penetration depth of light in scattering tissues such as the brain. The use of two-photon imaging of fluorescent indicators has pushed the imaging depth limit of laser scanning microscopy from less than 100 µm with

single-photon excitation to almost 1 mm, about the depth of the entire mouse cortex (Helmchen & Denk 2005).

Fluorescent microscopy is based on the principle of exciting a fluorophore with monochromatic light and collecting the emitted photons from the fluorescent probe. Absorbing a photon elevates a fluorophore to an excited state. This state is unstable and the fluorophore returns to its ground state rapidly, again emitting a photon (Lichtman & Conchello 2005). As the emitted photon is has slightly less energy, the emitted light has a longer wavelength than the excitation light (**Fig. 7 A**). This difference in wavelengths is called Stokes-shift (Resch-Genger et al 2008). In order to rapidly detect fluorescence with a high spatial resolution, the laser beam is typically scanned across a rectangular field of view (**Fig. 7 B**) using fast galvanometric or resonant mirrors. Different scanning methods also exist (Yang & Yuste 2017), but will not be discussed here. Because the laser only illuminates a defined spot at a certain time, a rapid detector with a very high sensitivity but only one pixel, such as a photomultiplier tube (PMT) can be used and the image is then reconstructed by assigning the fluorescence level at a certain time back to the location the laser has hit.

In the case of single-photon laser scanning microscopy (typically with blue light), the highest light intensity will be found in the focal spot, but the cone above and below will also get illuminated and thus generate out of focus fluorescence (**Fig. 7 C**). This can be largely overcome by the application of nonlinear two-photon excitation, which makes use of the fact that the energy of two photons can add up if they arrive at the same location within about 0.5 fs from each other (Göppert-Mayer 1931). This means that the same fluorophores as in single-photon laser scanning microscopy can be excited by light with longer wavelengths (in the near infrared spectrum), i.e. less energy (**Fig. 7 A**). This brings a lot of advantages such as deeper penetration depth (Oheim et al 2001) and lower phototoxicity (Svoboda & Block 1994). Furthermore, as the addition of energies is a nonlinear process, the amount of out of

focus fluorescence is much lower in two-photon than in single-photon microscopy (**Fig. 7 C**). Since photons that have been generated outside of the focal point hit the objective at slightly different angles than those originating from the focal point, they can be blocked out by a pinhole to maintain a high resolution as is typically done in confocal microscopy. If using nonlinear multi-photon illumination, on the other hand, all photons can be expected to result from the focal point and thus no pinhole is needed.

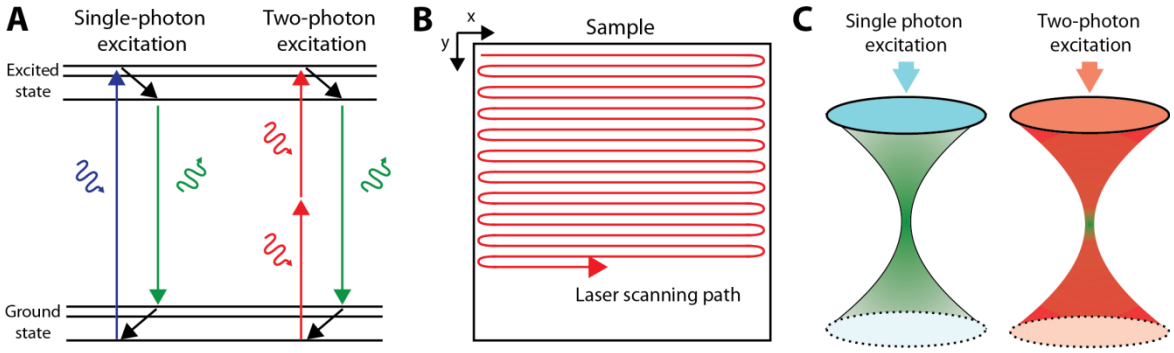

Fig. 7: The basics of two-photon microscopy. *A)* Jablonski diagram illustrating single-photon and two-photon absorption. *B)* Typical laser path in laser scanning microscopy. *C)* Spatial confinement of signal generation with nonlinear excitation. Panels *A* and *C* based on (Helmchen & Denk 2005) and (Lichtman & Conchello 2005).

The biggest limiting factor of light microscopy is light scattering. The brain is a highly scattering tissue, which means that photons are forced from their ballistic linear path after penetrating only few tens of micrometers into the tissue (Oheim et al 2001). This limits the recording depth of confocal microscopy as photons that were emitted from the fluorophore get scattered on their way back towards the objective and get blocked out by the pinhole, which results in a much lower signal as compared to two-photon imaging where no pinhole is used. On the contrary, two-photon microscopes are usually equipped with objectives with a high acceptance angle, i.e. numerical aperture (NA) to collect as many scattered photons as possible. Also those photons emitted by the laser get scattered on their way towards the fluorophore, which leads to a lower brightness of the focal point in both methods. In single-

photon excitation, however, the scattered photons additionally contribute to the amount of out of focus fluorescence, whereas, in the two-photon case, the use of laser light with approximately double the wavelength, i.e. half the energy, leaves scattered photons with too little energy to excite the fluorophore (Helmchen & Denk 2005).

While two-photon imaging theoretically allowed researchers to perform imaging experiments in depths up to 1 mm (Theer et al 2003), the analysis of neuronal activity was mainly limited to the cortical layer 2/3 for a long time. In the last years, however, huge advances have been made and allow for functional two-photon imaging in deeper cortical layers (Tischbirek et al 2017, Yang & Yuste 2017). These include the development of red-shifted fluorophores with longer excitation and emission wavelengths (Akerboom et al 2013, Dana et al 2016, Tischbirek et al 2015) and the targeted labelling of fewer neurons to reduce the background fluorescence (Birkner et al 2017). Other methodological advances for deeper imaging include the use of three-photon excitation, the implantation of lenses or prisms into the cortex and shaping the wave front of the laser to counteract inhomogeneity of the tissue (Yang & Yuste 2017). However, these techniques are not widely used yet.

1.2.2 *In vivo* analysis of neuronal activity by two-photon imaging in mouse models of AD

Rationale

The hippocampus is a brain area that is of particular interest to many neuroscientists. It is a key player in the formation and maintenance of memory in healthy patients and major disruptions of the integrity of hippocampal circuits invariably lead to memory loss, independent of the underlying disease (Eichenbaum 2017, Scoville & Milner 1957, Vargha-Khadem et al 1997).

Even though AD pathology can affect the whole brain, the hippocampus is especially prone to be disrupted by the disease. Neuropathological and, more recently, imaging studies

in AD patients have revealed that the hippocampus highly susceptible to tangle formation and atrophy (Braak & Braak 1991, Devanand et al 2007), as well as amyloid plaque pathology (Thal et al 2002). Also, the loss of memory functions of AD patients is paralleled by marked functional hippocampal impairments in their brains (Sperling et al 2010, Zott et al 2018). The most striking aspect of hippocampal dysfunction in early AD stages is an increase in neuronal activity, which can be found in human AD patients as well as in mouse models of AD. Moreover, several studies in mice have revealed Aβ-dependent impairments of synaptic plasticity in the hippocampus of mice[6]. In consequence, I decided to perform the majority of my experiments in hippocampal neurons.

Methodology

My graduate work is largely based on previous observations of an Aβ-induced increase of baseline activity in wild-type and transgenic mice (Busche et al 2012, Busche et al 2008, Busche et al 2015a, Keskin et al 2017). Baseline activity of neuronal networks is induced by excitatory and inhibitory synaptic inputs. In consequence, neuronal baseline activity should be recorded under conditions which leave the network as intact as possible, such as *in vivo* two-photon Ca^{2+}-imaging. Unfortunately, the hippocampus is not accessible to classical two-photon imaging approaches, as, in mice, it is covered by more than 1 mm of neocortex and white matter (Mizrahi et al 2004). However, exposing the dorsal hippocampus by carefully removing the covering cortex makes it accessible to two-photon imaging (Busche et al 2012, Dombeck et al 2010, Kuga et al 2011). Even though it is rather invasive, this manipulation did not result in any structural or functional changes of hippocampal neurons, probably because the overlying cortex is not strongly connected to the hippocampus (Dombeck et al 2010). Due to the recent advancements in two- and three-photon imaging, proof of principle studies have recently reported that it is possible to record neuronal activity in the hippocampus without removing the cortex (Kondo et al 2017, Ouzounov et al 2017). It

[6] A more detailed introduction into Aβ-induced hippocampal pathology can be found in chapter 1.1.3.

remains to be shown whether these approaches will be widely applied in the near future. In my experiments, I chose to acutely remove the parts of the sensory cortex overlying the hippocampus without implanting a cortical window (**Fig. 8**). This approach allowed for pharmacological manipulations through the application of drugs in the bath solution or by pipette injection.

2 Methods

2.1 Mouse models

All experimental procedures were performed in compliance with institutional animal welfare guidelines and were explicitly approved by the local government. *In vivo* experiments were performed in male and female Bl/6 C57N mice, called wild-type mice in the following (Charles River, Wilmington, USA), at the age of 5-9 week or age-matched female APP23 x PS45 mice. This transgenic mouse line is derived from crossing APP23 mice with a PS45 line. The APP23 line expresses a humanized form of APP harboring the so-called Swedish mutation under the control of a Thy-1 promoter (Sturchler-Pierrat et al 1997). The regulation of the construct by the Thy-1 promoter leads to an overexpression of Aβ in pyramidal cells. The Swedish mutation is a double mutation in position 670 and 671 of the APP, which was discovered in a group of patients suffering from FAD in Sweden (Mullan et al 1992). It does not affect the sequence of amino-acids within the Aβ peptide but is located directly next to the site of β-secretase cleavage. As a result, APP is less frequently cleaved by α-secretase, which would lead to non-amyloidogenic products, and more regularly cleaved by BACE, thus increasing the production of Aβ (Haass et al 1995). The PS45 mouse line expresses the humanized PS1 protein with the G384A mutation under the Thy-1 promotor (Herzig et al 2004). This mutation was found to promote very early onset AD in two Belgian families (Martin et al 1991). Crossing these two mouse-lines led to early onset and rapid accumulation of soluble Aβ in the double-transgenic mice. At the age I used them (5-9 weeks), APP23 x PS45 mice were reported to have increased levels of soluble Aβ in the brain but no apparent amyloid plaques (Busche et al 2012).

Slice two-photon Ca^{2+} imaging experiments and electrophysiological experiments were performed in 10-25 days old wild-type mice of both sexes.

2.2 Surgery

For *in vivo* experiments, mice were initially anesthetized with Isoflurane (CP pharma, Burgdorf, Germany, 2% vol/vol in pure O_2). Preemptive analgesia was provided by the injection of 2% Xylocaine (AstraZeneca, Wedel, Germany, ca. 50µl) under the scalp and the subcutaneous application of metamizole (Bela-pharm, Vechta, Germany, 200 mg/kg bodyweight). After a waiting period of 10 min to allow for the analgesic treatment to take full effect, the mice were transferred to a heating plate and the temperature was maintained at 37.5 ± 0.5°C during the whole experiment. The scalp was partially removed and a custom-made plastic recording chamber with a central opening was attached to the skull using cyanoacrylic glue (UHU, Buhl-Baden, Germany). A stereotactic mouse brain atlas (Paxinos & Franklin 2012) was used to determine the coordinates of the hippocampal Cornu ammonis 1 (CA1) region (posterior to bregma: 2.5 mm, lateral from the midline: 2.2 mm) and the skull was thinned with a dental drill (Meisinger, Neuss, Germany) in a circle with a diameter of approximately 2 mm with the center at the identified coordinates. At this point, the recording chamber was filled with artificial cerebrospinal fluid (ACSF; 125 mM NaCl, 4.5 mM KCl, 26 mM $NaHCO_3$, 1.25 mM NaH_2PO_4, 2 mM $CaCl_2$, 1 mM $MgCl_2$, 20 mM glucose, pH 7.4, when bubbled with carbogen gas (95 % O_2 and 5 % CO_2)), which had been heated to 37°C. The bone was carefully removed with a thin cannula (30G, Braun, Kronberg, Germany) to open a cranial window directly above CA1. In hippocampal Ca^{2+}-imaging experiments, the dura was removed using fine forceps (Fine Science Tools, Heidelberg, Germany) After this, the cortical tissue covering the hippocampus was removed by suction and the ensuing bleeding was stopped by continuous rinsing with ACSF. To stain the CA1 pyramidal cells, multi-cell bolus loading was performed as previously described (Stosiek et al 2003). The

organic Ca^{2+}-indicator Cal-520 AM (Tada et al 2014) (AAT Bioquest, USA) was pre-diluted in dimethyl sulfoxide (DMSO) containing 20 % Pluronic F-127 (Life technology, Carlsbad, USA) and vortexed at 1000 RPM for 60 seconds. This dye-containing solution was then diluted with Ca^{2+} free ACSF to a final concentration of 0.5-1 mM. Patch-electrodes were pulled using a vertical puller (Narishige, Japan) to have a tip resistance of 2-3MΩ. The diluted Cal-520 solution was filled into one of these pipettes and the tip was carefully lowered into the hippocampal tissue to a depth of 200 µm, using a micro-manipulator (Luigs & Neumann, Ratingen, Germany). The back end of the pipette was connected to a picospritzer II (General Valve Co. Fairfield, USA) and the Ca^{2+}-indicator was pressure-injected (60 sec, 600 mBar) into the hippocampus. To stabilize the preparation, a small drop of heated agarose (2%, 37°C) was carefully placed on the hippocampal surface. After the surgery was completed, the concentration of Isoflurane was reduced to 0.6 to 0.8% vol/vol. Cortical recordings were performed in the primary visual cortex (V1) in a similar manner as the hippocampal recordings. The stereotactic coordinates for V1 were identified as 3.8 mm caudal of bregma and 2.2 mm lateral to midline. The skull was removed exactly as described above, but the dura and cortical tissue were left intact. Cal-520 AM was diluted and pressure-injected as described at the depth of 200 µm for recordings in cortical layer 2/3 and at 550 µm for imaging layer 5.

2.3 *In vitro* hippocampal slice preparation and staining

The mice were anesthetized by the inhalation of CO_2 and subsequently decapitated. The brain was surgically removed and submerged in ice-cold slicing solution (24.7 mM glucose, 2.48 mM KCl, 65.47 mM NaCl, 25.98 mM $NaHCO_3$, 105 mM sucrose, 0.5 mM $CaCl_2$, 7 mM $MgCl_2$, 1.25 mM NaH_2PO_4, and 1.7 mM ascorbic acid) with an osmolarity of 290-300 mOsm and a pH of 7.4, which was stabilized by bubbling with carbogen gas. The brain was then glued onto a metal plate and horizontal slices (300 µm thickness) were cut using a vibratome

(VT1200S; Leica, Wetzlar, Germany). The slices were allowed to recover at room temperature for at least one hour in a recovering solution containing 2 mM $CaCl_2$, 12.5 mM glucose, 2.5 mM KCl, 2 mM $MgCl_2$, 119 mM NaCl, 26 mM $NaHCO_3$, 1.25 mM NaH_2PO_4, 2 mM thiourea (Sigma, St. louis, USA), 5 mM Na-ascorbate (Sigma), 3 mM Na-pyruvate (Sigma), and 1 mM glutathion monoethyl ester (Santa Cruz Biotechnology, Dallas, U.S.A). The pH value was adjusted to 7.4 with HCl, and the osmolality was 290 mOsm. Before the experiment, the slices were transferred into the recording setup and superfused with ACSF. For Ca^{2+}-imaging experiments, Cal-520 AM was injected into the hippocampal CA1 area as described above.

2.4 Two-photon calcium imaging

In vivo and *in vitro* two-photon Ca^{2+}-imaging was performed in a custom-made multi-photon recording setup. Two-photon excitation was provided by a Coherent Chameleon tunable Ti:sapphire laser with a pulse-width of 75 fs and a pulse repetition rate of 80 MHz. The laser-power was adjusted using a pockel-cell (Conoptics, Danbury, USA). The scanning unit for x-y scanning was a custom-built galvo-resonance scanner combination with an 8 kHz line-rate, which was fixed to an upright microscope (BX51W; Olympus, Shinjuku, Japan). The laser-beam was focused by a 40x 0.8 NA water-immersion objective with a working distance of 1.2 mm (Nikon, Tokyo, Japan). This setup allowed for imaging relatively large fields of view of up to 300 µm x 300 µm at a frame rate of 40 Hz and a resolution of 400 x 400 pixels. The emitted fluorescence was reflected by a beam-splitter and detected by a hybrid-photomultiplier tube (Hamamatsu, Japan). Image acquisition was performed using custom-written software based on LabVIEW (National instruments, Austin, USA) and the data was stored for offline-analysis.

2.5 Targeted application of synthetic Aβ dimers

Where not specified otherwise, synthetically produced Aβ dimers were used. These were produced by replacing the Serine in position 26 of the human Aβ1-40 peptide by a Cysteine. After oxidation, two of these mutated peptides form a disulfide bond between their respective cysteine residues and thus dimerize the two Aβ peptides (Shankar et al 2008). Aβ1-40 S26C dimers were purchased from JPT (Berlin, Germany), dissolved in DMSO and stored at -20°C. Immediately before the experiment, the Aβ containing solution was thawed and dissolved with ACSF to a final concentration of 500 nM. This solution was then filled into a glass patch pipette and directly pressure-applied to the hippocampal cells (300 mBar, 30 sec) as previously described (Busche et al 2012). In some experiments, Aβ containing ACSF was directly superfused over the brain slice.

2.6 Targeted application of human Aβ preparations

Human brain extracts were a gift from Dominic Walsh. They were obtained from the brain of a patient with sporadic AD as previously described (Hong et al 2018, Jin et al 2018). After death, a piece of cortical gray matter was cut into small pieces and dissolved in ACSF containing protease inhibitors (Hong et al 2018). The tissue was homogenized using a Dounce homogenizer (Fisher, Ottawa, Canada) and spun for 110 min in a centrifuge (Beckman Coulter, Fullerton, USA). The supernatant was divided in two portions, one of which was treated with the anti-Aβ antibody AW7 to immunodeplete Aβ (ID extract). The other half was mock- immunodepleted without removing Aβ (AD extraxt). After ID or mock ID, the samples contained 32.66 ng/ml Aβx-42 or 1.72 ng/ml Aβx-42 respectively. Immediately before the experiment, the samples were thawed and diluted 1:10 in ACSF. This solution was filled into a glass patch pipette and directly pressure-applied to the hippocampal cells (300 mBar, 30 sec).

Human brain-derived monomers and dimers were a gift from Dominic Walsh. In order to obtain a sufficient amount of Aβ dimers from human tissues, amyloid plaques were dissolved in formic acid and the Aβ was separated according to its molecular weight. The fractions used in this study contained either monomers or dimers as confirmed by mass spectrometry (Dominic Walsh, personal communication). The samples were dissolved in ammonium bicarbonate-containing ACSF at a concentration of 1 µg/ml and stored at -80°C. It is not possible to calculate the exact molar concentration of Aβ for this solution as it contains a mix of different species of various sizes. However, most of these species have similar molar weights (~4 kDa for monomers and ~7 kDa for dimers). Thus, a rough estimation can be made. Accordingly, the undiluted 1 µg/ml monomer or dimer solutions contained about 250 nM of monomer or 143 nM of dimers, respectively, with unknown but lower concentrations of different subspecies. Immediately before the experiment, the aliquots were thawed and diluted 1:5, 1:20, 1:50 or 1:200 in ACSF. This solution was then filled into a glass patch pipette and directly pressure-applied to the hippocampal cells (300 mBar, 30 sec).

2.7 Pharmacologal experiments

For pharmacological experiments, the following substances were used:

Name	Aim	Concentration	Source	Application
Bicuculline	$GABA_A$ receptor blocker	10-100 µM	Enzo (BML-EA1090050)	Bath
CNQX	AMPAR blocker	50 µM	Tocris (0190)	Bath/pipette
D-AP5	NMDAR blocker	50 µM	Abcam (Ab120003)	Bath/pipette
DL-TBOA (= TBOA)	Inhibitor of EAATs	2.5-250 µM	Tocris (1223)	Bath/pipette
L-Glutamic acid	Glutamate	40-80µM	Sigma (G12521)	Bath
Glutathione monoethyl ester	Antioxidant for slice preservation	1 mM	Santa Cruz (SC-203974)	Bath
Gyki53655	AMPA receptor blocker	10 µM	Tocris (2555)	Bath
Tetrodotoxin citrate (TTX)	Voltage gated Na^+ channel blocker	1 µM	Abcam (Ab120055)	Bath

Table 1: List of drugs and reagents

Bath and/or pipette application was performed as indicated in **Table 1**. The drugs were dissolved in water or DMSO and stored at -20°C. Immediately before the experiments, the aliquots were thawed and the drug was dissolved in ACSF as indicated above. In pipette application experiments, the drug was filled into a glass patch pipette (tip resistance 2-3 MΩ), which was carefully lowered into the brain or the hippocampal slice and maneuvered into the center of the field of view. After a baseline recording with the pipette in place, the drug was the carefully pressure applied (300 mBar, 30 sec) into the brain while monitoring the neuronal activity. After a washout period of 5-10 minutes, another recording was made while the pipette was left in place. For bath-applications, the drug was dissolved in ACSF, which was superfused over the brain or the hippocampal slice after performing several recordings at baseline conditions. Another series of recordings was started after the drug-containing solution had perfused the surface for several minutes.

2.8 Electrophysiological recordings

For electrophysiological recordings, hippocampal slices were prepared as described in chapter 2.3. Individual slices were transferred to the recording setup and perfused with ACSF containing 10 µM bicuculline (Enzo, U.S.A) to block $GABA_A$ receptor-mediated synaptic transmission. In NMDAR-EPSC experiments, 10 µM GYKI53655 (Tocris, United Kingdom) was additionally dissolved in the ACSF to block AMPA receptors. To minimize recurrent excitation, the Schaffer collaterals between CA3 and CA1 were cut using a razor blade. An upright light microscope was used to identify CA1 pyramidal neurons, which were carefully approached by a glass pipette with a tip resistance of approximately 7MΩ connected to an EPC 9/2 patch-clamp amplifier (HEKA, Germany). The patch pipette was filled with an internal solution containing 122.5 mM cesium gluconate, 5 mM HEPES, 10 mM cesium BAPTA, 6 mM $MgCl_2$, and 10 mM phosphocreatine at a pH of 7.2, adjusted with gluconic acid (Arnth-Jensen et al 2002). Whole-cell patch clamp recordings were performed and in NMDAR-EPSC experiments,

the membrane potential was held at +40 mV, without correcting for liquid junction potentials. In PPF experiments, the cell was not depolarized.

A second glass electrode (5-7 MΩ) filled with 2 M NaCl was used to elicit synaptic responses in 5 second intervals (NMDAR-EPSC) or two pulses with inter-pulse intervals of 30-500 msec (PPF experiments). The pulse amplitude was adjusted to approximately twice the value that gave the smallest synaptic response, typically around 10 V and the pulse-length was 100 µsec. After recording baseline data, Aβ (500 nM) or TBOA (2.5, 5, 10 or 25 µM) were applied in the bath solution and the recording was repeated after several minutes of superfusion of the drug. The data was collected with PULSE software (HEKA) at 10 kHz, Bessel-filtered at 2.9 kHz and stored for offline analysis.

2.9 Data analysis

Ca^{2+}-traces were extracted from the imaging data using custom-written software based on LabVIEW (Jia et al 2010). Neurons were visually identified according to their morphology and regions of interest (ROIs) were drawn around their somata. Astrocytes were excluded from the analysis due to their morphology and their high fluorescence levels (Nimmerjahn & Helmchen 2012). The Ca^{2+} fluorescence of each ROI over time was extracted and low-pass filtered (cutoff frequency 10 Hz). The relative fluorescence was then calculated as $\Delta F(t) = (F_1(t)-F_0)/F_0$, with $F_1(t)$ being the measured fluorescence at time point t and F_0 being the baseline fluorescence. These traces were analyzed with Igor Pro (Wavemetrics, Lake Oswego, USA) and Matlab (Mathworks, Natick, USA). Fluorescence changes were accepted as neuronal Ca^{2+}-transients if their peak amplitude was three times larger than the standard deviation of the noise band. In drug application experiments, only cells that were visible in the field of view during baseline, drug application and washout were analyzed. The area under the curve (AUC) was calculated for individual Ca^{2+}-traces using a custom-written Matlab algorithm. $\Delta_{activity}$ was calculated as the number of Ca^{2+}-transients per minute during

the application of Aβ or TBOA minus the number of Ca^{2+}-transients during baseline conditions:

$$\Delta_{activity} = Ca^{2+}\text{-transients}_{A\beta} - Ca^{2+}\text{-transients}_{Baseline}$$

The application-dependent activity was considered to be increased if $\Delta_{activity}$ was larger than +1 and decreased if it was smaller than -1. The normalized change of activity was calculated for each mouse or slice separately. The mean frequency of Ca^{2+}-transients during drug or Aβ application was divided by the number of Ca^{2+}-transients/min during baseline conditions and is indicated as "Ca^{2+}-transients (normalized)" in the figures.

The electrophysiological data was analyzed using Igor Pro software (WaveMetrics, U.S.A). Statistical analysis was performed with Matlab. The full width at half maximum (FWHM) of NMDAR-EPSCs was measured manually. The decay time was fitted as a bi-exponential fit with a fast component τ_1 and a slow component τ_2 and $\tau_{weighted}$ was calculated as previously described (Ferreira et al 2017, Stocca & Vicini 1998):

$$\tau_w = (A_1\tau_1 + A_2\tau_2)/(A_1 + A_2)$$

A_1 and A_2 were the amplitudes of the first and second decay components, respectively. The PPR was calculated as PPR = A_{P2}/A_{P1} where A_{P1} and A_{P2} were the amplitude of the first and the second EPSC, respectively.

2.10 Statistical analysis

All statistical tests were performed in Matlab. Wilcoxon signed-rank test, Wilcoxon rank sum test or Kolmogorov-Smirnov Test were used as indicated and multiple comparison testing was employed where appropriate. Linear regression analysis was performed with Matlab. p-values of < 0.05 were considered to be statistically significant. N corresponds to the number of mice in *in vivo* experiments or the number of slices in *in vitro* experiments, while n corresponds to the number of cells. Average values are indicated as mean ± SEM.

3 Results

The goal of my graduate work was to explore the basic mechanisms underlying Aβ-induced neuronal dysfunctions. In this study, I employed *in vivo* and *in vitro* two-photon imaging to investigate neuronal hyperactivity in mouse models of AD and after the targeted injection of Aβ in wild-type mice. Additionally, I used intracellular electrophysiology to determine the effect of Aβ on synaptic transmission. These experiments were performed in the hippocampal CA1 region or the neocortex.

3.1 Soluble Aβ dimers induce neuronal hyperactivity in the hippocampal CA1 region

As a first step, I characterized the previously described Aβ-dependent neuronal hyperactivity in the hippocampal CA1 region *in vivo* (Busche et al 2012). To this end, I adapted an *in vivo* two-photon Ca^{2+}-imaging approach that had previously been developed in the Konnerth laboratory (Busche et al 2012). In mice, the hippocampal CA1 region is not accessible to standard two-photon microscopy (Helmchen & Denk 2005) because it is covered in large parts by the somatosensory cortex, which is more than one millimeter thick (Paxinos & Franklin 2012). Therefore, the overlying cortical tissue had to be carefully removed before bolus loading of the Ca^{2+}-indicator Cal-520 AM into the hippocampus (Stosiek et al 2003, Tada et al 2014). The imaging plane was adjusted to the pyramidal layer 100-150 µm below the hippocampal surface, which is densely packed with glutamatergic excitatory neurons (Bliss 2007). Two-photon imaging was performed at a framerate of 40 Hz and a wavelength of 920 nm under anesthesia with low levels of isoflurane (**Fig. 8 A**). 30 to 60 minutes after bolus loading, the neurons were clearly visible as round or ellipsoid structures with sharp edges and characterized by their typical fluorescence pattern: higher fluorescence intensities

around the edges and lower fluorescence intensities in the center (**Fig. 8 B**). In line with earlier work from the Konnerth lab (Busche et al 2012, Stosiek et al 2003), I did not observe any voids of fluorescence, which would be indicative of unlabeled cells. Astrocytes, which are also labelled by organic Ca^{2+}-indicators (Nimmerjahn & Helmchen 2012), were rarely found in the pyramidal layer and excluded from the analysis according to their irregular shape and high brightness. For drug applications, I placed the tip of a patch pipette in the center of the field of view. Using this methodology, I was able to detect Ca^{2+}-transients in individual neurons as a change of the fluorescence intensity (**Fig. 8 C**) and to determine the neuronal activity status for all recorded cells before, during and after drug application.

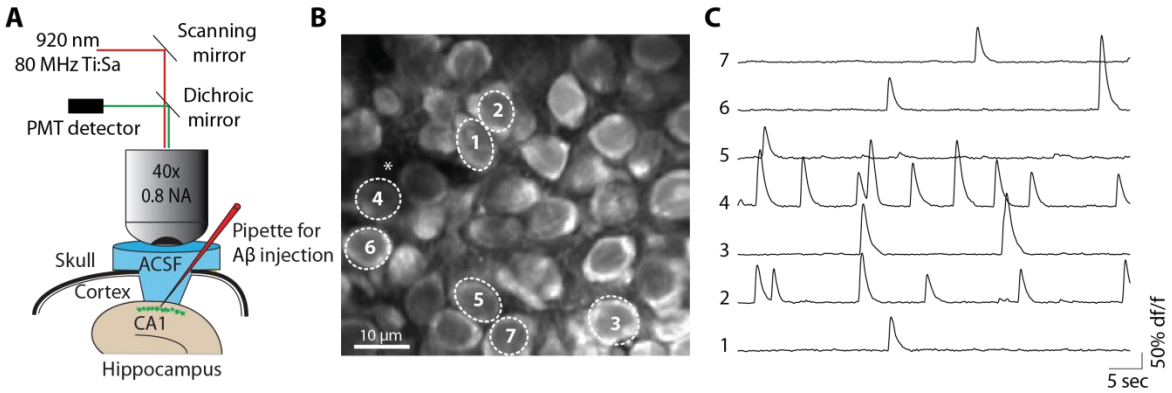

Fig. 8: *In vivo* two-photon Ca^{2+}-imaging in the hippocampal CA1 region of an anesthetized wild-type mouse. *A)* Two-photon imaging setup. *B)* Representative example of a two-photon image from the CA1 pyramidal layer of an anesthetized wild-type mouse. Asterisk: shadow of the injection pipette. *C)* Representative Ca^{2+}-traces from seven neurons (cycled in *B*).

Once I could reliably record neuronal activity in the CA1 region *in vivo*, I replicated earlier findings from the Konnerth laboratory demonstrating that the application of soluble Aβ induces neuronal hyperactivity in hippocampal CA1 neurons (Busche et al 2012). The Aβ preparation used in this study was the synthetic S26C dimer (Shankar et al 2008). I filled a glass patch pipette with a tip resistance of 2-3 MΩ with 500 nM of S26C dimer dissolved in ACSF and carefully lowered it into the hippocampus at an angle of about 45°. The Aβ-containing solution was then carefully pressure-applied (5-7 psi) to the extracellular space for

30 seconds (**Fig. 9**). In accordance with the findings from (Busche et al 2012), the application of Aβ robustly increased the neuronal activity, as detected by an increased frequency of Ca^{2+}-transients (**Fig. 9 B**, N = 7 mice, p = 0.016). The increase in activity was almost immediate and lasted longer than the application itself (**Fig. 9 A**). After a washout period of five to ten minutes, however, the neuronal activity had returned to baseline levels (Aβ vs. WO p = 0.0156; BL vs. WO p = 0.69) (**Fig. 9 B**).

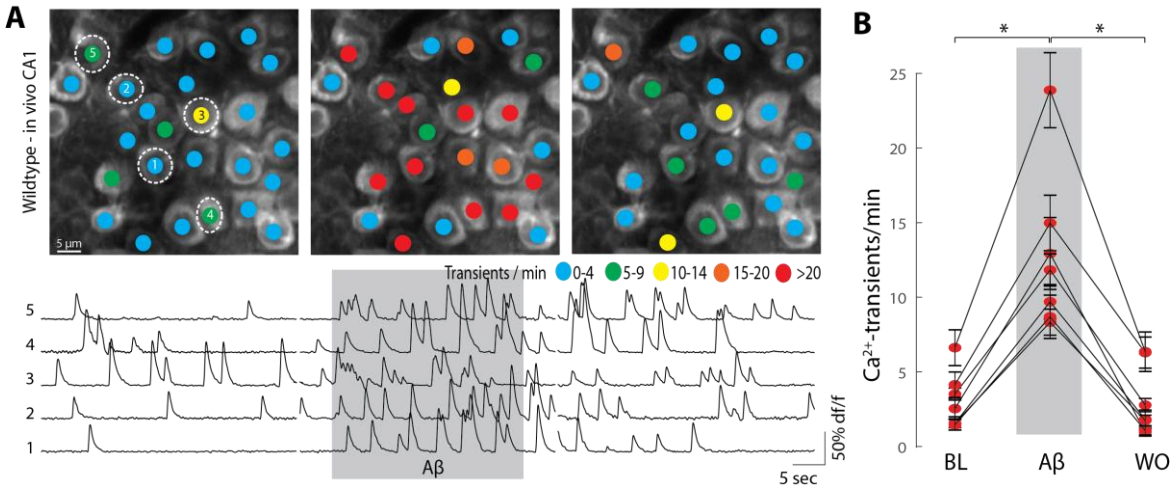

Fig. 9: Aβ dimers induce neuronal hyperactivity *in vivo*. *A)* Top: representative two-photon image of the hippocampal CA1 region of a wild-type mouse for baseline (left), Aβ application (middle) and washout (right) conditions. The colored dots on the neurons represent the number of Ca^{2+}-transients per minute. Bottom: Ca^{2+}-traces for the circled neurons. The grey shaded area represents the time of Aβ application. *B)* Summary data for N = 7 mice. Each dot represents the mean number of Ca^{2+}-transients per minute for all neurons in one mouse under baseline (BL), Aβ application and washout (WO) conditions. Error bars denote SEM, * $p < 0.05$, Wilcoxon signed rank test

To ensure that the hyperactivity-inducing effect was specific to Aβ dimers as opposed to a pressure-induced artifact or an unspecific effect of the application of large peptides, I next performed a series of control experiments, in which the dimers were heat-denatured (95°C for 30 minutes) and applied using the protocol described above. The application of 500 nM of the denatured dimers had no effect on the neuronal activity (**Fig. 10 A**, N = 5, p = 0.63). To enable a direct comparison between the applications of different substances, I calculated the number of Ca^{2+}-transients during the application normalized to baseline conditions for each

mouse (**Fig. 10 B**). The application of Aβ increased the number of Ca^{2+}-transients almost fivefold (4.8 ± 1.2), while the frequency of Ca^{2+}-transients was unchanged for denatured Aβ (1.2 ± 0.35). In consequence, the difference between the application of native and denatured dimers was highly significant (p = 0.0025).

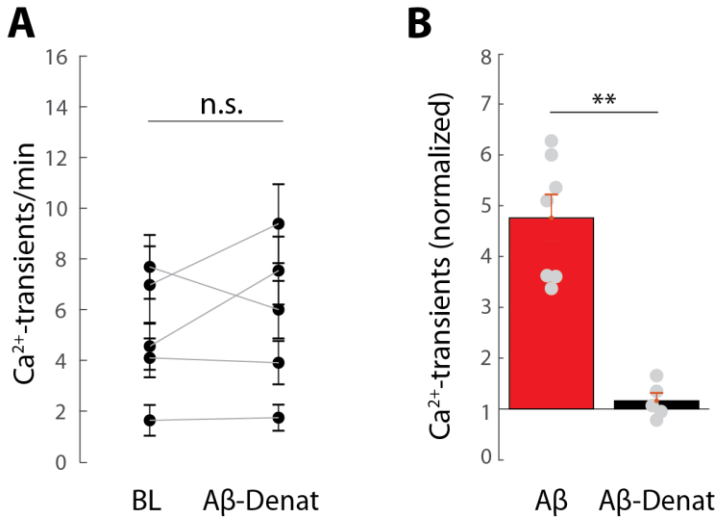

Fig. 10: Denatured Aβ dimers do not induce neuronal hyperactivity *in vivo*. *A)* Ca^{2+}-transients/min under baseline conditions and during the application of denatured Aβ dimers. Each dot represents the mean number of Ca^{2+}-transients per minute for all neurons in one mouse under baseline (BL) and denatured Aβ application conditions (N = 5). *B)* Normalized change of activity for the application of Aβ (left, N = 7) and denatured Aβ (right, N = 5). Each dot represents the mean number of Ca^{2+} transients, normalized to baseline, from one mouse. n.s. not significant ** p < 0.005, Wilcoxon signed rank test (*A*) or Wilcoxon rank sum test (*B*). Error bars denote SEM

Next, I analyzed the effect of Aβ on the activity of each neuron on a single-cell level. Accordingly, I calculated the difference of activity $\Delta_{activity}$ between baseline and Aβ application conditions[7]. Remarkably, the application of Aβ increased the activity in the vast majority of cells (**Fig. 11 A**, 89%, 220/248 cells), while only a small number of cells decreased their activity (3%, 8/248 cells) or remained unchanged (8%, 20/248 cells). The median change of activity was 8 transients/min (**Fig. 11 A**). Because $\Delta_{activity}$ was distributed over a wide range of values from -5 to +33 transients/min, I next asked what caused this variability. One possible explanation was that the Aβ-induced change of activity was dependent on the

[7] A description of how $\Delta_{activity}$ was calculated can be found in the methods section.

baseline activity level of the respective neuron. To test this hypothesis, $\Delta_{activity}$ was plotted as a function of the number of Ca^{2+}-transients at baseline (**Fig. 11 B**). Because $\Delta_{activity}$ was higher for increased levels of baseline activity, I performed a linear regression analysis (**Fig. 11 C**), which revealed a strong dependence of the Aβ-induced $\Delta_{activity}$ on the number of Ca^{2+}-transients at baseline (R^2 = 0.90). Thus, I concluded that Aβ increases the activity in almost all neurons, but the magnitude of the increase depends on the preceding baseline activity of the respective neuron.

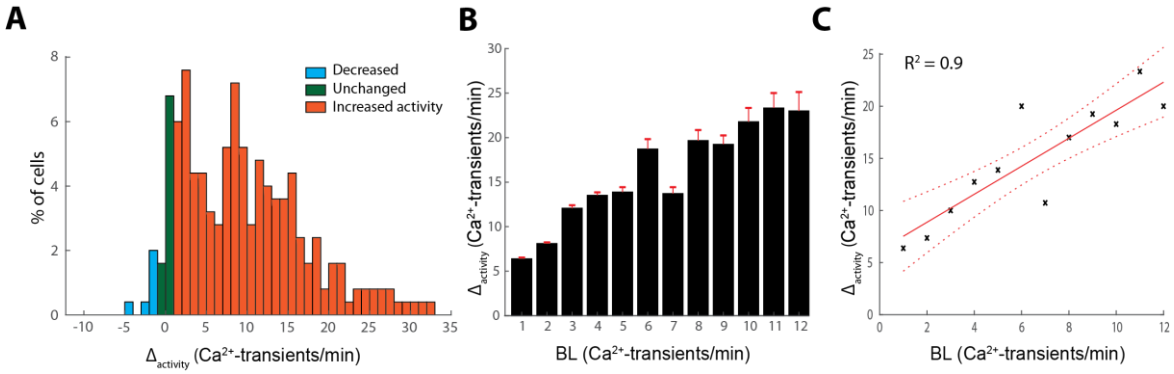

Fig. 11: Analysis of the Aβ-induced neuronal hyperactivity *in vivo*. *A)* Histogram of the difference in activity between Aβ application and baseline conditions ($\Delta_{activity}$) for n = 248 cells. *B* and *C)* Bar graph (*B*) and linear regression (*C*) of the average difference of activity ($\Delta_{activity}$) compared to baseline (BL) activity.

An especially noteworthy finding of these experiments is that the effect of Aβ could be observed almost instantaneously. To determine the time-course of the Aβ-dependent hyperactivity, I calculated the area under the curve (AUC) for each neuron in one-second bins (**Fig. 12 A**). This is a good approximation of neuronal activity since the AUC faithfully tracked all neuronal Ca^{2+}-transients. Furthermore, I found that the AUC strongly depended the number of Ca^{2+}-transients on a single cell level for all conditions (baseline, Aβ application and washout), as illustrated for a representative mouse in **Fig. 12 B** (R^2 = 0.81). Due to the strong linear correlation between the number of Ca^{2+}-transients and the AUC, the normalized average AUC was calculated for all 248 neurons in one-second bins and plotted against the

time (**Fig. 12 C**). This analysis revealed that the neuronal activity rises immediately after the beginning of the Aβ injection. In fact, the AUC was already increased in the first one-second bin after the onset of application, stayed elevated during the whole application period and beyond. After the five- to ten-minute washout period, the AUC had returned to baseline (**Fig. 12 C**).

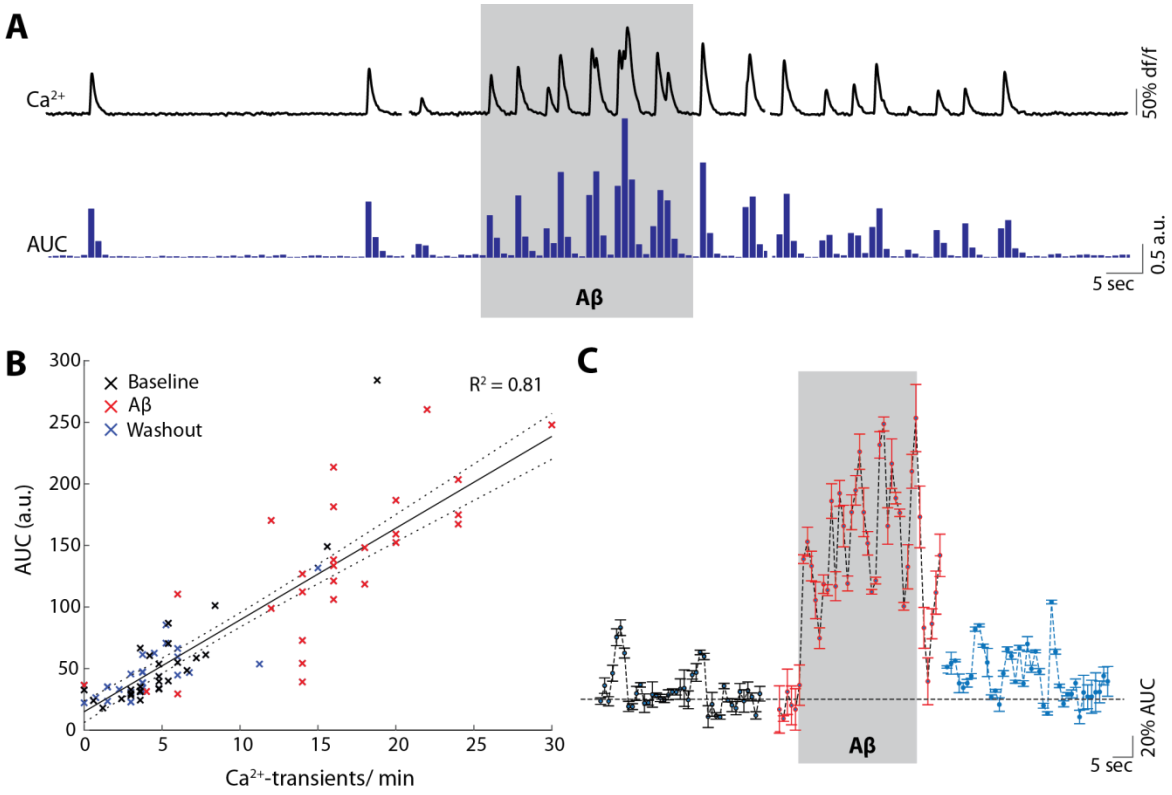

Fig. 12: Aβ application rapidly induces neuronal hyperactivity. *A)* Ca^{2+}-trace and calculated AUC of the Ca^{2+}-trace in one-second bins (bottom) for a representative neuron under baseline (left), Aβ application (middle) and washout (right) conditions. The grey shaded area represents the time of Aβ application. *B)* Linear regression analysis of the number of Ca^{2+}-transients/min and the AUC for all neurons of one mouse for baseline (black), Aβ application (red) and washout (blue) conditions (R^2 = 0.81). *C)* Averaged AUC in one-second bins normalized to baseline for all 248 cells from N = 7 mice for baseline (left), Aβ application (middle) and washout (right) conditions. The grey shaded area represents the time of Aβ application. a.u. arbitrary units. Error bars denote SEM

3.2 The Aβ effect critically depends on the levels of the preceding baseline activity

Subsequently, I performed a series of *in vivo* and *in vitro* experiments to further investigate the observation that the Aβ-induced change in activity depended on the number of Ca^{2+}-traces at baseline on a single-cell level.

3.2.1 Surprisingly, Aβ does not induce neuronal hyperactivity *in vitro*

In the next set of experiments, I worked together with Manuel Simon, a MD-student in the Konnerth laboratory, to investigate whether Aβ could also induce neuronal hyperactivity in hippocampal slices. We wanted to perform the experiments in acute slices, because they are more accessible to pharmacological manipulations than *in vivo* preparations. The neurons were stained with bolus loading of Cal-520 AM, just like in the *in vivo* experiments and the slice was placed under a two-photon microscope (**Fig. 13**). We applied Aβ as described before for the *in vivo* experiments, that is, we carefully pressure applied 500 nM Aβ S26C dimer for 30 seconds through a patch pipette, which was placed in the center of the field of view. Remarkably, Aβ application did not induce neuronal hyperactivity in these hippocampal slices (**Fig. 14**, p = 0.55, N = 9). This puzzling finding could likely be explained by a difference between the *in vivo* and the *in vitro* slice conditions, since the groups of neurons from the same brain area became hyperactivated after Aβ application *in vivo* but not *in vitro*. One of the obvious differences between the two conditions is the level of spontaneous baseline activity. Neurons in the hippocampus are highly active *in vivo* (Kamondi et al 1998), even under isoflurane anesthesia (Busche et al 2012, Hudetz et al 2011), while neuronal network activity usually breaks down after slice preparation because excitatory afferent connections get severed (Hájos et al 2009). In fact, in our hands, the baseline activity *in vivo* (N = 7) was much higher than in slices (N = 9, p = 0.00019), where it was virtually absent (**Fig. 15 A**).

Moreover, the distribution of activity was highly different and revealed a shift towards lower levels across the whole frequency spectrum in slices compared to *in vivo* conditions (**Fig. 15 B**, $p < 0.0001$, n = 248 for *in vivo* and n = 217 for *in vitro* conditions,).

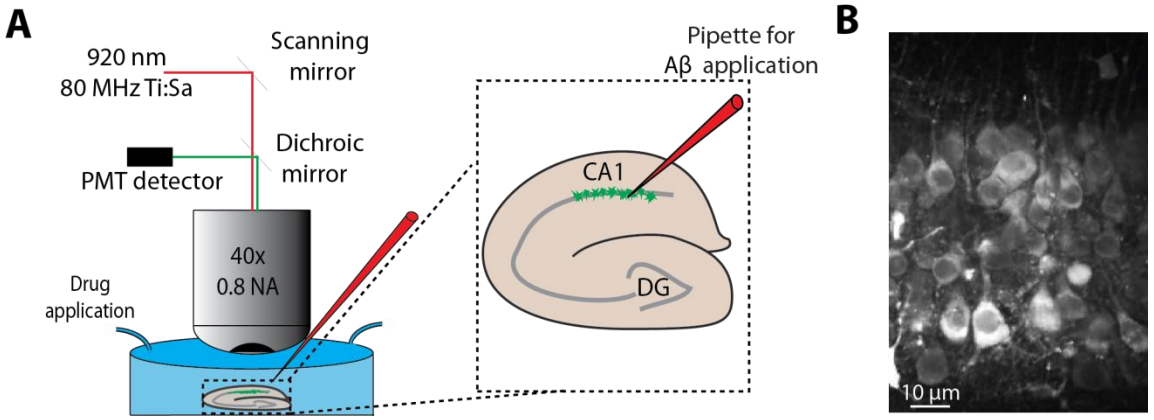

Fig. 13: Two-photon imaging of neuronal activity in acute hippocampal slices. *A)* Hippocampal slice recording setup. The hippocampal CA1 neurons were stained with Cal-520 (inset, green). *B)* Representative two-photon image of the hippocampal CA1 area of an acute hippocampal slice.

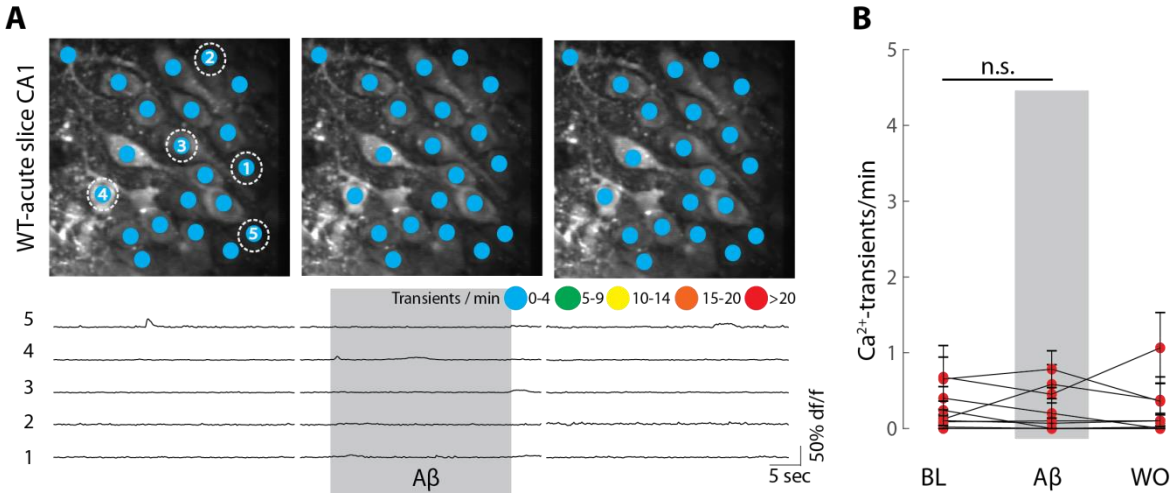

Fig. 14: Aβ application does not induce neuronal hyperactivity in hippocampal CA1 slices. A) Top: representative two-photon image of the CA1 region in a hippocampal slice from a wild-type mouse for baseline (left) Aβ application (middle) and washout (right) conditions. The colored dots on the neurons represent the number of Ca^{2+}-transients per minute. *Bottom:* Ca^{2+}-traces of the circled neurons. The grey shaded area represents the time of Aβ application. B) Summary data for N = 9 slices. Each dot represents the mean number of Ca^{2+}-transients per minute for all neurons in one slice under baseline (BL), Aβ application and washout (WO) conditions. Error bars denote SEM. n.s. not significant, Wilcoxon signed rank test

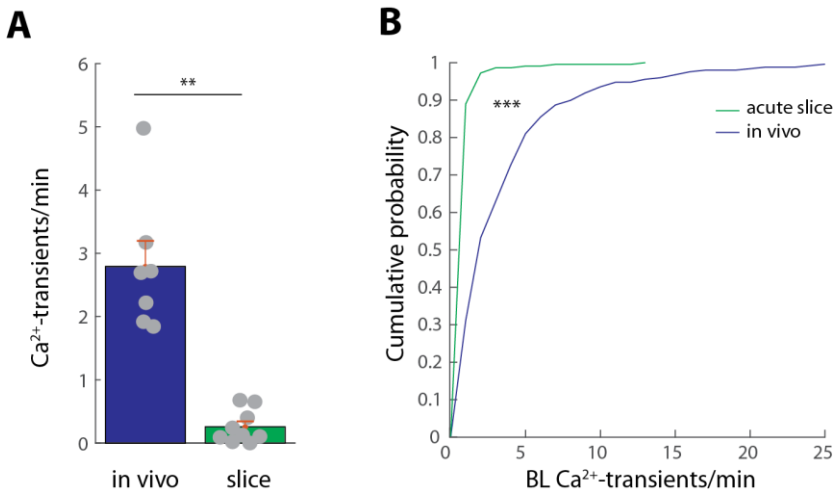

Fig. 15: Hippocampal CA1 baseline activity is lower in slices than *in vivo*. *A)* Comparison of the average baseline activity in the hippocampal CA1 region *in vivo* (N=7) and in acute hippocampal slices (N = 9). ** $p < 0.005$, Wilcoxon rank sum test. *B)* Cumulative distributions of spontaneous Ca^{2+}-transients of hippocampal CA1 neurons *in vivo* (n = 248) and in slices (n = 217). *** $p < 0.0001$, Kolmogorov-Smirnov test. Error bars denote SEM

3.2.2 Inducing neuronal baseline activity in hippocampal slices makes them susceptible to Aβ-induced neuronal hyperactivity

In order to examine whether the occurrence of baseline activity is sufficient to make CA1 neurons susceptible to Aβ-induced hyperactivity, we next tested several protocols to induce baseline activity in hippocampal slices. Since the slices in our preparation were submerged in an ACSF bath, it was possible to change the ion composition of the ACSF and add drugs to the bath while monitoring the neuronal activity by two-photon microscopy. Thus, in a first set of experiment, we carefully increased the extracellular potassium (K^+) concentration, a manipulation which is known to induce neuronal activity by shifting the membrane potential towards depolarization (Somjen 1979). This method is also often used to study epilepsy in the hippocampus (Jensen & Yaari 1997, Traynelis & Dingledine 1988). By careful titration of the extracellular potassium level for each slice individually, we were able to induce sparse neuronal activity in the slices, which was reminiscent of the baseline activity *in vivo* without triggering epileptiform activity (**Fig. 16 A-C**). This effect could typically be achieved at

extracellular potassium concentrations of 6.5 to 8 mM (N = 7). In a second set of experiments, we dissolved low concentrations of glutamate in the ACSF in order to induce neuronal activity by an increase in the excitatory input (Herman & Jahr 2007) . Indeed, an extracellular glutamate concentration of 40-60 µM induced sparse neuronal activity in hippocampal slices (N = 9). In a third approach, we applied high doses (60-80µM) of the $GABA_A$ receptor antagonist bicuculline in the ACSF to fully block GABAergic transmission. In these slices, we cut the Schaffer collateral pathway (Barnes et al 1997) to prevent the occurrence of bicuculline-induced seizures (Williamson & Wheal 1992). Since bicuculline application was not sufficient to induce neuronal activity in some slices, we then slowly increased the extracellular potassium levels, until we detected neuronal hyperactivity by two-photon Ca^{2+}-imaging (typically at 5.5 to 6.5 mM). All three manipulations significantly increased the neuronal activity in the slices (**Fig. 16 D**, ACSF vs. K^+: p = 0.018; ACSF vs. Glu: p = 0.0052; ACSF vs. BIC: p = 0.0017) to levels observed *in vivo* under baseline conditions (p = 1 for all three groups vs. *in vivo* baseline activity).

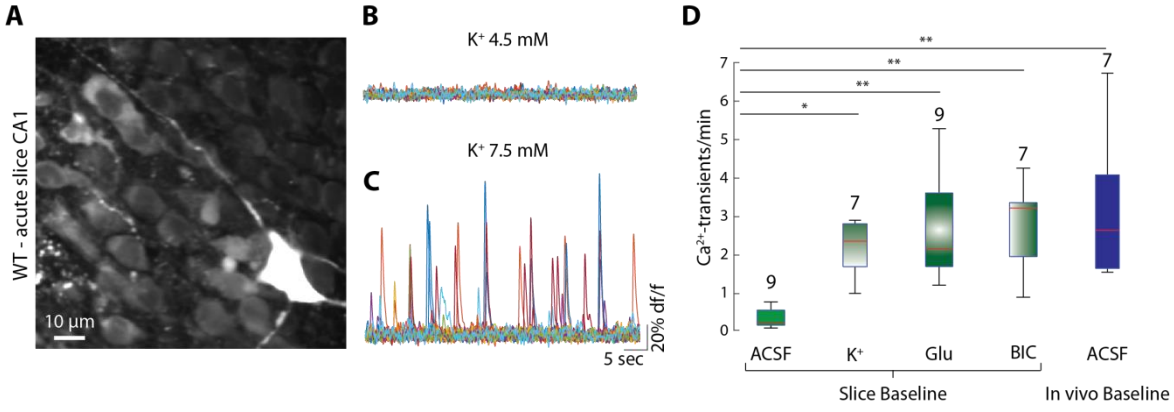

Fig. 16: Induction of baseline activity in acute hippocampal slices. *A)* representative two-photon image of a slice imaged under baseline conditions. The asterisk indicates an Astrocyte. *B)* Overlay of the Ca^{2+}-traces of all neurons identified in the slice in *A*, superfused with standard ACSF (n = 34). *C)* Same as in *B*, but during the superfusion of high- K^+ ACSF. *D)* Boxplot of the average baseline activities in under different conditions. The N-numbers for each experiment are indicated over the respective boxes. *p<0.05, **p<0.005, Kruskal Wallis test with Dunn-Sidak post-hoc comparison

Once we were able to induce stable levels of neuronal baseline activity in hippocampal slices, we returned to applying Aβ in those preparations. Remarkably, Aβ application reliably triggered hyperactivity under these conditions. We first demonstrated this in slices in which the activity had been increased by blocking GABAergic receptors and increasing extracellular potassium (**Fig. 17 A**). Just like under *in vivo* conditions (**Fig. 9**), Aβ increased neuronal activity (normalized activity: 2.9 ± 0.34) in all recorded slices (**Fig. 17 B**, N = 7, p = 0.016). After a washout period of five to ten minutes, the activity had returned to baseline levels (Aβ vs. WO p = 0.016; BL vs. WO p = 1). It is important to note, that in order to avoid concentration gradients between the solution in the ACSF bath and the solution puffed out from the pipette, Aβ was dissolved in the same ACSF containing bicuculline and increased levels of potassium that also superfused the respective slice. Thus, in control experiments, the vehicle solution was pressure applied onto the CA1 to ensure that the effect of the Aβ application was not an artifact of the application or the composition of the vehicle solution (**Fig. 18 A**). As expected, applying the vehicle solution did not increase neuronal activity (0.99 ± 0.06, N = 6) and the effect was significantly different from the application of the Aβ-containing vehicle (p = 0.0012). Since we had observed an activity-dependence of the Aβ-induced action on a single-cell level under *in vivo* conditions (**Fig. 11**), we next tested, whether this was also true for the slice conditions. Indeed, linear regression analysis, revealed a strong dependence of the Aβ-induced activity on the baseline activity (**Fig. 18 B,** R^2 = 0.78). The fact that Aβ could induce neuronal hyperactivity when high doses of bicuculline were applied are especially noteworthy, since many authors consider the neuronal hyperactivity in mouse models of AD to be a product of a decrease in GABAergic inhibition (Busche et al 2008, Palop et al 2007, Verret et al 2012)[8].

[8] See chapter 4.2 for a discussion of the role of GABAergic inhibition in Aβ-induced hyperactivity.

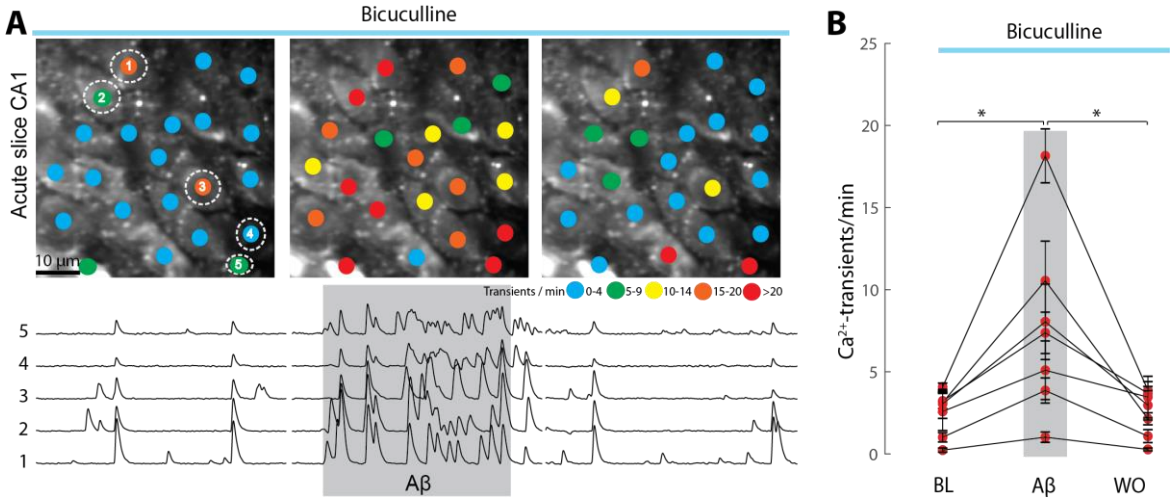

Fig. 17: Aβ induces neuronal hyperactivity in bicuculline-treated hippocampal slices. *A)* Top: representative two-photon image of a hippocampal slice from a wild-type mouse for baseline (left) Aβ application (middle) and washout (right) conditions. The colored dots on the neurons represent the number of Ca^{2+}-transients per minute. *Bottom*: Ca^{2+}-traces of the circled neurons. The grey shaded area represents the time of Aβ application. *B)* Summary data for N = 7 slices. Each dot represents the mean number of Ca^{2+}-transients per minute for all neurons in one slice under baseline (BL), Aβ and washout (WO) conditions. * $p < 0.05$, Wilcoxon signed rank test. Error bars denote SEM

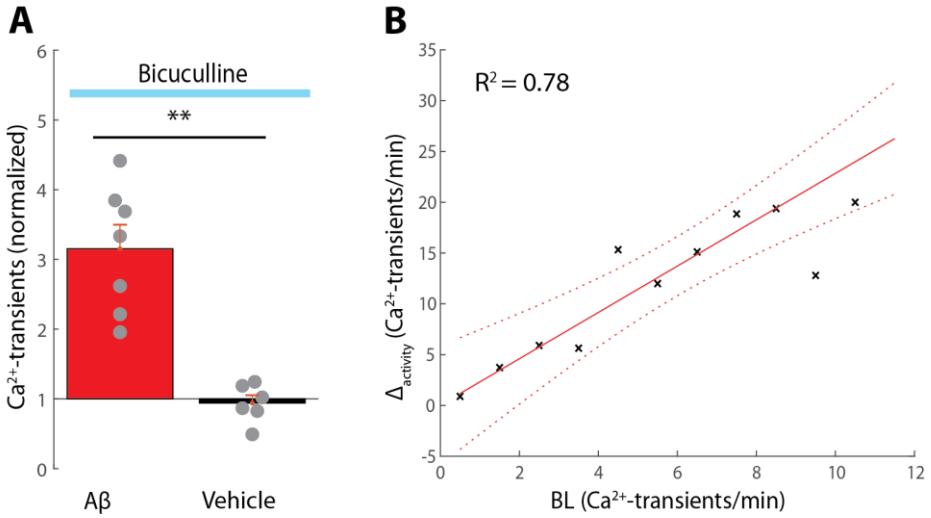

Fig. 18: Analysis of the Aβ-induced neuronal hyperactivity *in vitro* *A)* Normalized change of activity for the application of Aβ (left, N = 7) or vehicle (right, N = 7) in hippocampal slices in which the neuronal baseline activity had been induced by the superfusion of high doses of bicuculline in ACSF containing elevated K^+-concentrations (5.5 - 6.5 mM). Each dot represents the mean of one slice. *B)* Linear regression analysis of the average difference of activity ($\Delta_{activity}$) compared to the baseline activity for Aβ application. $R^2 = 0.78$. ** $p < 0.005$. Wilcoxon rank sum test. Error bars denote SEM

In line with the previous results, inducing neuronal hyperactivity by other pharmacological manipulations made the slices susceptible for Aβ-induced neuronal hyperactivity as well.

Thus, Aβ readily induced neuronal hyperactivity in slices which were superfused with ACSF containing high levels of potassium (**Fig. 19 A, B**, N = 6, normalized activity: 2.5 ± 0.26, p = 0.031). The application of the vehicle had no effect in these slices (N = 6, normalized activity: 0.94 ± 0.11, Aβ vs. vehicle p = 0.0022). Moreover, Aβ application could activate CA1 neurons, when their baseline activity was increased by glutamate application (**Fig. 19 C, D**). In these experiments, Aβ had again a strong effect on all slices (N = 7, normalized activity: 5.5 ± 0.58, p = 0.016), while vehicle application did not change neuronal activity (n = 6, normalized activity: 1.2 ± 0.10, Aβ vs. vehicle p = 0.0012). Next, we compared the activity-inducing effect of Aβ for all three manipulations (**Fig. 19 E**). Surprisingly, Aβ application had a stronger hyperactivity-inducing effect in slices, in which the baseline activity had been induced by glutamate application when compared to bicuculline- and potassium-treated ones (Bic vs. K^+, p = 0.84; Bic vs. Glu, p = 0.034; K^+ vs. Glu, p = 0.0046). This intriguing finding could not be explained by differences in the baseline activity (**Fig. 16**).

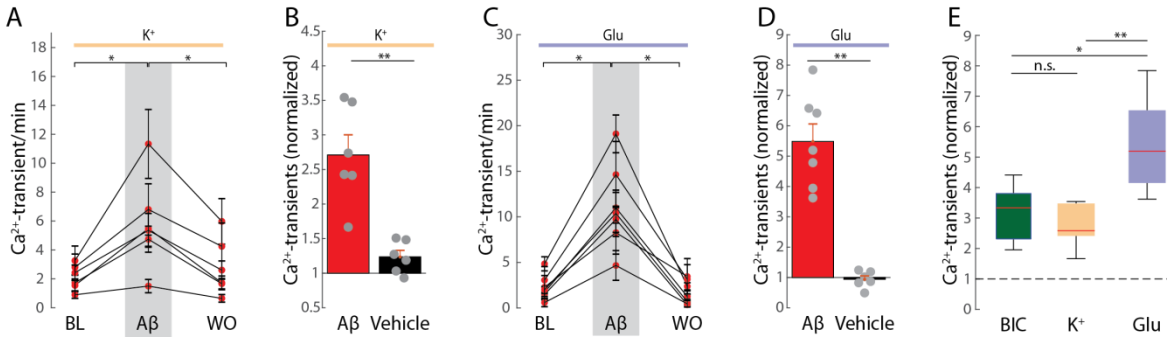

Fig. 19: K^+- or glutamate-dependent induction of baseline activity makes hippocampal slices susceptible to Aβ-induced neuronal hyperactivity. *A)* Summary data for N = 6 slices superfused with high K^+-ACSF. Each dot represents the mean number of Ca^{2+}-transients per minute for all neurons in one slice under baseline (BL), Aβ application and washout (WO) conditions. *B)* Normalized change of activity for the application of Aβ (left, N = 6) and vehicle (right, N = 6) in slices superfused with high K^+-ACSF. Each dot represents the mean of one slice. *C* and *D)* Same as *A* and *B* for slices superfused with 40-60 µM of glutamate (Aβ, N = 7; vehicle, N = 6). *E)* Boxplot of the normalized activity after bicuculline (BIC, N = 7) high K^+ (N = 6) or glutamate (Glu, N =7) superfusion of the slice. * p < 0.05, ** p < 0.005. Wilcoxon signed rank test (*A, C*), Wilcoxon rank sum test (*B, D*), Kruskal Wallis test with Dunn-Sidak post-hoc comparison (*E*). Error bars denote SEM

One possible explanation for the bigger impact of Aβ in glutamate-treated slices was that Aβ could in many cases induce baseline activity in neurons that remained silent even after glutamate superfusion. Silent neurons in bicuculline-treated slices, on the other hand, almost always stayed silent during Aβ application (**Fig. 20**). Thus, we turned our attention to those cells for a more in-depth analysis (**Fig. 21**). More than half of the silent neurons (n = 88) under glutamate-application conditions increased their activity beyond 1 transient/30 seconds during Aβ application (**Fig. 21 B**) while only 5% of neurons (n = 65) from bicuculline-treated slices could be activated by Aβ (**Fig. 21 A**). Also the number of Ca^{2+}-transients in these activated neurons was much higher for glutamate than for bicuculline conditions (**Fig. 21 C**). In fact, the analysis of the distribution of the activities (**Fig. 21 D**) revealed a marked shift towards higher activities for glutamate as compared to bicuculline treatment and Aβ application ($p < 0.0001$). In consequence, the enhanced effect of Aβ on slices treated with glutamate compared to bicuculline or potassium-superfused slices (**Fig. 19 E**) can at least partially be explained by the fact that glutamate application made silent neurons susceptible to Aβ-induced hyperactivity, while bicuculline superfusion did not.

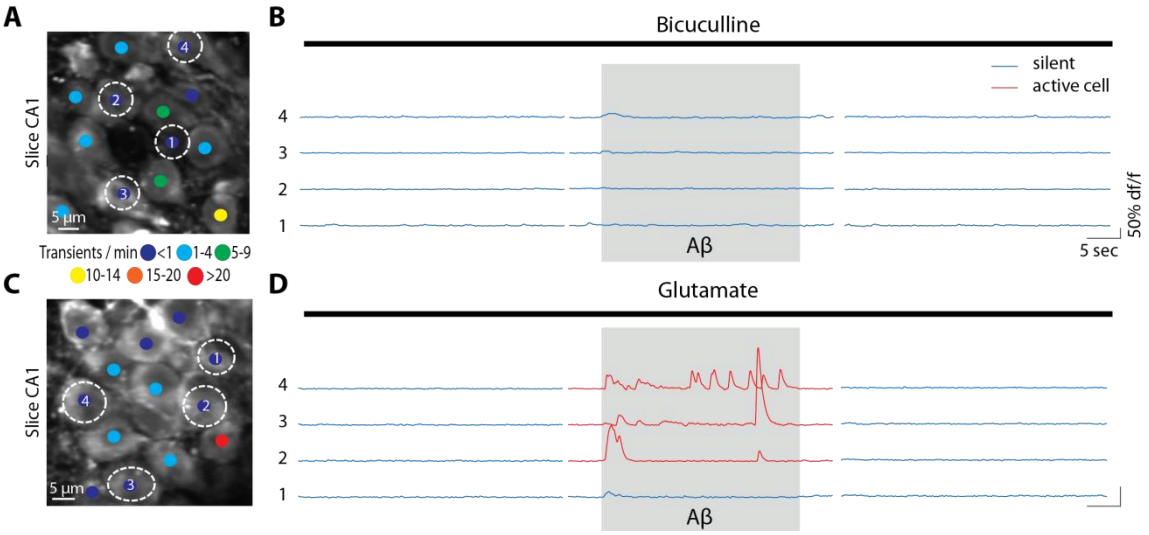

Fig. 20: Glutamate superfusion makes silent neurons susceptible to Aβ-dependent activation. *A)* Representative two-photon image of a hippocampal slice superfused with bicuculline. The colored dots on the neurons represent the number of Ca^{2+}-transients per minute. *B)* Ca^{2+}-traces of the circled neurons in *A* for baseline (left) Aβ application (middle) and washout (right) conditions. The grey

shaded area represents the time of Aβ application. *C* and *D)* Same as *A* and *B*, but for a slice superfused with glutamate.

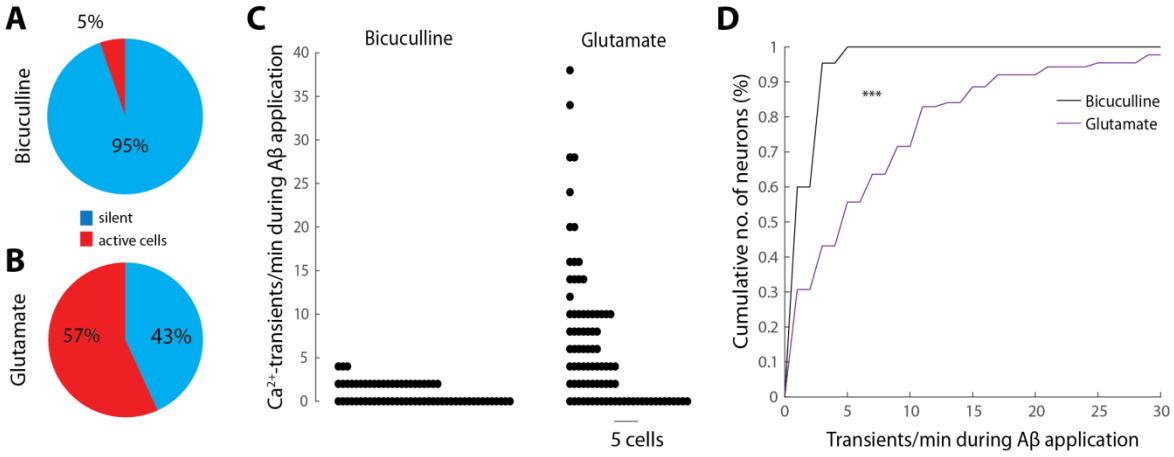

Fig. 21: Glutamate but not bicuculline superfusion makes silent neurons susceptible to Aβ-dependent activation. *A* and *B)* Pie chart depicting the number of silent neurons that get activated after Aβ application from slices superfused with bicuculline (*A*, n = 65) or glutamate (*B,* n = 88). *C)* Number of Ca^{2+}-traces during Aβ application for all silent neurons from bicuculline (left) or glutamate (right) superfused slices. Each dot represents one cell. *D)* Cumulative distributions of the number of Ca^{2+}-transients during Aβ application for all silent neurons from bicuculline or glutamate superfused slices. *** $p < 0.0001$, Kolmogorov-Smirnov test

3.2.3 Blocking neuronal baseline activity *in vivo* prevents the Aβ-induced neuronal hyperactivation

So far, we established that Aβ-induced neuronal hyperactivity critically depends on the level of previous baseline activity in hippocampal slices. In consequence, I next asked whether this also applies to *in vivo* conditions, that is, whether blocking baseline activity *in vivo* could prevent the Aβ-induced neuronal hyperactivity. To address this question, I superfused the hippocampus *in vivo* for thirty minutes with the ionotropic glutamate receptor blockers D-APV and CNQX (50 µM each) (**Fig. 22**). As previously described (Busche et al 2008), these drugs blocked the spontaneous neuronal activity in all neurons. In line with my previous findings from the *in vitro* experiments, Aβ application was ineffective under these conditions (**Fig. 22**) and could not increase the neuronal activity (N = 5, p = 0.50). These results were independently confirmed in a second experiment, in which the hippocampus was silenced by the superfusion of the sodium channel blocker TTX (1µM). Similar to the previous

experiment, all neurons were completely inactive under these conditions and the application of Aβ had no effect on the neuronal activity under these circumstances (**Fig. 23**, N = 4, p = 0.8). In summary, these experiments demonstrate that the Aβ-induced neuronal hyperactivation of hippocampal CA1 neurons critically depends on their baseline activity both *in vitro* and *in vivo*.

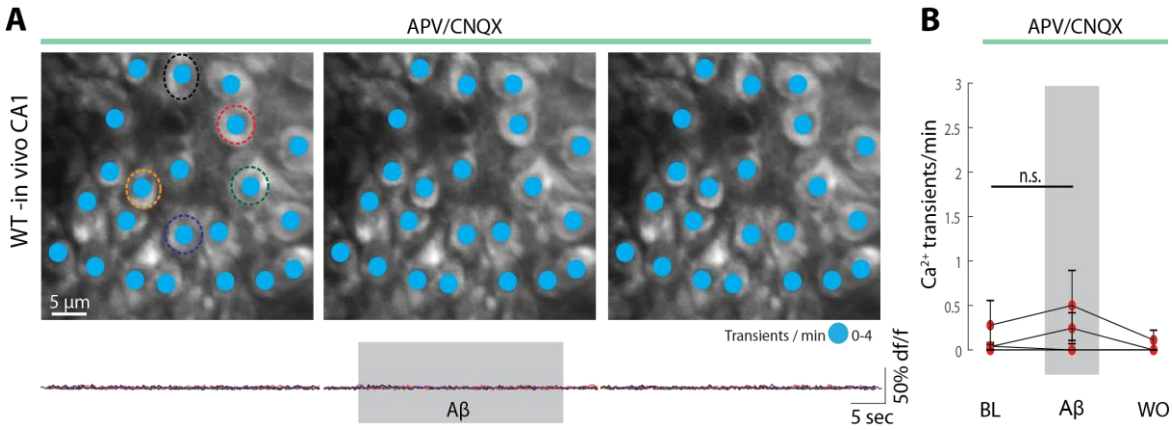

Fig. 22: The superfusion of D-APV and CNQX prevents the Aβ-induced neuronal hyperactivity *in vivo*. *A)* Top: representative two-photon image of the hippocampal CA1 region from a wild-type mouse during the superfusion of APV and CNQX for baseline (left), Aβ application (middle) and washout (right) conditions. The colored dots on the neurons represent the number of Ca^{2+}-transients per minute. Bottom: Overlay of the Ca^{2+}-traces from the five circled neurons. The grey shaded area represents the time of Aβ application. *B)* Summary data for N = 5 mice. Each dot represents the mean number of Ca^{2+}-transients per minute for all neurons in one mouse under baseline (BL), Aβ application and washout (WO) conditions. n.s. not significant, Wilcoxon signed rank test. Error bars denote SEM

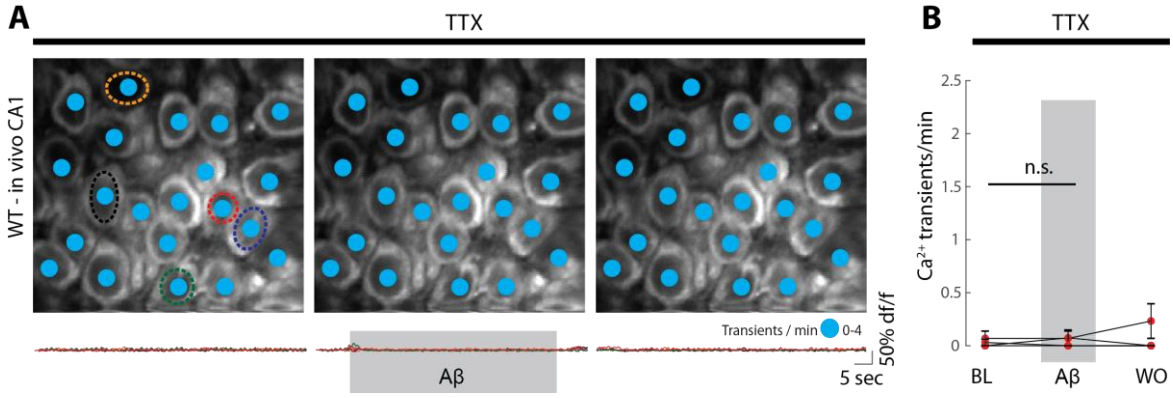

Fig. 23: The superfusion of TTX prevents the Aβ-induced neuronal hyperactivity *in vivo*. *A)* Top: representative two-photon image of the hippocampal CA1 region from a wild-type (WT) mouse during the superfusion of TTX for baseline (left), Aβ application (middle) and washout (right) conditions. The colored dots on the neurons represent the number of Ca^{2+}-transients per minute. Bottom: Overlay of the Ca^{2+}-traces from the five circled neurons. The grey shaded area represents the time of Aβ application. *B)* Summary data for N = 5

mice. Each dot represents the mean number of Ca^{2+}-transients per minute for all neurons in one mouse under baseline (BL), Aβ application and washout (WO) conditions. n.s. not significant, Wilcoxon signed rank test Error bars denote SEM

3.2.4 Aβ application induces neuronal hyperactivity in CA1 but not in all cortical circuits

In the previous experiments, I have demonstrated that neuronal activity is necessary to make hippocampal CA1 neurons susceptible to Aβ-induced neuronal dysfunction. Next, I investigated whether this activity-dependence is also relevant for cortical areas, where Aβ pathology manifests earlier than in the hippocampus in AD patients (Palmqvist et al 2017). The spontaneous activity of cortical layer 2/3 neurons has been well characterized because it is accessible to classical two-photon imaging applications (Grienberger & Konnerth 2012). The baseline activity in this cortical region is much lower than in the hippocampus (Busche et al 2012, Kerr et al 2005, Rochefort et al 2009). Also, the neuronal hyperactivity in AD mice has previously been described in layer 2/3 (Busche et al 2015a, Grienberger et al 2012, Keskin et al 2017). As expected, I found rather low levels of spontaneous baseline activity in cortical layer 2/3 (**Fig. 24 A, B**). In contrast, the spontaneous baseline activity in layer 5 was expected to be much higher (De Kock et al 2007, Niell & Stryker 2008, Tischbirek et al 2015). Since recent advances in two-photon imaging (Tischbirek et al 2015) have enabled us to image deeper cortical layers, I specifically stained cortical layer 5 neurons with bolus loading of Cal-520 AM by carefully injecting a small volume of the indicator at a depth of 550 µm from the surface (Birkner et al 2017). I then adjusted the imaging plane to the dendritic trunks of these neurons at a depth of about 350 µm (**Fig. 24 C**). This facilitates the detection of individual Ca^{2+}-transients in these highly active neurons, because the decay time of the fluorescent signals are much shorter in the trunk than in the cell body (Tischbirek et al 2017). As expected, I found that the neuronal activity in layer 5 was much higher than in layer 2/3 (**Fig. 24 D**).

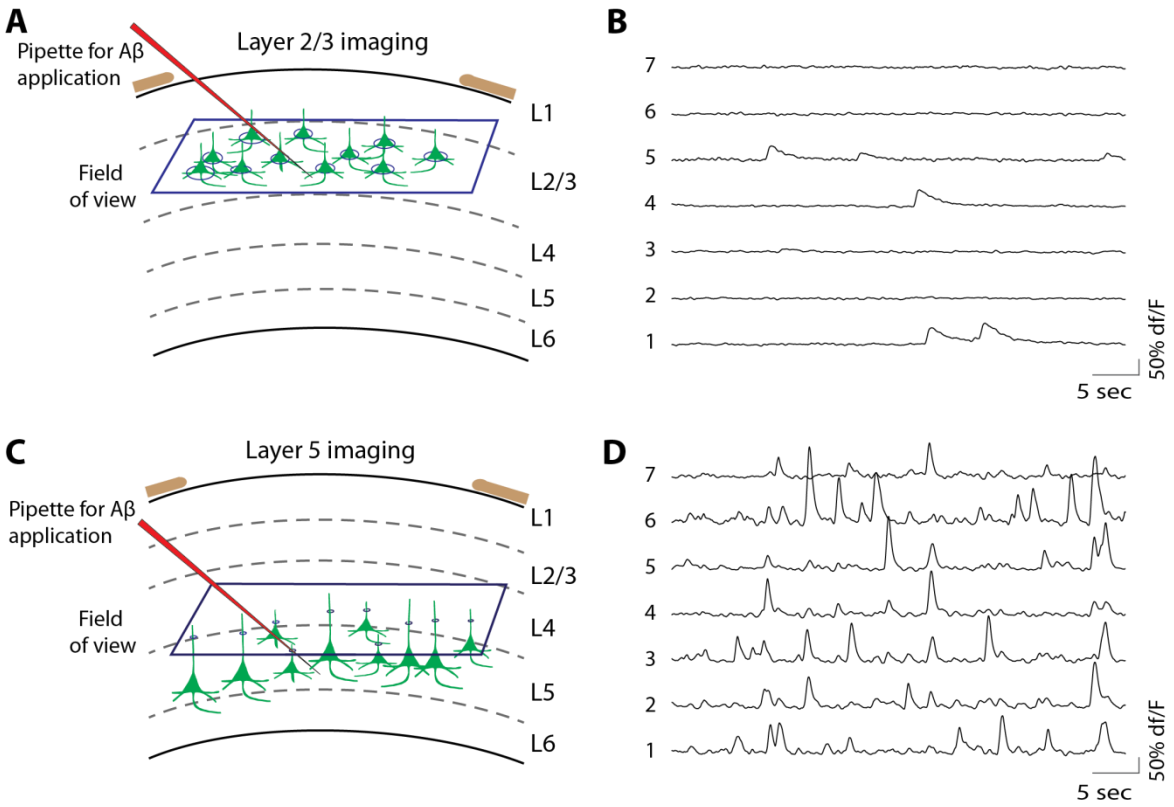

Fig. 24: Neuronal baseline activity in cortical layer 2/3 and layer 5 *in vivo* *A)* Cartoon of the preparation for layer 2/3 imaging. *B)* Baseline activity of seven representative layer 2/3 neurons from a wild-type mouse. *C)* Cartoon of the preparation for layer 5 imaging. Note that the imaging plane was adjusted to record from the dendritic trunk of the neurons. *D)* Baseline activity of seven representative layer 5 neurons from a wild-type mouse.

Next, I tested whether Aβ could induce neuronal hyperactivity in those two different layers. To achieve this, I applied Aβ into layer 2/3 or layer 5 (**Fig. 24 A, C**). The Aβ application was performed as previously described, that is, 500 nM of S26C Aβ dimers dissolved in ACSF were puffed from a patch pipette into the extracellular space around the neuronal cell bodies for 30 seconds. Remarkably, the application of Aβ in layer 2/3 did not change the activity of the surrounding neurons (**Fig. 25 A**). In layer 5, however, Aβ application robustly increased the number of Ca^{2+}-transients in most neurons (**Fig. 25 B**). Since, especially in layer 5, it was difficult to count individual Ca^{2+}-transients, I used the AUC of the Ca^{2+}-traces as an approximation of the neuronal activity. Thus, I calculated the AUC for each neuron in three-second bins, as previously described (**Fig. 12 A, B**). In layer 2/3, the average AUC was low at

baseline conditions and stayed at similar levels during Aβ application (**Fig. 26 A**). In layer 5, conversely, the AUC was higher under baseline conditions and increased further during Aβ application (**Fig. 26 B**). To compare both applications, I calculated the normalized AUC for all neurons during baseline, Aβ application and washout-conditions (**Fig. 26 C, D**). In layer 2/3, the AUC during the Aβ application was not different from baseline conditions (**Fig. 26 C**, n = 129 cells from 5 mice, p = 0.35). In layer 5, on the other hand, the Aβ application robustly increased the AUC in the neurons surrounding the pipette tip (**Fig. 26 D**, n = 144 cells from 4 mice, p < 0.0001). These results indicate that the activity-dependency of the Aβ-induced action I had previously observed in the hippocampus is also relevant for cortical circuits *in vivo*.

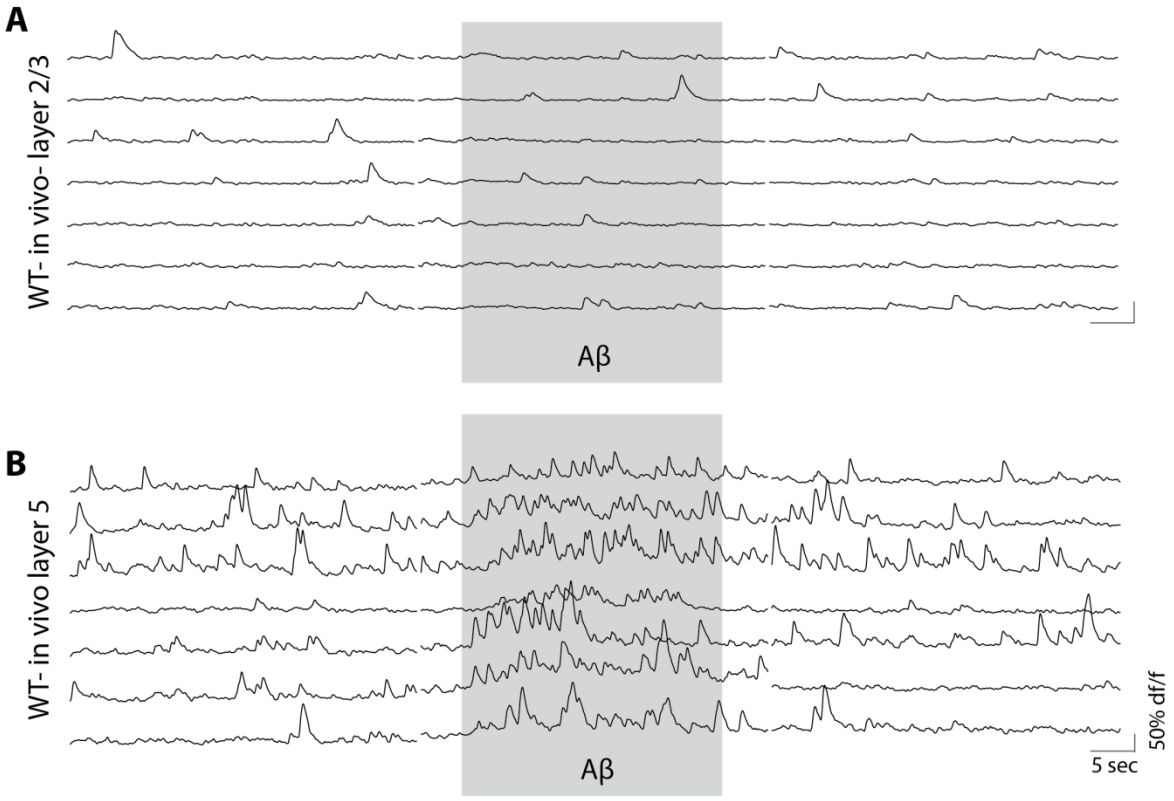

Fig. 25: Aβ induces neuronal hyperactivity in cortical layer 5 but not in layer 2/3 *in vivo*. *A)* Ca^{2+}-traces of seven representative layer 2/3 neurons from a wild-type mouse for baseline (left), Aβ application (middle) and washout (right) conditions. The grey shaded area represents the time of Aβ application. *B)* Same as in A, but for layer 5 cortical neurons.

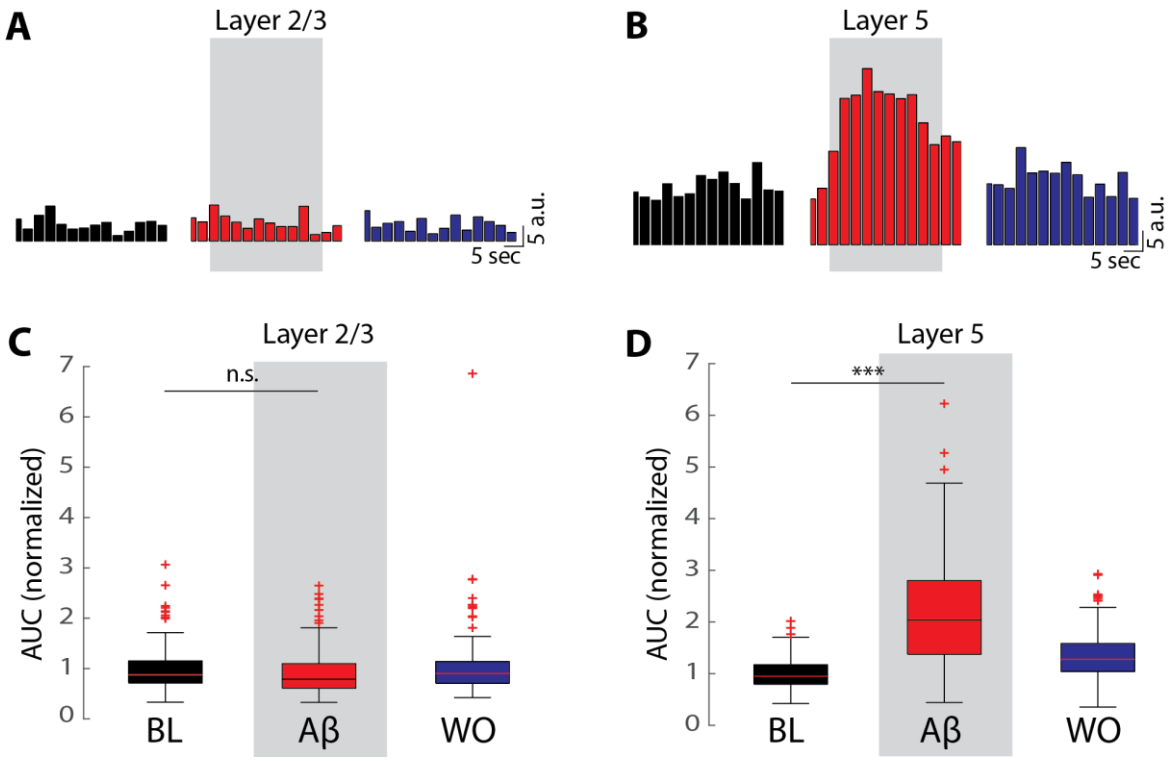

Fig. 26: Analysis of the Aβ-induced effects in cortical circuits *in vivo*. *A)* Average AUC, calculated in three-second bins, of the seven layer 2/3 neurons from Fig. 25 for baseline (left), Aβ application (middle) and washout conditions. The grey shaded area corresponds to the time of Aβ application. *B)* Same as *A*, but for the seven layer 5 neurons in Fig. 25. *C)* Boxplot of the normalized AUC from all recorded layer 2/3 neurons (n = 129 cells from 5 mice) for baseline (left), Aβ application (middle) and washout conditions. *D)* Same as *C*, but for all recorded layer 5 neurons (n = 144 from 4 mice). a.u. arbitrary units, n.s. not significant, *** $p < 0.0001$. Wilcoxon signed rank test

3.3 Impaired glutamate uptake as a cellular mechanism of Aβ-induced neuronal hyperactivity *in vivo*

Action potentials in pyramidal neurons are largely driven by glutamatergic inputs (Spruston 2008). In the previous experiments, I revealed that the Aβ-induced neuronal dysfunction critically depends on the neuronal activity status, both in the hippocampus and the cortex. Thus, I hypothesized that the cellular mechanism of the Aβ-dependent neuronal

hyperactivity involved an impairment of the cerebral glutamate metabolism as previously indicated (Li et al 2009, Li et al 2011, O'Shea et al 2008).

3.3.1 Co-application of iGluR-antagonists prevents the effect of Aβ

In order to test whether the cellular mechanism of the Aβ-induced neuronal hyperactivation involved an increase of extracellular glutamate, I first investigated whether the activation of ionotropic glutamate receptors (iGluRs) was necessary to mediate the Aβ-induced neuronal hyperactivity. Thus, I co-applied Aβ (500 nM) with D-APV (50 µM) and CNQX (50 µM) in the CA1 region of wild-type mice as described above. The co-application of the three substances did not induce neuronal hyperactivity (**Fig. 27**). Rather, there was a trend towards decreased neuronal activity during the application of all three substances (N = 5, p = 0.063). Moreover, the effects of Aβ application alone (N = 7) and Aβ co-application with D-APV and CNQX (N = 5), were significantly different (**Fig. 28 A**, p = 0.0025). Since the co-application of Aβ with the iGluR-blockers not only blocked the Aβ action, but rather decreased neuronal activity, I asked whether the Aβ action was dominated by the iGluR-blockers. Thus, I next applied the iGluR blockers alone, which had a similar effect as their co-application with Aβ. (**Fig. 28 B**, N = 5, p = 0.31). Unlike the bath-application of the same concentrations (**Fig. 22**), the local application of D-APV and CNQX did not block all neuronal activity in the field of view.

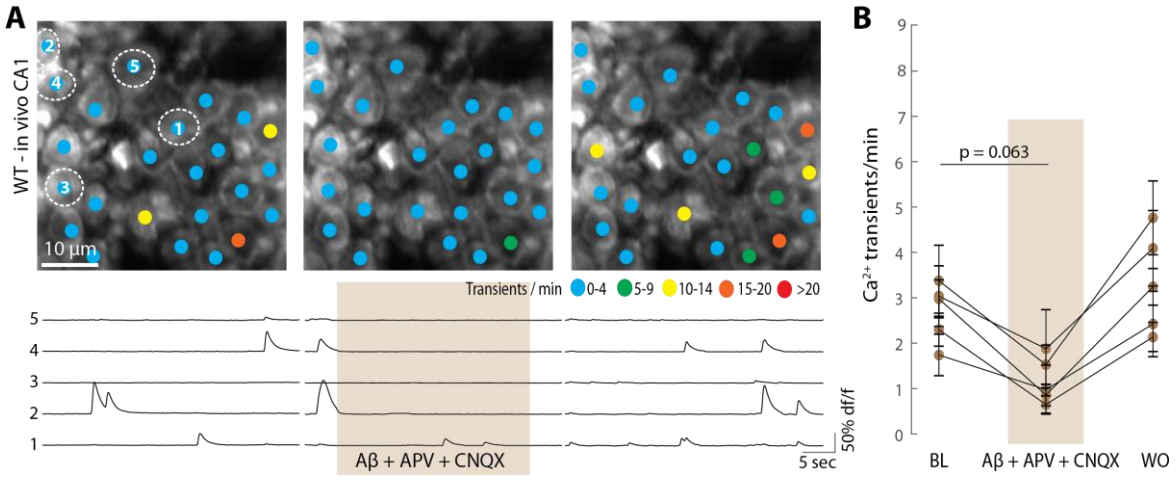

Fig. 27: Co-application with iGluR blockers prevents the hyperactivity-inducing effects of Aβ. *A)* Top: representative two-photon image of the hippocampal CA1 region of a wild-type mouse *in vivo* for baseline (left), Aβ, D-APV (abbreviated as APV in the figure) and CNQX application (middle) and washout (right) conditions. The colored dots on the neurons represent the number of Ca^{2+}-transients per minute. Bottom: Ca^{2+}-traces for the circled neurons. The brown shaded area represents the time of application. *B)* Summary data for N = 5 mice. Each dot represents the mean number of Ca^{2+}-transients per minute for all neurons in one mouse under baseline (BL), Aβ, D-APV and CNQX application and washout (WO) conditions. P = 0.063, Wilcoxon signed rank test. Error bars denote SEM

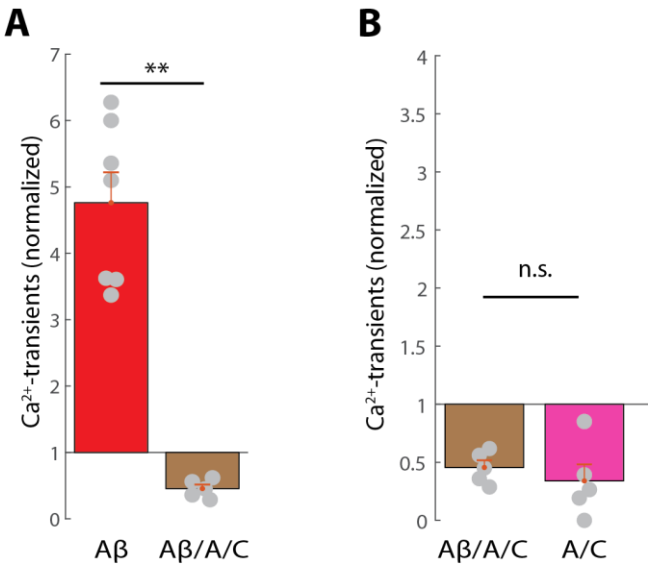

Fig. 28: The application of iGluR blockers dominates the action of Aβ. *A)* Normalized change of activity for the application of Aβ (left, N = 7) and Aβ, D-APV and CNQX (right, N = 5) *in vivo*. Each dot represents the mean of one mouse. *B)* Normalized Ca^{2+} transients for the application of Aβ, D-APV and CNQX (left) and D-APV and CNQX (N = 5) *in vivo*. Each dot represents the mean of one mouse. n.s. not significant, ** p< 0.005. Wilcoxon rank sum test

3.3.2 Aβ-dependent block of glutamate uptake at excitatory synapses

Because the Aβ-induced neuronal hyperactivity was absent when iGluRs were blocked (**Fig. 27**), I hypothesized that the mechanism of the observed activity-dependence of the Aβ-induced neuronal hyperactivation involved an increase in extracellular glutamate. The levels of extracellular glutamate are controlled by glutamate release and glutamate uptake (Danbolt 2001, Zhou & Danbolt 2014). Unlike other neurotransmitters, glutamate cannot be enzymatically degraded in the extracellular space. Thus, dwell-time of glutamate in the synaptic cleft is limited by neuronal and astrocytic uptake mechanisms. Previous *in vitro*

studies have reported that the non-transportable glutamate uptake blocker TBOA had very similar effects on synaptic plasticity as Aβ (Li et al 2009, Li et al 2011). To test, whether blocking glutamate uptake could also mimic the Aβ action *in vivo*, I injected 250 µM of TBOA in the hippocampus of wild-type mice just as I had applied Aβ in the previous experiments (**Fig. 29 A**). Remarkably, TBOA faithfully induced neuronal hyperactivity in all tested mice (**Fig. 29 B**, N = 6, p = 0.031). Moreover, the effect of TBOA application was very similar to that of the Aβ application (**Fig. 30 A**). Both the application of TBOA (N = 6) or Aβ (N = 7) increased the neuronal activity almost five-fold (TBOA 4.6 ± 0.33; Aβ 4.8 ± 0.46, p = 0.63). Like the Aβ application (**Fig. 11 A**), TBOA increased the number of Ca^{2+}-transients in almost all neurons (**Fig. 30 B**). During the application, the activity of 91% (268/295) of all cells was increased, decreased in only 3% (8/295) of all neurons and unchanged in 6% (19/295). The median increase in activity during TBOA application was +12 transients/min.

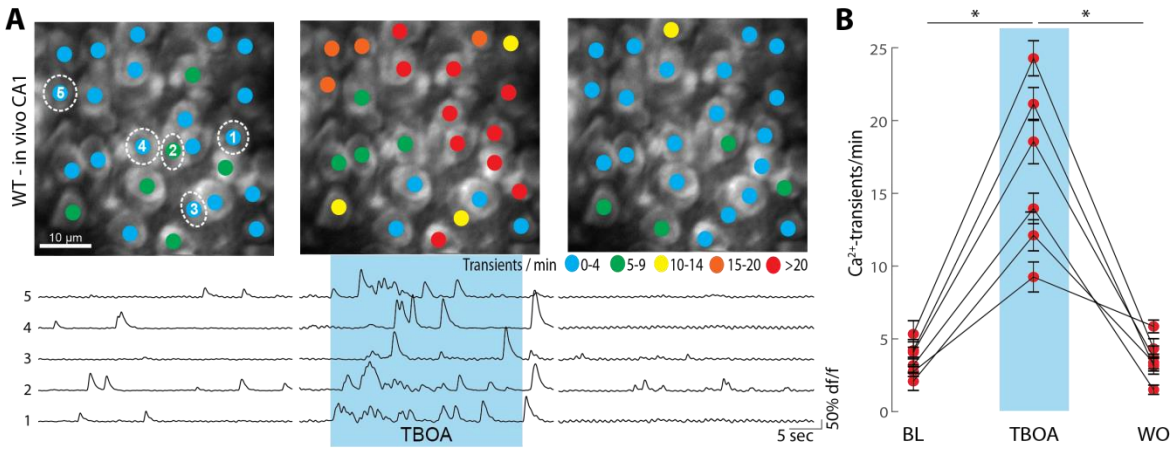

Fig. 29: TBOA induces neuronal hyperactivity *in vivo.* *A)* Top: representative two-photon image of the hippocampal CA1 region of a wild-type mouse for baseline (left), TBOA-application (middle) and washout (right) conditions. The colored dots on the neurons represent the number of Ca^{2+}-transients per minute. Bottom: Ca^{2+}-traces for the circled neurons. The blue shaded area represents the time of Aβ application. *B)* Summary data for N = 6 mice. Each dot represents the mean number of Ca^{2+}-transients per minute for all neurons in one mouse under baseline (BL), TBOA and washout (WO) conditions. Error bars denote SEM, * p< 0.05, Wilcoxon signed rank test

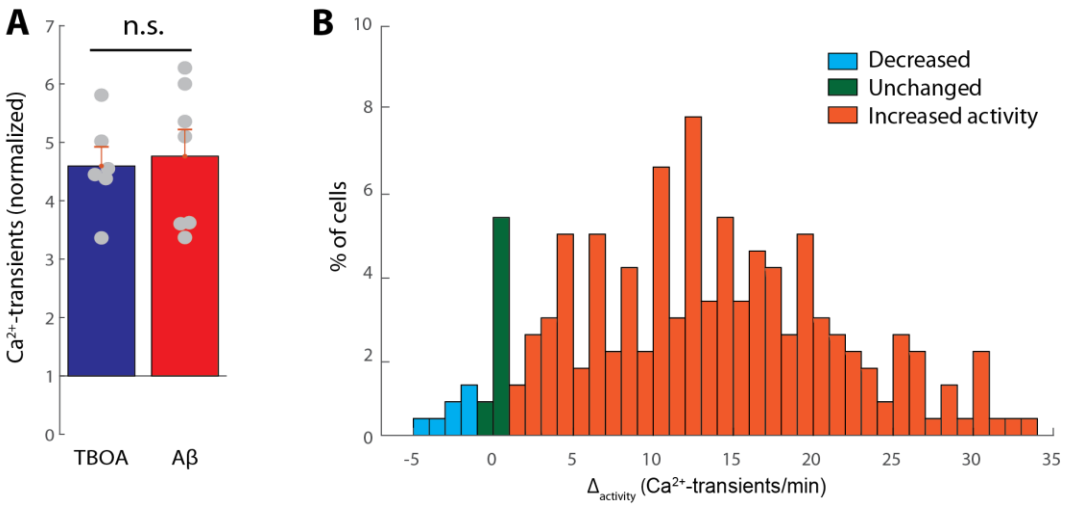

Fig. 30: Analysis of the TBOA-induced neuronal hyperactivity *in vivo*. *A)* Normalized change of activity for the application of Aβ (left, N = 7) or TBOA (right, N = 6). Each dot represents the mean of one mouse. *B)* Histogram of the difference in activity between Aβ application and baseline conditions ($\Delta_{activity}$). n.s. not significant. Wilcoxon rank sum test. Error bares denote SEM

3.3.3 Impaired glutamate uptake in mouse models of AD

Next, I turned my attention to the neuronal activity in a mouse model of β-amyloidosis, the APP23 x PS45 mouse model. As previously demonstrated in the Konnerth laboratory (Busche et al 2012), at early ages, a significant fraction of neurons in the hippocampal CA1 region of this mouse model is hyperactive. This was observed even before plaques were formed, when only the levels of soluble Aβ were increased. In consequence, the neuronal hyperactivity in this mouse model was hypothesized to be caused by increased levels of soluble Aβ (Busche et al 2012). In a first set of experiments, I replicated these findings independently. As expected, two-photon Ca^{2+}-imaging in six week-old wild-type (**Fig. 31 A, B**) and APP23 x PS45 transgenic mice (**Fig. 31 C, D**) revealed that more neurons are hyperactive in the transgenic mouse model. To quantify the number of hyperactive cells, the neurons were classified according to their activity status as previously described (Busche et al 2012). Neurons were categorized as functionally silent if they did not have a single Ca^{2+}-transient in five minutes, and as hyperactive if they had more than 20 Ca^{2+}-transients per minute on average. All

neurons that had activity levels between these two values were categorized as normal (**Fig. 32**). In wild-type mice, 10% of all cells (n = 542 from 8 mice) were functionally silent, while 88% had normal activity levels and only 2% were hyperactive (**Fig. 32 A, B**). In the transgenic mice, on the other hand, only 3 % of all neurons (n = 299 from 6 mice) were silent, much more cells (14%) were hyperactive and 84% had normal activity levels (**Fig. 32 C, D**).

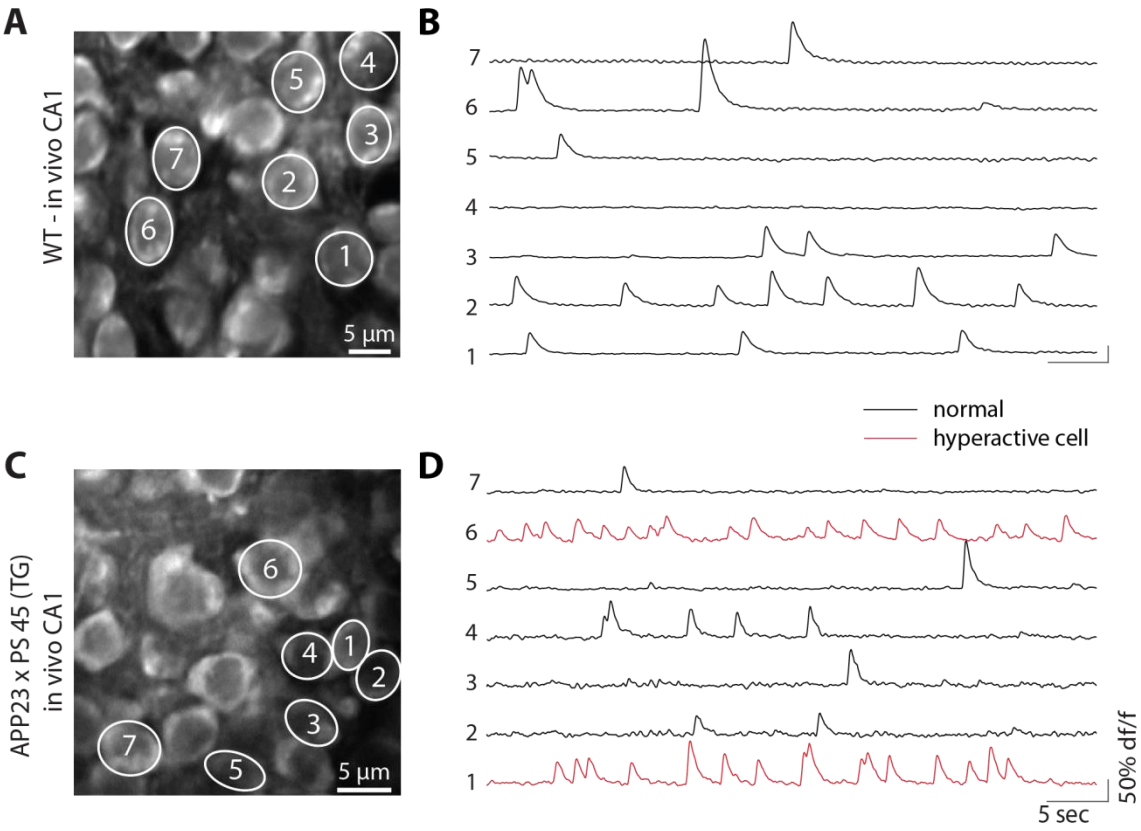

Fig. 31: *In vivo* baseline activity in a wild-type (WT) and an APP23 x PS45 transgenic (TG) mouse. *A)* Representative two-photon image of the hippocampal CA1 region of a wild-type mouse. *B)* Ca^{2+}-traces of the four circled neurons in *A*. *C)* Representative two-photon image of the hippocampal CA1 region of a TG mouse. *D)* Ca^{2+}-traces of the four circled neurons in *C*. Traces from hyperactive cells are shown in red.

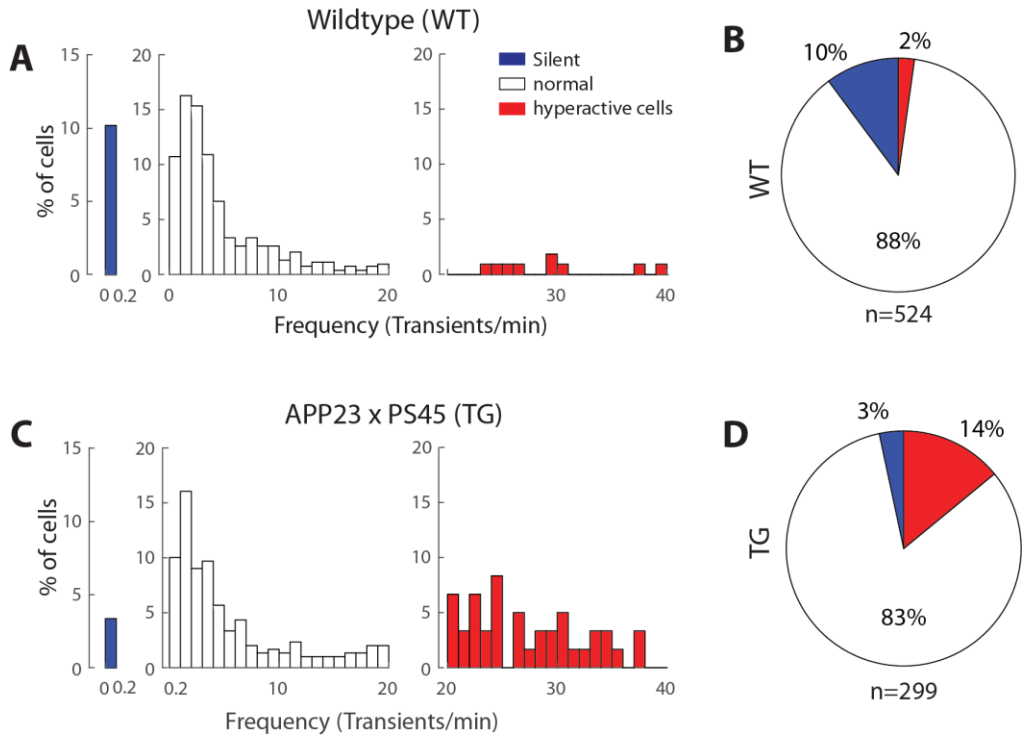

Fig. 32: Neuronal hyperactivity in APP23 x PS45 transgenic (TG) mice. *A)* Activity histogram depicting the frequency of Ca^{2+}-transients under baseline conditions in wild-type mice (n = 524 cells from 8 mice). *B)* Pie chart of the percentage of silent, normal and hyperactive neurons. *C)* Activity histogram depicting the frequency of Ca^{2+}-transients under baseline conditions in TG mice (n = 299 cells from 6 mice). *D)* Pie chart of the percentage of silent, normal and hyperactive neurons.

If Aβ and TBOA both inhibit glutamate uptake, then the TBOA effect should be less severe in mouse models of AD with high intrinsic levels of Aβ. In other words, the neuronal activity, which is already increased in mouse models of AD, would not increase much further after TBOA application, because the high intrinsic levels of soluble Aβ in this mouse model of AD (Busche et al 2012, Busche et al 2015a, Keskin et al 2017) would already inhibit some of the glutamate uptake. Thus, I next applied TBOA in the CA1 region of the APP23 x PS45 mouse model (**Fig. 33**). While, in wild-type mice, the application of TBOA led to a pronounced increase of neuronal activity (normalized activity: 4.6 ± 0.33, **Fig. 29**, **Fig. 33 B**), the effect was much weaker in the transgenic mice (normalized activity: 1.8 ± 0.019, **Fig. 33 A, Fig. 34 A**) and the difference was highly significant (**Fig. 34 B,** p= 0.0095). This indicates that the TBOA effect is partially saturated in transgenic mice. Also, the neuronal activity after TBOA

application was not significantly different in the two mouse lines (WT 17 ± 2.3 Ca^{2+}-transients/min, TG 11 ± 1.3, p = 0.17). Next, I applied Aβ in the AD mice to test whether a further increase of Aβ would lead to an additional increase in neuronal activity (**Fig. 34 C, D**). Even though the number of Ca^{2+}-transients still increased slightly, the effect of Aβ was much smaller in transgenic mice (1.3 ± 0.08 fold increase compared to baseline) than in wild-type mice (4.81 ± 1.3, p = 0.0012). The neuronal activity after Aβ application was slightly, but not significantly higher in in wild-type mice (13 ± 2.0 Ca^{2+}-transients/min) compared to AD mice (8.4 ± 1.2, p = 0.07).

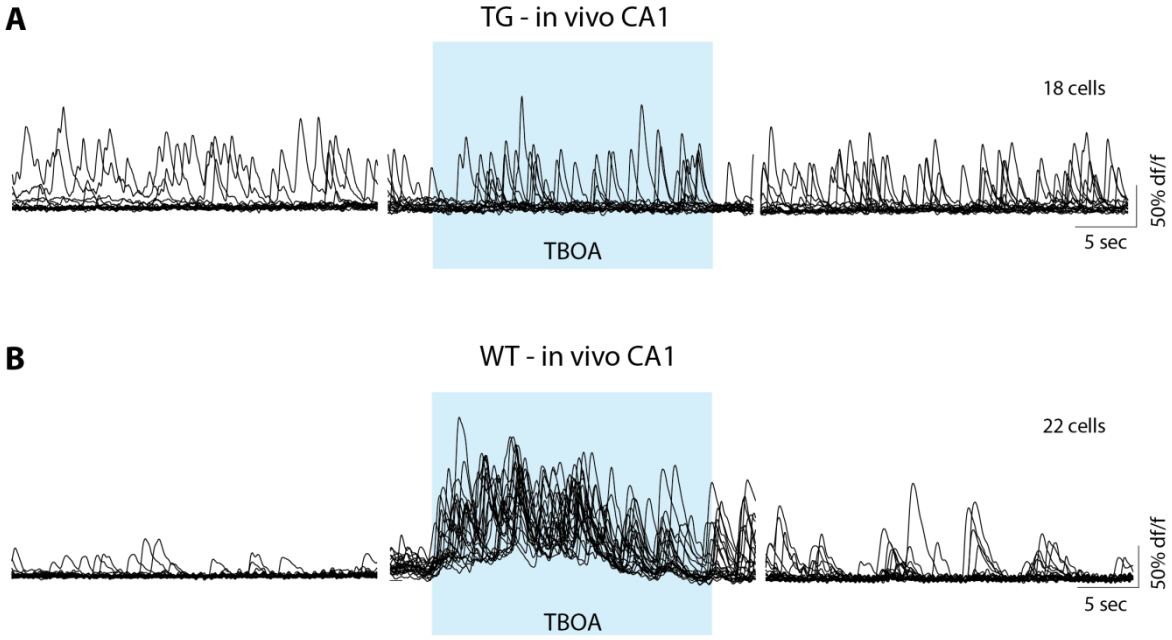

Fig. 33: The TBOA effect is partially saturated in a mouse model of AD. *A)* Overlay of the Ca^{2+}-traces from all cells (n = 18) in one APP23 x PS 45 transgenic (TG) mouse for baseline, TBOA application and washout conditions. The blue shaded area represents the time of Aβ application. *B)* Same as *A*, but for all cells from one wild-type (WT) mouse (n = 22).

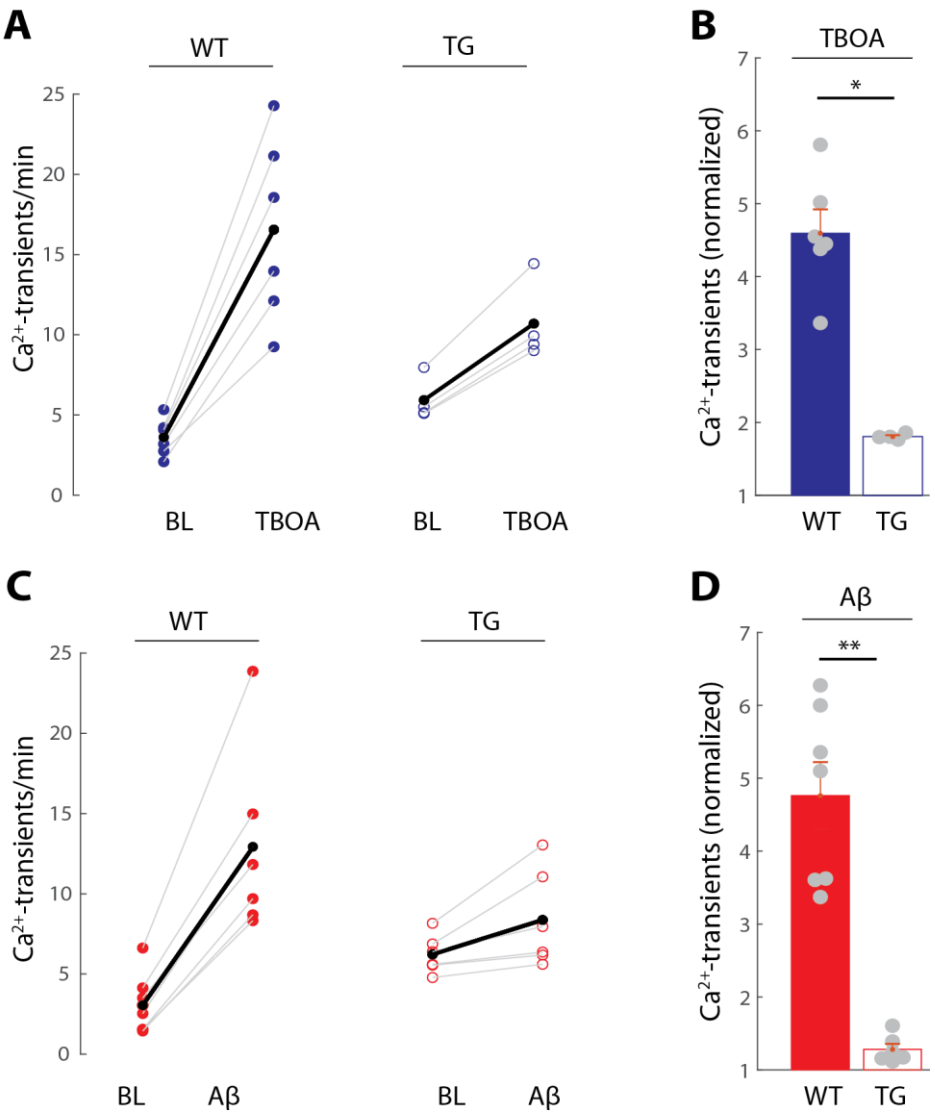

Fig. 34: The TBOA and Aβ effects are partially saturated in a mouse model of AD. *A)* Average frequency of Ca^{2+}-transients for baseline and TBOA application in wild-type (WT, left, N = 7) and APP23 x PS45 transgenic (TG, right, N = 4) mice. The colored dots represent the mean of Ca^{2+}-transients of one mouse. The black dots indicate the mean of all mice. *B)* Normalized activity change of TBOA application in wild-type (left, solid bar) and TG mice (right, open bar). The grey dots represent the mean of one mouse. *C* and *D)* Same as *A* and *B*, but for Aβ application (WT, N = 7; TG, N = 6). * $p < 0.05$. **$p < 0.005$, Wilcoxon rank sum test

3.3.4 Aβ can impair glutamate uptake *in vitro*

Even though TBOA increases neuronal activity just like Aβ and the TBOA effect is partially saturated in AD mice, the two substances could possibly have the same effect via different pathways. Thus, I next turned my attention to investigating whether Aβ indeed increases the

levels of extracellular glutamate. These experiments were performed in collaboration with Hsing-Jung Chen, a postdoc in the Konnerth laboratory. The inhibition of glutamate uptake should result in a longer dwell-time of glutamate in the extracellular space. In fact, glutamate which has been released from the presynaptic site can reach very high concentrations rapidly, but only remains in the synaptic cleft for around one millisecond (Clements et al 1992). In the hippocampus, stimulating the axonal connection from CA3 to CA1 (i.e. the Schaffer collateral pathway) will lead to a release of glutamate in the CA1 region (Collingridge et al 1983). At the postsynaptic site, glutamate triggers an excitatory postsynaptic current (EPSC) in CA1 pyramidal neurons by enabling cation influx through α-amino-3-hydroxy-5-methyl-4-isoxazolepropionic acid receptors (AMPARs) and NMDARs, which can be detected by whole cell patch-clamp recordings of the postsynaptic cell (Keller et al 1991). While the AMPARs have fast kinetics, the NMDARs bind glutamate with a high affinity and can thus stay activated for more than 100 milliseconds, depending on the receptor subunit composition (Cull-Candy et al 2001, Hestrin et al 1990, Lester et al 1990). Because NMDARs are usually blocked by a magnesium (Mg^{2+}) ion at the resting membrane potential, it is possible to experimentally isolate the NMDAR-dependent EPSC (NMDAR-EPSC) by depolarizing the cell and/or by the pharmacological block of AMPARs in the absence of Mg^{2+} (Keller et al 1991). An inhibition of glutamate uptake can be detected as a prolongation of the postsynaptic NMDAR-EPSC and the application of TBOA was reported to increase the decay time of the NMDAR-currents both after the application of exogenous glutamate (Jabaudon et al 1999) or after triggering synaptic glutamate release by electrical stimulation of the presynaptic axons (Arnth-Jensen et al 2002).

In a first set of experiments, we replicated these experiments (**Fig. 35**). To isolate the NMDAR-EPSCs, we depolarized the cells to +40 mV under whole cell patch-clamp conditions and blocked AMPARs with 10 µM GYKI. Synaptic glutamate release was then triggered by electrical stimulation of the Schaffer collaterals (typically 10 V, 100 µs) and the EPSC was

recorded under baseline conditions and after wash-in of TBOA for 10 min. As expected, the application of low doses of TBOA in the bath (10 µM) led to a prolongation of the NMDAR-EPSC, as shown for an example cell in **Fig. 35 A-D**. Even though the amplitude was slightly increased in some cells, the average amplitude change was not significant (**Fig. 35 E,** p = 0.29, n = 7). However, TBOA application robustly increased the full width at half maximum (FWHM) (**Fig. 35 F**, p = 0.016), as well as the decay time $\tau_{weighted}$ in all cells[9] (**Fig. 35 G**, p = 0.016)**.** Next, we tested whether the application of Aβ affected the NMDAR-EPSC the same way as TBOA does (**Fig. 36**). Thus, we performed the same recordings in a different set of cells (n = 8) under baseline conditions and after wash-in of 500nM Aβ dimers (**Fig. 36 A-D**). Just like TBOA, the application of Aβ did not significantly change the EPSC amplitude (**Fig. 36 E**, p = 0.15) but robustly increased the FWHM (**Fig. 36 F**, p = 0.0078) and $\tau_{weighted}$ (**Fig. 36 G**, p = 0.0078). Most of these findings are in line with a previous study using Aβ from cell culture (Li et al 2009). The authors of this study reported an increase in decay time for the application of Aβ, but also saw a strong decrease in amplitude, which we did not observe.

Finally, we examined whether the effect of the decay time was dose-dependent for the TBOA application in order to determine which dose of TBOA has the same effect as 500 nM of Aβ dimer (**Fig. 37**). To this end, we applied TBOA at the concentrations of 2.5 µM (n = 5), 5 µM (n = 10), 10 µM (n = 7) and 25 µM (n = 9) and compared the effects on the FWHM with the application of 500 nM Aβ dimers (**Fig. 37 A**). We estimated, that 500 nM of Aβ have a similar effect as 5-10 µM of TBOA (**Fig. 37 B**). Taken together, these findings demonstrate that Aβ has the same effect on the NMDA-EPSC as TBOA and provides strong evidence that both substances increase extracellular glutamate via the same mode of action, that is, by an inhibition of glutamate uptake.

[9] A full description how $\tau_{weighted}$ was calculated can be found in the methods section.

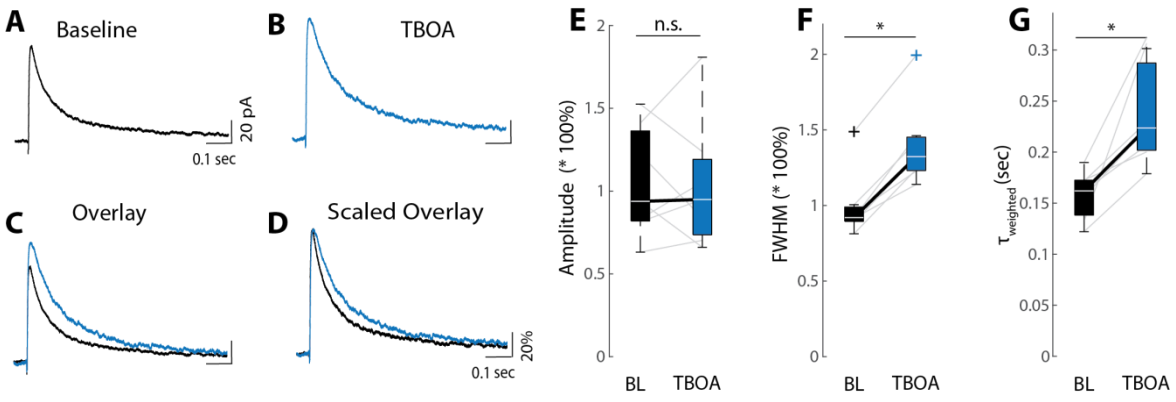

Fig. 35: TBOA prolongs the decay time of the NMDAR-EPSC in acute hippocampal slices. *A, B)* Average of the synaptically evoked NMDAR-EPSC of one representative hippocampal CA1 neuron from a wild-type mouse for baseline (*A*) and TBOA (10 µM) superfusion (*B*). *C, D)* Overlay (*C*) and scaled overlay (*D*) of the traces in *A* and *B*. *E-G)* Boxplot of the normalized EPSC amplitudes (*E*), normalized FWHM (*F*) and $\tau_{weighted}$ (*G*) for baseline (left) and TBOA superfusion conditions (right, n = 7). Each grey line represents one cell; the thick black line depicts the median. n.s. not significant, *p < 0.05. Wilcoxon signed rank test

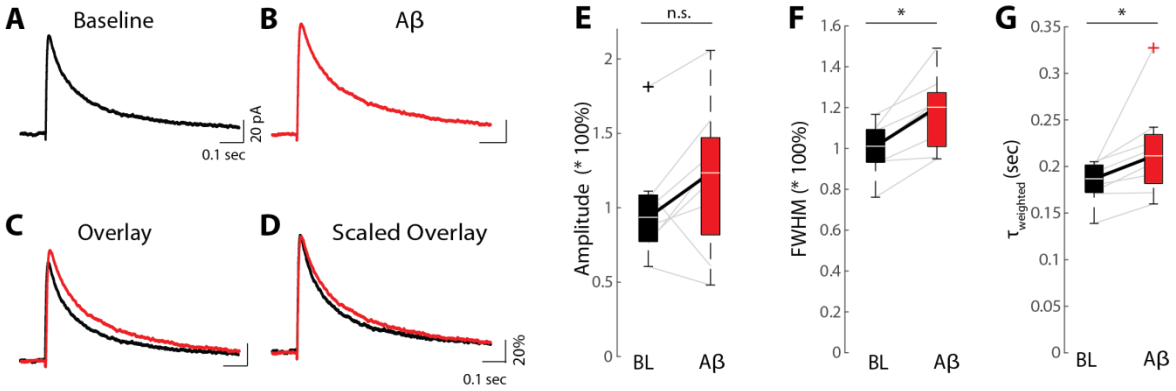

Fig. 36: Aβ prolongs the decay time of the NMDAR-EPSC in acute hippocampal slices. *A, B)* Average of the synaptically evoked NMDAR-EPSC of one representative hippocampal CA1 neuron from a wild-type mouse for baseline (*A*) and Aβ (500 nM) superfusion (*B*). *C, D)* Overlay (*C*) and scaled overlay (*D*) of the traces in *A* and *B*. E-G) Boxplot of the normalized EPSC amplitudes (*E*), normalized FWHM (*F*) and $\tau_{weighted}$ (*G*) for baseline (left) and Aβ superfusion conditions (right, n = 8). Each grey line represents one cell; the thick black line depicts the median. n.s. not significant, *p < 0.05. Wilcoxon signed rank test

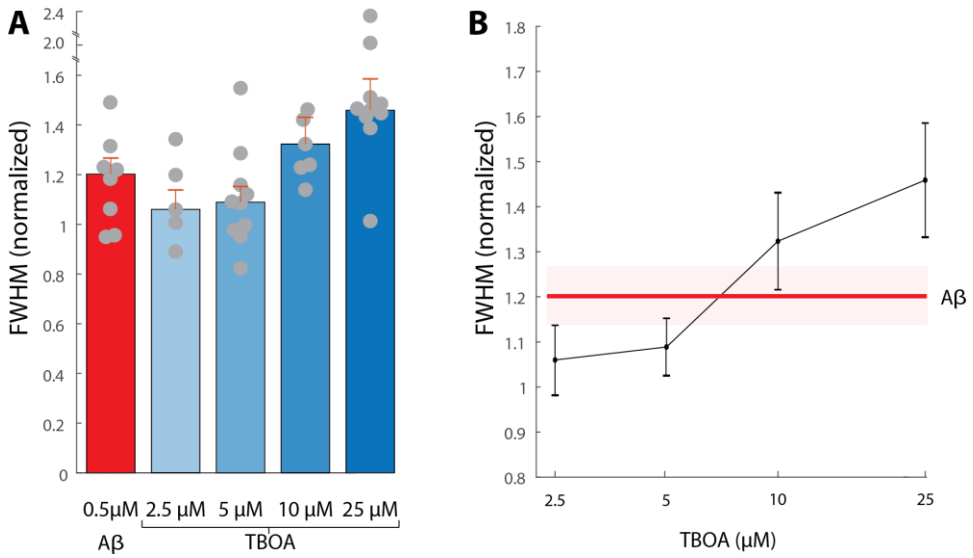

Fig. 37: Estimation of the TBOA concentration which has the same effect as 500 nM Aβ. *A)* Bar graph of the normalized FWHM of the synaptically evoked NMDAR-EPSC after the superfusion of 500nM Aβ dimer (n = 8), 2.5 µM TBOA (n = 5), 5µM TBOA (n = 9), 10 µM TBOA (n = 7) and 25µM TBOA (n = 9). Each dot represents the mean of one neuron. The error bars indicate SEM. *B)* Semi-logarithmic plot of the concentration of TBOA and its effect on the FWHM (mean ± SEM). The red line and red shaded area indicate the mean and SEM of the Aβ-dependent effect on the FWHM

3.3.5 Aβ does not affect the presynaptic glutamate release

An increase in extracellular glutamate could not only be caused by an impairment of the glutamate uptake, but also by an increase in glutamate release from presynaptic sites. Thus, we next examined whether an increase of the presynaptic glutamate release could contribute to the observed effects. In order to determine, whether Aβ changed the release probability of glutamate at the presynaptic site, we performed paired pulse facilitation (PPF) experiments. When a synapse is stimulated twice in rapid succession (10 – 200 msec), the second stimulus typically leads to an enhanced postsynaptic EPSC, typically presenting as an increase in the paired pulse ratio (PPR)[10] (Thomson 2000, Zucker & Regehr 2002). The mechanism of PPF is thought to be based on residual Ca^{2+} in the presynapse, leading to the exocytosis of larger quantities of glutamate (Fioravante & Regehr 2011). The PPR is altered

[10] A full description of how the PPR is calculated can be found in the methods section

after pharmacological manipulations which change the release property of glutamate at the presynapse but is unaffected by manipulations at the postsynaptic site (Manabe et al 1993). In consequence, PPF can be viewed as a sensitive tool to detect changes in the release probability of glutamate at the presynaptic site.

I performed these experiments in collaboration with Hsing-Jung Chen. We induced PPF in slices that were perfused with ACSF (n = 8 cells), ACSF containing 500 nM Aβ dimer (n = 8 cells) or 5 µM TBOA (n = 5 cells). We observed similar levels of potentiation for all three conditions at an inter-stimulus interval of 200 msec (**Fig. 38 A, B, C**). PPF is expected to be more pronounced when the two pulses are delivered within very short succession (<100 msec) and the PPR is expected to decrease as a function of the length of the inter-pulse intervals (Wu & Saggau 1994). Thus, we also performed PPF at different inter-pulse intervals ranging from 30 to 500 milliseconds. As expected, the PPR was larger than one for short inter-pulse intervals and decayed towards one with increasing intervals (**Fig. 38 D**). We did, however, not detect any difference when the slice was superfused with ACSF, Aβ or TBOA for all of the tested intervals (30 msec, $p = 0.36$; 50 msec, $p = 0.46$; 100 msec, $p = 0.80$; 200 msec, $p = 0.77$; 500 msec, $p = 0.39$). Thus, we found no evidence that Aβ or TBOA significantly alter the release probability of glutamate at the presynaptic site and conclude that the observed increases in the decay times of the NMDAR-EPSC were rather caused by an inhibition of glutamate uptake. These results were not surprising, since many previous studies did not report any change in PPF after the application of other Aβ preparations (Cerpa et al 2010, Li et al 2009, Schmid et al 2008, Shankar et al 2008, Talantova et al 2013, Zhao et al 2018).

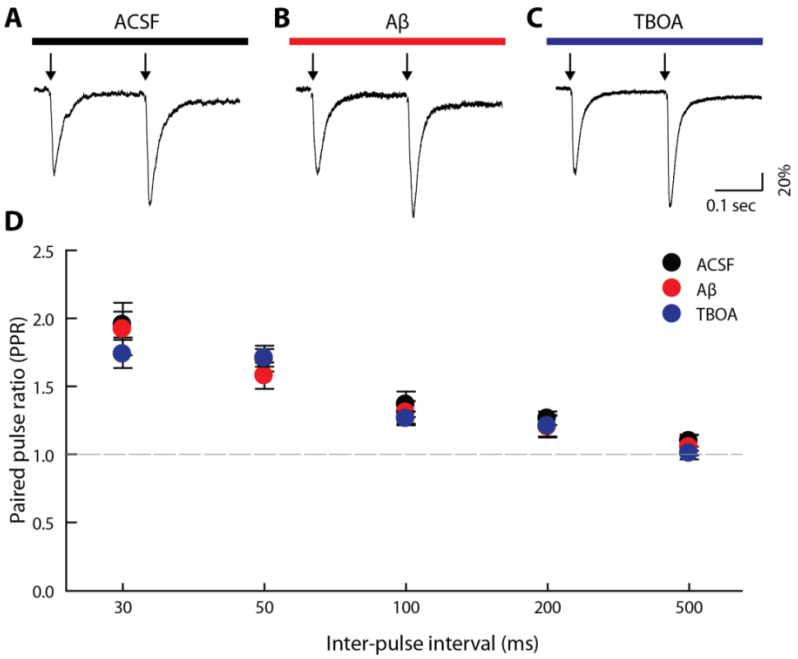

Fig. 38: Aβ or TBOA superfusion have no impact on the paired pulse ratio (PPR) at Schaffer collateral – CA1 synapses. *A-C)* Average EPSCs recorded from *in vitro* CA1 pyramidal neurons during paired pulse stimulation of the Schaffer collateral pathway with an inter-pulse interval of 200 msec (arrows). The superfusion of ACSF (*A*), 500 nM Aβ (*B*) or 5 µM TBOA (*C*) is indicated by the colored bars on the top. D) Paired pulse ratio (PPR) for inter-pulse intervals ranging from 30 to 500 msec for cells superfused with ACSF (black, n = 8), Aβ (red, n = 8) or TBOA (blue, n = 5). Error bars denote SEM. The differences between the three applications are not significant for all inter-pulse intervals. Kruskal Wallis test

3.4 Aβ from human AD patients induces neuronal hyperactivity *in vivo*

When working with soluble Aβ, it is important to choose the Aβ preparation with great care. In the first part of my thesis, I only used the synthetic Aβ 1-40 S26C dimer, (Shankar et al 2008). Thus I next tested whether the results obtained so far can also be reproduced with Aβ which has been derived from human AD brains. In the following experiments, I investigated whether brain extract obtained from a patient suffering from sporadic AD (hence called AD extract) had the same hyperactivity-inducing effect as the synthetic dimer (**Fig. 39**). The Aβ was extracted from post-mortem brain tissue via homogenization and centrifugation (Barry et al 2011, Hong et al 2018, Shankar et al 2008, Wang et al 2017). Since this homogenate contains many forms of Aβ, it is hard to quantify the Aβ concentration of the sample, but western blot analysis revealed that it contained 0.2 ng/ml Aβx-42 before and 3.3 ng/ml Aβx-

42 after denaturation of the oligomers with guanidium chloride. The AD extract was pressure applied *in vivo* in the CA1 hippocampal region of wild-type mice, the same way as the dimer had been applied in the above experiments. Remarkably, the targeted application of AD extract robustly increased the neuronal activity in all mice (**Fig. 39**, N = 6, p = 0.031). To prove that the hyperactivity-inducing effect of the AD extract is attributable to Aβ, I next performed control experiments with brain extracts from the same AD patient, in which only the Aβ had been removed by immunodepletion with Aβ antibodies (Hong et al 2018, Jin et al 2018). The application of this immunodepleted extract (hence called ID extract) had no effect on the number of neuronal Ca^{2+}-transients (**Fig. 40 B**, N = 5) and I observed a significant difference between the normalized effect on neuronal activity for both extracts (**Fig. 40 C**, p = 0.0043). To test, whether the effect of the AD extract was activity-dependent, I next repeated the application in the hippocampus of mice, in which the baseline activity had been blocked by the superfusion of 50 µM D-APV and CNQX (**Fig. 40**). Just like the Aβ dimer (**Fig. 22**), the application of the AD extract did not induce hyperactivity in the absence of baseline activity (**Fig. 41** N = 5, p = 0.25). Thus, I conclude that human brain extract induces neuronal hyperactivity in an activity-dependent manner.

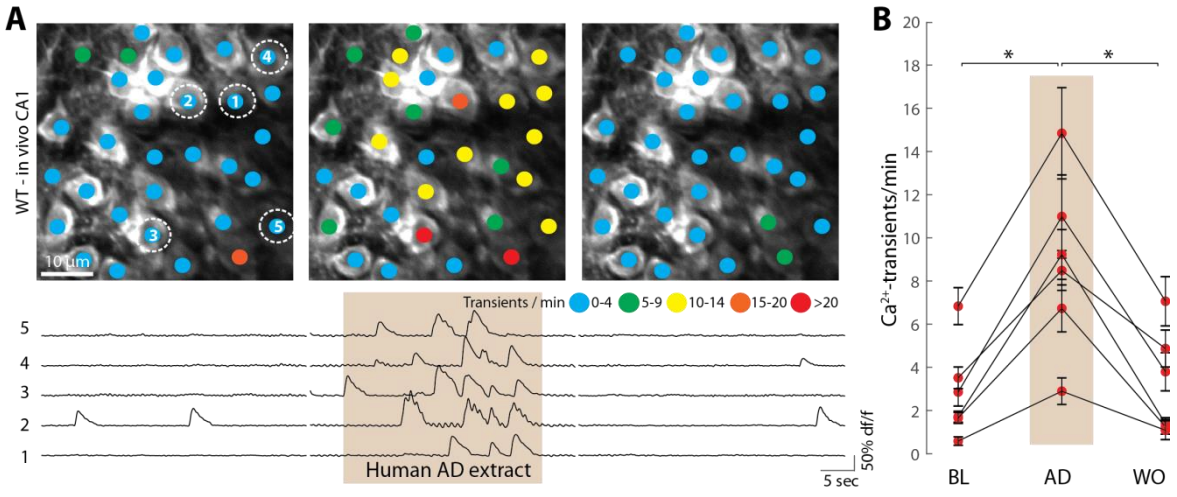

Fig. 39: Human AD extract induces neuronal hyperactivity *in vivo*. *A)* Top: representative two-photon image of the hippocampal CA1 region of a wild-type mouse for baseline (left), AD extract application

(middle) and washout (right) conditions. The colored dots on the neurons represent the number of Ca^{2+}-transients per minute. Bottom: Ca^{2+}-traces of the circled neurons. The brown shaded area represents the time of AD extract application. *B)* Summary data for N = 6 mice. Each dot represents the mean number of Ca^{2+}-transients per minute for all neurons in one mouse under baseline (BL), AD extract application and washout (WO) conditions. Error bars denote SEM, * $p < 0.05$, Wilcoxon signed rank test

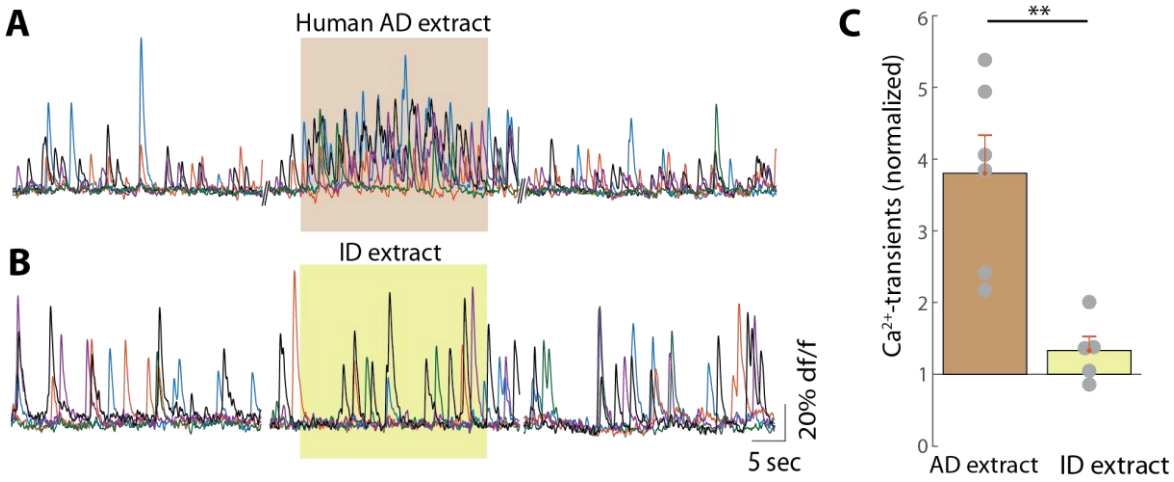

Fig. 40: Human ID extract does not induce neuronal hyperactivity *in vivo*. *A)* Ca^{2+}-traces from five representative hippocampal CA1 neurons of a wild-type mouse for baseline (left), AD extract application (middle) and washout (right) conditions. *B)* Same as in *A*, but for the application of ID extract. The green shaded area represents the time of ID extract application. *C)* Normalized change of activity for the application of AD extract (left, N = 6) and ID extract (right, N = 5). Each dot represents the mean for all neurons in one mouse. Error bars denote SEM, ** $p < 0.005$, Wilcoxon rank sum test

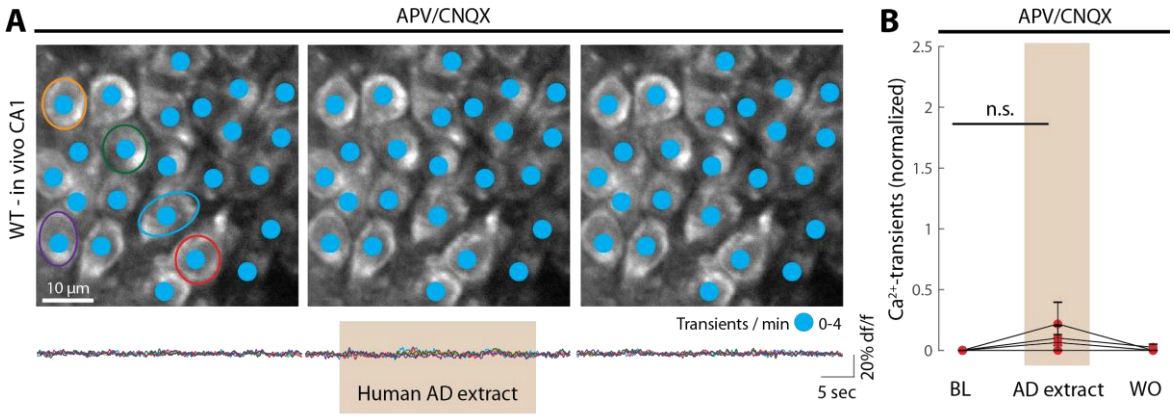

Fig. 41: The application of D-APV and CNQX prevents the AD extract-induced neuronal hyperactivity *in vivo*. *A)* Top: representative two-photon image of the hippocampal CA1 region from a wild-type (WT) mouse during the superfusion of D-APV and CNQX for baseline (left), AD extract-application

(middle) and washout (right) conditions. The colored dots on the neurons represent the number of Ca^{2+}-transients per minute. Bottom: Overlay of the Ca^{2+}-traces from the five circled neurons. The brown shaded area represents the time of AD extract application. *B)* Summary data for N = 5 mice. Each dot represents the mean number of Ca^{2+}-transients per minute for all neurons in one mouse under baseline (BL), AD extract and washout (WO) conditions. Error bars denote SEM, n.s. not significant, Wilcoxon signed rank test

Next, I turned my attention to the question which of the Aβ species in the brain of AD patients is responsible for inducing neuronal hyperactivity. Various studies of synaptic plasticity have reported that especially LMW oligomers and dimers are highly toxic, while monomers as well as larger assemblies were inefficient in impairing LTP or inducing LTD (Cleary et al 2004, Lesné et al 2006, Shankar et al 2008, Yang et al 2017). Because of the remarkable effect of synthetic dimers (see above), I next tested the effects of Aβ dimers which had been derived from the post-mortem brains of AD patients. The application of these human Aβ dimers (200 ng/ml)[11] potently induced neuronal hyperactivity in murine hippocampal CA1 pyramidal neurons *in vivo* (**Fig. 42**, N = 6, p = 0.031). The analysis of the activity changes on a single cell level revealed that the effect of the synthetic and the human Aβ dimers were remarkably similar (**Fig. 43**). Just as the synthetic dimers (**Fig. 11**), the application of human dimers increased neuronal activity in the majority of neurons (80 %, 188/235 cells), decreased the activity in only 2% (5/235) and left 18% (42/235) unchanged (**Fig. 43 A**). The median increase of activity was +6 Ca^{2+}-transients/min. Moreover, linear regression analysis revealed a strong dependence of the Aβ-induced activity on the baseline activity (**Fig. 43 B**, $R^2 = 0.77$).

[11] It is impossible to calculate the exact molar concentration of Aβ in this solution containing a mix of different peptides. An approximation can however be found in the methods section.

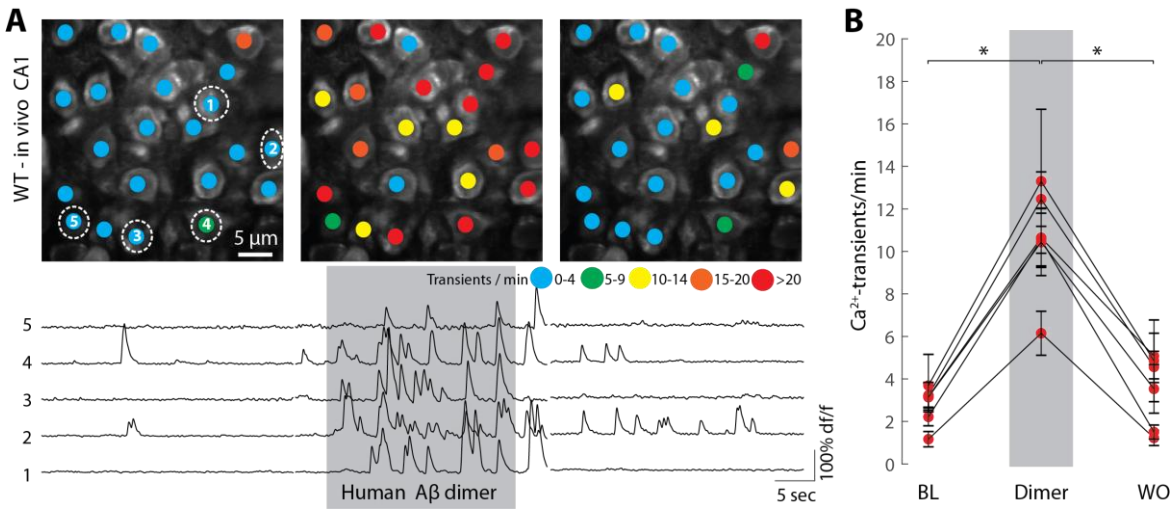

Fig. 42: Aβ dimers isolated from human brain induce neuronal hyperactivity *in vivo*. *A)* Top: representative two-photon image of the hippocampal CA1 region of a wild-type mouse for baseline (left), human Aβ dimer application (middle) and washout (right) conditions. The colored dots on the neurons represent the number of Ca^{2+}-transients per minute. Bottom: Ca^{2+}-traces for the circled neurons. The grey shaded area represents the time of AD extract application. *B)* Summary data for N = 6 mice. Each dot represents the mean number of Ca^{2+}-transients per minute for all neurons in one mouse under baseline (BL), human Aβ dimer applicaion and washout (WO) conditions. Error bars denote SEM, * $p < 0.05$, Wilcoxon signed rank test

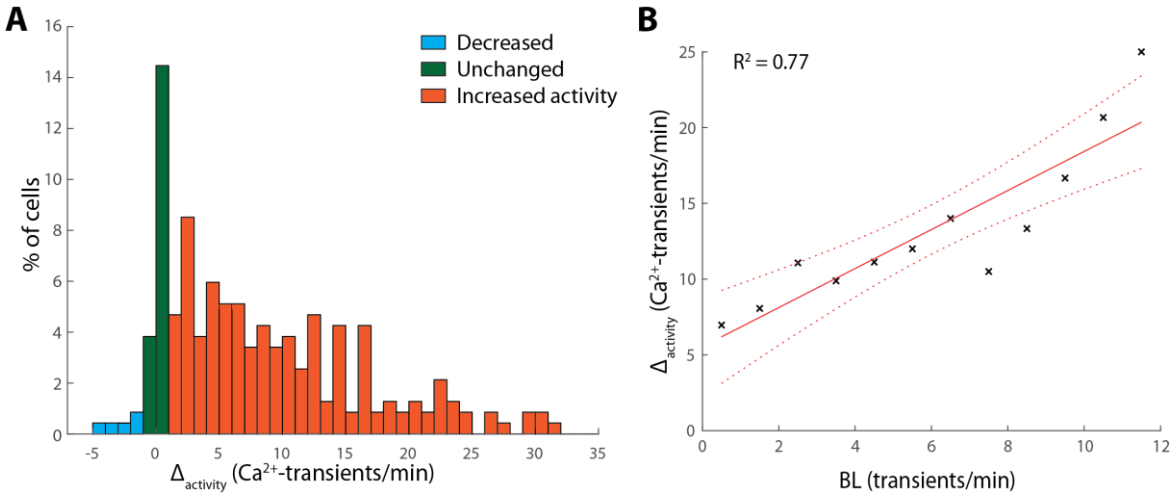

Fig. 43: Analysis of the human Aβ dimer-induced neuronal hyperactivity *in vivo*. *A)* Histogram of the difference in activity between human Aβ dimer application and baseline conditions ($\Delta_{activity}$) for n = 235 cells. *B)* Linear regression analysis of the average difference of activity ($\Delta_{activity}$) compared to baseline activity

To test whether the hyperactivity-inducing effect was specific for dimers, I next applied similar concentrations (200 ng/ml)[12] of isolated human monomers from the same AD patients. As shown in **Fig. 44**, the application of Aβ monomers *in vivo* only had a small, yet significant effect of increasing the neuronal activity (N = 6, p = 0.031). Whether this minor change in neuronal activity is due to a small effect of monomeric Aβ or whether the hydrophobic Aβ monomers start to aggregate in the application pipette once they are dissolved in ACSF, remains unclear. A closer analysis of the activity changes on a single-cell level revealed that the small increase of activity triggered by the application of Aβ monomers was due to a small number of neurons with relatively strong increases of their firing rate as opposed to a general right-shift of the neuronal activity (**Fig. 45 A**). Thus, the application of human Aβ monomers did not change the activity in 53% (100/189) of cells, while 30% (56/189) of the cells had increased and 17% (33/189) decreased activities compared to baseline conditions. The median activity change was 0.0. Also, the application of the human Aβ dimers had a much stronger effect than the application of the monomers (**Fig. 45 B,** p = 0.0039).

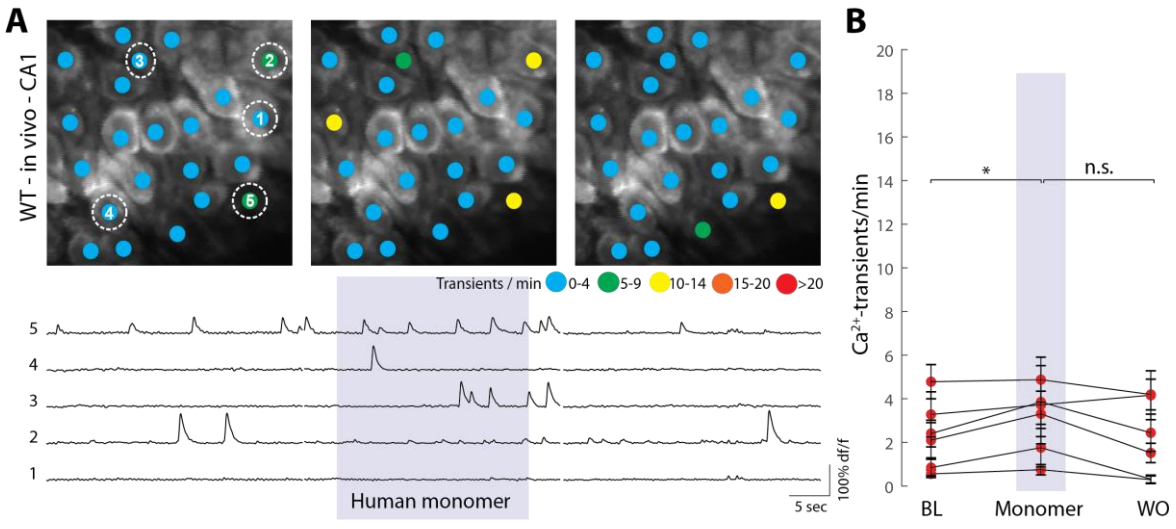

Fig. 44: Aβ monomers isolated from human brain slightly increase the neuronal activity *in vivo*. *A)* Top: representative two-photon image of the hippocampal CA1 region of a wild-type mouse for

[12] It is impossible to calculate the exact molar concentration of Aβ in this solution containing a mix of different peptides. An approximation can however be found in the methods section.

baseline (left), human Aβ monomer application (middle) and washout (right) conditions. The colored dots on the neurons represent the number of Ca^{2+}-transients per minute. Bottom: Ca^{2+}-traces for the circled neurons. The purple shaded area represents the time of AD extract application. B) Summary data for N = 6 mice. Each dot represents the mean number of Ca^{2+}-transients per minute for all neurons in one mouse under baseline (BL), human Aβ monomer and washout (WO) conditions. Error bars denote SEM, * $p < 0.05$, Wilcoxon signed rank test

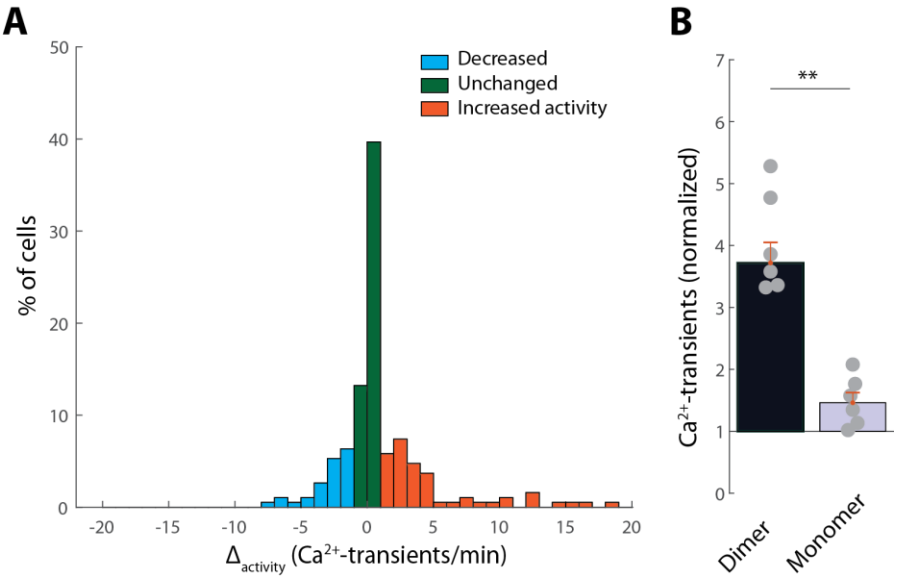

Fig. 45: The hyperactivity-inducing effect of human Aβ dimers *in vivo* is much stronger than that of monomers. *A)* Histogram of the difference in activity between human Aβ monomer application and baseline conditions ($\Delta_{activity}$) for n = 189 cells. *B)* Normalized activity change for the application of human Aβ dimers (left, N = 6) and human Aβ monomers (right, N = 6). Each dot represents the mean number of one mouse. Error bars denote SEM, ** $p< 0.005$, Wilcoxon rank sum test

Finally, I asked, whether the effect of human Aβ could be observed at physiological Aβ levels. One prominent point of criticism when working with soluble Aβ is that in most application studies, authors typically apply Aβ concentrations in the high nanomolar or even low micromolar range (Selkoe 2008), while the concentration of soluble Aβ in the brains of AD patients was reported to be in the low picomolar range (Moore et al 2012) with similar levels in mouse models of AD (Keskin et al 2017). Thus, I applied the human Aβ dimers in decreasing concentrations ranging from 200 ng/ml to 5 ng/ml. Remarkably, the application of 20 ng/ml Aβ dimer still had a stronger effect than the application of 200 ng/ml Aβ

monomer or vehicle (**Fig. 46**). These findings demonstrate that human Aβ dimers increase neuronal activity even at very low concentrations.

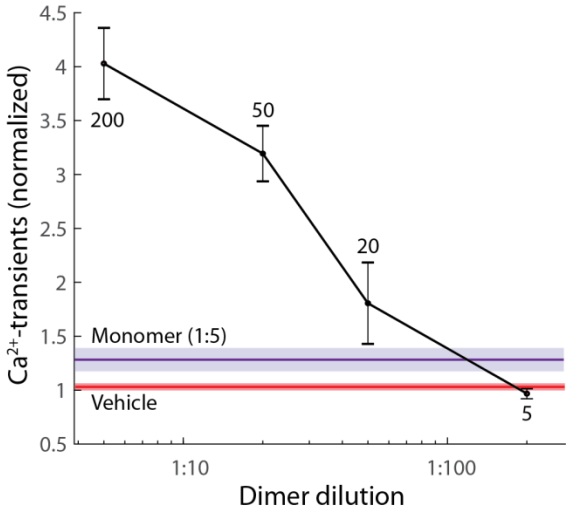

Fig. 46: Low concentrations of human Aβ dimers induce neuronal hyperactivity. Semi-logarithmic plot of the human Aβ dimer-induced increase in neuronal activity (black line). The numbers indicate the concentration of human Aβ dimer in ng/ml (200, N = 7; 50, N = 7; 20, N = 3; 5, N = 3). The purple line and shaded area indicate the effect of 200 ng/ml of monomers (mean ± SEM, N = 7). The red line and shaded area indicate the effect of vehicle applications (mean ± SEM, N = 3). Error bars denote SEM

4 Discussion

A huge body of literature on pathological changes in the brain of AD patients is available. However, we are only beginning to understand the exact disease-associated impairments of neuronal and circuit function. Multimodal imaging studies in humans facilitate the identification of brain regions which are especially susceptible to AD-induced alterations and the analysis of mouse models helps us to understand the underlying cellular pathology. Accumulating evidence, both from observations in mouse models and humans, indicates that an early dysfunction in AD is the Aβ-dependent hyperactivity in a subset of neurons. However, the cellular mechanism(s) of this hyperactivity have thus far remained unknown. In my graduate work, I have addressed this question in several Aβ application experiments, both *in vivo* and *in vitro.* I provide substantial evidence that a vicious cycle of Aβ-dependent neuronal hyperactivation which is driven by an impairment of glutamate uptake is a linchpin of the Aβ-induced neuronal dysfunction.

4.1 Baseline-activity dependence of the Aβ-induced neuronal hyperactivity

Previously, the Konnerth laboratory demonstrated that neuronal hyperactivity in the APP23 x PS45 transgenic mouse model of AD does not affect all brain circuits at the same time. More precisely, neuronal hyperactivity could be found in the hippocampus of young transgenic mice at an age at which the activity in cortical layer 2/3 was still comparable to wild-type mice. In 6-10 month old transgenic mice, on the other hand, neuronal hyperactivity was detected in the both of these regions (Busche et al 2012, Busche et al 2008). At the time, it was not clear whether this was due to a difference in Aβ concentrations or due to brain regions' distinct susceptibilities to Aβ. My results now offer, for the first time, an explanation

for the lack of layer 2/3 hyperactivity in young AD mice. I demonstrated that, in isoflurane anesthetized young wild-type mice, hippocampal CA1 neurons were susceptible to Aβ-induced hyperactivity (**Fig. 9**), while Aβ application in cortical layer 2/3 had no effect on the neuronal activity. Moreover, the application of Aβ in cortical layer 5 readily induced neuronal hyperactivity (**Fig. 25, 26**). What causes this surprising difference in susceptibility to Aβ-induced neuronal dysfunctions? One of the major differences between those brain areas is their frequency of Ca^{2+} transients under baseline conditions, which is high in hippocampal CA1 and cortical layer 5, and lower in cortical layer 2/3. In consequence, I hypothesized that the lower spontaneous baseline activity of layer 2/3 is not sufficient to render this area susceptible to the Aβ-induced neuronal hyperactivation. I could establish a mechanistic link between baseline activity and susceptibility to Aβ in a series of *in vivo* and *in vitro* experiments in the hippocampal CA1 area. Remarkably, Aβ application in hippocampal slices only induced neuronal hyperactivity after the baseline activity of those slices had been pharmacologically raised to levels of activity observed *in vivo* (**Fig. 14-19**). This could be achieved by increasing the extracellular potassium levels, by blocking GABAergic inhibition with bicuculline or by applying glutamate. Conversely, the hyperactivity-inducing effect of Aβ in the CA1 area *in vivo* could be prevented by abolishing neuronal baseline activity in the CA1 area by pharmacological manipulations including the block of excitatory synaptic transmission with D-APV and CNQX or the block of neuronal spiking with TTX (**Fig. 22, 23**). Moreover, linear regression analysis suggests that, on a single cell level, the baseline activity of the respective neuron determines its susceptibility to Aβ-induced dysfunctions, both for synthetic and human Aβ (**Fig. 11, 43**). Due to these observations, I hypothesize that the baseline activity of layer 2/3 is not high enough to allow for Aβ-induced hyperactivation *in vivo*, as opposed to cortical layer 5 and the hippocampal CA1 region. The remaining question is why the cortical layer 2/3 of older transgenic mice is susceptible to Aβ-induced dysfunctions (Busche et al 2008). A possible explanation could be that neuronal activity levels

increase with aging. Indeed, a tendency towards higher neuronal activity levels was reported for aged wild-type mice in the hippocampus (Wilson et al 2005) as well as cortical layer 2/3 (Lerdkrai et al 2018). It was beyond the scope of this study to verify whether the increased neuronal activity in aged mice is can make neurons in cortical layer 2/3 prone to Aβ-dependent hyperactivation.

What are the implications of the observed activity dependence for human AD cases? *In vivo* imaging studies of AD patients have revealed that early functional impairments of brain circuits can be detected in some brain regions before others (Brier et al 2014, Drzezga et al 2011, Jones et al 2016). More specifically, the hippocampus and certain cortical areas (together referred to as the DMN) show functional impairments at very early disease stages when other brain regions are still largely unaffected (Palop & Mucke 2016, Sperling et al 2010, Zott et al 2018)[13]. The exceptional susceptibility of the hippocampus and the DMN to AD-induced pathology is likely not just a consequence of Aβ production, since the expression patterns of APP, BACE and γ-secretase do not offer a satisfactory explanation (Bero et al 2011, Goedert 1987, Lahiri & Ge 2004). Instead, higher levels of neuronal connectivity (Buckner et al 2008, Utevsky et al 2014) and baseline activity (Buckner et al 2005, Lustig et al 2003) compared to other brain regions could put them at the center of the disease process. Similar to mice, healthy aging in humans is typically associated with higher neuronal baseline activity levels. During healthy aging, many genes involving GABAergic inhibition are downregulated (Loerch et al 2008), which in turn could lead to increased levels of activity compared to young adults (Bishop et al 2010). Moreover, in memory tests, aged patients usually recruit more brain areas (Cabeza et al 2002) and show higher levels of activation (Yassa et al 2011). In consequence, as humans age, some of their brain regions get more active, which might make them more prone to Aβ-dependent neuronal dysfunctions such as

[13] A detailed description of the functional impairments in the brains of AD patients can be found in chapter 1.1.3.

neuronal hyperactivity. In consequence, persons with elevated Aβ brain levels might start to develop AD-specific network dysfunctions once the activity status of certain brain areas reaches critical levels.

4.2 Impaired glutamate uptake as a cellular mechanism for the Aβ-induced neuronal hyperactivity

In my thesis, I have provided compelling evidence that soluble Aβ increases the extracellular glutamate concentration by an inhibition of glutamate uptake. Accordingly, the hyperactivity-inducing effects of Aβ *in vivo* were blocked by a simultaneous application of the glutamate receptor antagonists D-APV and CNQX (**Fig. 22**). In slices that were superfused with bicuculline, Aβ increased the neuronal activity almost exclusively in neurons with preceding baseline activity. In the presence of glutamate, on the other hand, Aβ was able to also induce hyperactivity in neurons which had previously been silent. These findings indicate that Aβ is more potent in the presence of glutamate (**Fig. 20, 21)**. The most convincing line of evidence, however, is based on the observation that the glutamate uptake blocker TBOA has similar effects as Aβ, both *in vivo* and *in vitro*. The application of TBOA could induce neuronal hyperactivity *in vivo* and thus mimic the effects of Aβ (**Fig. 29**). Moreover, the TBOA effects were less pronounced in mouse models of AD (**Fig. 33, 34**), suggesting that the TBOA action was saturated, potentially due to a preexisting glutamate uptake inhibition by the increased levels of intrinsic soluble Aβ in these mice. Next we asked whether Aβ and TBOA acted on a similar mechanism *in vitro*. The application of TBOA in hippocampal slices was repeatedly reported to lead to an increased decay time of the NMDAR-EPSC (Arnth-Jensen et al 2002, Jabaudon et al 1999, Nie & Weng 2009), which was attributed to an increased dwell-time of glutamate in or around the synaptic cleft. Our experiments revealed that Aβ and TBOA indeed have similar effects on the NMDAR-EPSC and both increase the decay-time of the current without significantly affecting the amplitude (**Fig. 35, 36**). Finally, PPF experiments

confirmed that Aβ did not change the presynaptic release property of glutamate (**Fig. 38**). Together, these findings demonstrate that the Aβ-induced neuronal hyperactivation is mainly caused by an Aβ-dependent inhibition of glutamate uptake.

Evidence for impaired glutamate uptake in AD patients and mouse models

Unlike other neurotransmitters, glutamate cannot be enzymatically degraded in the extracellular space. In consequence, the glutamate dependent signaling process has to be terminated by removal from the synaptic cleft by neuronal and astrocytic uptake mechanisms (Danbolt 2001). Some synapses can transmit individual signals up to a frequency of 100 Hz. Accordingly, the uptake mechanisms have to act very fast. Indeed, glutamate uptake transporters limit the dwell-time of glutamate in the synaptic cleft to a few milliseconds (Clements et al 1992) and keep the extrasynaptic concentration of glutamate at levels below 1 µM (De Bundel et al 2011). There are five excitatory amino acid transporters (EAATs) in the brain, out of which EAAT1 (or GLAST in rodents) and EAAT2 (or GLT-1 in rodents) are primarily expressed in Astrocytes, while EAAT3 is usually found in neurons, and the other two only play minor roles (Zhou & Danbolt 2014). Electron microscopy studies have revealed that glutamatergic synapses are tightly wrapped in astrocytic membrane, forming a "tripartite synapse" (Perea et al 2009) which consists of the presynaptic terminal, the postsynapse and the ensheathing astrocytic membrane. In consequence, 90% of the glutamate uptake in the brain is attributed to the predominantly astrocytic EAAT2 (Kim et al 2011).

Over the last years, accumulating evidence has pointed to an impairment of glutamate uptake in AD. Thus, post-mortem studies have reported decreased levels and impaired functionality of EAAT2 in patients suffering from AD (Li et al 1997, Masliah et al 1996, Scott et al 2011). Additionally, AD patients have lower levels of the vesicular glutamate transporter, which is required to transport glutamate into presynaptic vesicles (Kashani et al

2008, Kirvell et al 2006). An impairment of glutamate uptake has also been reported in mouse models of AD. Levels of GLT-1 protein expression were reported to be decreased in aged mice of multiple mouse models of AD but normal in young AD mice (Hefendehl et al 2016, Schallier et al 2011, Takahashi et al 2015, Zumkehr et al 2015). Previously, advances in protein engineering have enabled the rapid and sensitive detection of glutamate in the brain using fluorescence microscopy (Marvin et al 2013) and recently, the group of Timothy Murphy reported an impairment of glutamate transients around cortical amyloid plaques (Hefendehl et al 2016).

In line with the findings in mouse models of AD, multiple studies have demonstrated that the acute exposure to Aβ is sufficient to impair glutamate transporter function. First studies in which full-length Aβ or fractions thereof were applied on cultured astrocytes impaired glutamate uptake following incubation times ranging from multiple days (Parpura-Gill et al 1997) to as little as 30 minutes (Fernández-Tomé et al 2004, Harris et al 1996), but see also (Abe & Misawa 2003, Rodriguez-Kern et al 2003). Furthermore, the application of Aβ onto hippocampal slices was reported to promote the mislocalization of GLT1 (Scimemi et al 2013). The most convincing evidence, however, comes from the group of Dennis Selkoe. They demonstrated that many different preparations of Aβ (including synthetic dimers oligomers as well as Aβ derived from CHO cells and human Aβ) impaired LTP and boosted LTD in the Schaffer collateral CA1 pathway of the hippocampus. Strikingly, the Aβ-induced effects on LTP and LTD could be mimicked by TBOA (Li et al 2009, Li et al 2011). Moreover, they investigated the effect of TBOA or Aβ on the NMDAR-EPSC. In line with my work (**Fig. 36**), these authors observed a prolongation of the EPSC after Aβ application (Li et al 2009). However, in contrast to my findings, they also reported a strong decrease of the NMDAR-EPSC amplitude. These discrepancies might be explained by the use of different Aβ preparations containing dissimilar species and/or doses of Aβ. It is important to note that, in our hands, the application of low doses of TBOA (5 µM) had no effect on the EPSC amplitude

(**Fig. 35**). The main conclusion of the two papers from the Selkoe group was that Aβ-dependent impairment of glutamate uptake led to spill over of glutamate and, in consequence, an activation of (predominantly extrasynaptic) NMDA receptors containing the NR2B subunit (Li et al 2011). However, the Selkoe group could not provide evidence that this impairment was relevant for the neuronal function *in vivo*. My data now demonstrates that the Aβ-dependent uptake inhibition of glutamate triggers substantial neuronal hyperactivity in the brain of wildtype mice and indicates by occlusion experiments that also the chronic presence of Aβ in the brain of AD mice inhibits glutamate uptake.

One of the surprising findings of my graduate work is that GABAergic signaling is unlikely to be the trigger of the observed Aβ-dependent neuronal hyperactivity. In theory, the Aβ-induced shift of the E/I balance towards excitation could be based on two factors: increased excitation and/or decreased inhibition (Busche & Konnerth 2016). While the results from my graduate work clearly indicate a strong role for the excitatory neurotransmitter glutamate, there was no evidence for a major contribution of the inhibitory system. Thus, the effect of Aβ was entirely blocked by a co-application of the glutamatergic antagonists D-APV and CNQX (**Fig. 27**) in the absence of GABA-receptor blockers. Moreover, Aβ still increased neuronal activity in slices that had been superfused with high doses of the receptor-antagonist bicuculline, which should lead to a complete block of $GABA_A$ receptors (Nowak et al 1982). Together, these findings render a major contribution of GABAergic inhibition on the observed Aβ-induced neuronal hyperactivity rather unlikely. This conclusion might be surprising, since neuronal hyperexcitability in mouse models of AD has repeatedly been attributed to an impairment of GABAergic interneurons (Martinez-Losa et al 2018, Palop & Mucke 2016, Schmid et al 2016, Verret et al 2012). Moreover, previous work from the Konnerth laboratory demonstrated that the neuronal hyperactivity in mouse models of AD was associated with a relative decrease in inhibition and that enhancing the GABAergic tone could restore the neuronal activity (Busche et al 2008). However, these results do not

exclude that the initial increase in activity was caused by an accumulation of glutamate and that enhancing the GABAergic tone merely restored the E/I balance. Moreover, since all these studies were performed in mouse models of AD, it is possible that the observed interneuron dysfunction is a chronic effect of the disease in transgenic mice and develops independently from the glutamate accumulation.

Does Aβ affect glutamate release?

In order to test whether Aβ also had an effect on presynaptic glutamate release, we performed PPF experiments (**Fig. 38**)[14]. In these experiments, neither Aβ nor TBOA induced a significant change of the PPR. These findings are in line with observations from several other groups indicating that the application of soluble Aβ does not change the release probability of glutamate (Cerpa et al 2010, Li et al 2009, Schmid et al 2008, Shankar et al 2008, Talantova et al 2013, Zhao et al 2018). On the other hand, few authors have reported an Aβ-dependent change in glutamate release (Bobich et al 2004, Kabogo et al 2010). The vast majority of the authors that have performed PPF in transgenic mouse models of AD reported no or only minor differences to wild-type mice (Marchetti & Marie 2011), but see also (Davis et al 2014).

Another source of excess glutamate in AD could be release from astrocytes. The application of soluble Aβ in astrocytic cell cultures can increase the extracellular glutamate concentration (Sanz-Blasco et al 2016, Talantova et al 2013). However, the authors did not address whether the inhibition of glutamate uptake contributed to their observations. Also, it remains to be determined whether glutamate release from astrocytes is pathologically relevant (Acosta et al 2017).

[14] A more detailed description of the physiological background of PPF experiments can be found in chapter 3.3.5.

Long-term toxicity of glutamate accumulation

Besides neuronal hyperactivity, an Aβ-induced block of glutamate uptake and the resulting glutamate accumulation could also have other long-term effects in AD mice and patients. Indeed, a chronic increase in glutamate due to knock-out (Tanaka et al 1997, Watase et al 1998) or inhibition (Rothstein et al 1996) of EAATs led to behavioral impairments, epilepsy and, in many cases, neuronal loss in mice. In line with these findings, the injection of TBOA into the CSF of rats caused marked neurodegeneration (McBean & Roberts 1985). Moreover, a transgenic mouse line overexpressing Glud1, a gene involved in glutamate synthesis, displayed hippocampal cell loss and impaired LTP at the age of 12-20 months. The extracellular glutamate concentration was only increased by 10% in these mice (Bao et al 2009). Remarkably, these phenotypes developed in the absence of AD-related pathological changes, indicating that an extracellular glutamate accumulation could contribute to the loss of neurons and synapses as well as memory impairments in AD patients independently from the underlying disease.

4.3 The molecular mechanism of the Aβ-dependent impairment of glutamate uptake

Even though it is beyond the scope of this thesis, it will be important to understand the molecular mechanism of the Aβ-dependent inhibition of glutamate uptake. Since the hyperactivity-inducing effect of Aβ was almost immediate (**Fig. 12**), the interaction between Aβ and the impairment of glutamate uptake has to be rather fast. Thus, the downregulation of EAAT2/GLT-1 numbers, as observed in AD patients and mice (Hefendehl et al 2016, Li et al 1997, Masliah et al 1996, Schallier et al 2011, Scott et al 2011, Takahashi et al 2015, Zumkehr et al 2015), is unlikely to be the only mechanism. Rather, Aβ could impair the functions of glutamate transporters on the cell membrane by direct or indirect interaction. Unlike for

TBOA (Boudker et al 2007), a binding site for Aβ has, to my knowledge, not been described in the literature. One possible mechanism could be an Aβ-dependent impairment of transporter mobility. It was recently reported that GLT-1 is highly mobile on the cell membrane and that this mobility is necessary for an efficient uptake of glutamate from the synaptic cleft (Murphy-Royal et al 2015). In consequence, it is tempting to speculate that Aβ might interfere with this lateral mobility. Indeed, Aβ has been reported to inhibit the lateral mobility of mGluR5 on the cell membrane (Renner et al 2010). Moreover, this hypothesis would be compatible with my findings. Even though the application of Aβ or TBOA led to very similar results *in vivo* (**Fig. 29**) and *in vitro*, (**Fig. 36-38**), the TBOA effect was not fully saturated in mouse models of AD with high intrinsic levels of Aβ (**Fig. 33, 34**), indicating that Aβ and TBOA might interact with different properties of glutamate transport. However, further experiments to determine the molecular mechanism of the Aβ-dependent inhibition of glutamate uptake are needed.

4.4 Soluble Aβ dimers as a key pathological factor in AD

Even though AD mouse models are a very useful tool to study certain AD features such as Aβ or tau pathology, synapse loss or functional changes associated with early AD (Götz et al 2018), their complexity makes it very difficult to study the toxicity of certain Aβ species in an isolated fashion. Thus, the method of choice to study the effect of Aβ oligomers is their direct application in cell culture, in slices or in *in vivo* wild-type mice (Barry et al 2011, Borlikova et al 2013, Freir et al 2001, Jin et al 2011, Klyubin et al 2008, Shankar et al 2008). However, limitations of such studies arise mainly from the use of unphysiological Aβ species or staggeringly high Aβ concentrations. There are four ways to obtain soluble Aβ, which can be summarized as *in vitro* or *ex vivo* (Benilova et al 2012). The *in vitro* generation includes synthetic generation of Aβ and Aβ-production by CHO-cells harboring one or more mutations common in FAD patients (Podlisny et al 1995). Alternatively, Aβ can be

derived from the *ex vivo* brains of AD mice or patients (Meyer-Luehmann et al 2006, Shankar et al 2008). In the majority of experiments, I used synthetic Aβ S26C dimers (Shankar et al 2008). Admittedly, these dimers do not exist in the brain of AD patients. The S26C mutation is artificially introduced to crosslink two monomers, a manipulation which does not happen *in vivo* (Shankar et al 2008). However, it is remarkable, how faithfully the application of synthetic S26C Aβ dimers in wild-type mice can reproduce neuronal pathology observed in AD mice such as the impairments of synaptic plasticity (Hong et al 2014, Hu et al 2008, Li et al 2011, Li et al 2018, Shankar et al 2008). Moreover, previous data from the Konnerth laboratory demonstrated that Aβ S26C dimers induce neuronal hyperactivity in the hippocampus of wild-type mice (Busche et al 2012) and reintroduced neuronal hyperactivity in AD mice, in which the neuronal activity had been restored by BACE inhibition (Keskin et al 2017). I have now confirmed and expanded these findings by applying Aβ in untreated AD mice, where it only had a small effect on neuronal activity (**Fig. 34)** compared to wild-type mice (**Fig. 9, 10**). This saturation of the effect of exogenous Aβ in transgenic mice with high levels of intrinsic Aβ (Busche et al 2012) indicates that their mode of action is not fundamentally different. Instead, the residual effect of Aβ in transgenic mice might rather be due to the high concentration of the applied dimers (500 nM), which was considerably larger than brain Aβ levels in AD mice and patients (Busche et al 2012, Busche et al 2008, McDonald et al 2012, Puzzo et al 2015). To ensure that the hyperactivity-inducing effect of Aβ was not limited to artificial dimers, I also tested the application of different human preparations of Aβ. Thus, Aβ-containing human brain extract from an AD patient potently induced neuronal hyperactivity (**Fig. 39**), while the removal of Aβ from this extract by immunodepletion prevented the effect (**Fig. 40**), indicating that the hyperactivity-inducing effect of the brain extract can be attributed to Aβ. Moreover, to further investigate the toxicity of Aβ dimers, I applied Aβ dimers derived from human material, which potently induced neuronal

hyperactivity (**Fig. 42**). Remarkably, the application of monomers did not have a comparable effect (**Fig. 44).**

As mentioned above, a valid point of criticism is often the use of very high Aβ concentrations in application experiments (Selkoe 2008). In order to overcome this limitation, I recorded a dose-dependency curve of the effect induced by human Aβ dimers (**Fig. 46**), which unveiled that even the application of very low concentrations of human Aβ dimers (20 ng/ml, corresponding to low nanomolar concentrations [15]) increased neuronal activity. Notably, Aβ dimers appear to be much more toxic than the synthetic S26C dimers because lower concentrations of human Aβ dimer (in the low nanomolar range) have similar effects as much higher doses of the synthetic product (500 nM). This observation encourages the further investigation of the toxicity of human brain derived materials.

4.5 A vicious cycle of Aβ-induced neuronal hyperactivation and therapeutic implications

My observation that high levels of baseline activity make neuronal networks susceptible to an Aβ-induced hyperactivation prompts the notion of a vicious cycle of Aβ-induced neuronal dysfunction. More precisely, in brain regions with high levels of glutamatergic inputs, Aβ blocks the uptake of synaptically released glutamate. This leads to an extracellular accumulation of glutamate which further increases the neuronal activity within the affected brain circuit, making it again more susceptible to the Aβ-induced hyperactivation (**Fig. 47**). There have been reports that an increase in neuronal activity boosts the neuronal Aβ production (Bero et al 2011, Cirrito et al 2005, Dolev et al 2013, Kamenetz et al 2003), which might further accelerate the vicious cycle. Conversely, since the Aβ uptake inhibition would be ineffective in the absence of glutamate, neuronal circuits with lower levels of glutamate-driven baseline activity would be expected to be less affected by this vicious cycle.

[15] A detailed description of the approximation of the human brain-derived Aβ concentrations can be found in the methods section.

An increase in activity in a group of neurons would raise the release of glutamate in the brain regions their axons project to. This should increase the level of glutamate in the latter brain area and, in consequence, make it more susceptible to Aβ-induced pathology. Moreover, the increased neuronal activity might raise the production of Aβ in the projecting region (Yamamoto et al 2015). In fact, in AD patients, there is substantial evidence that the neuronal dysfunctions spreads between functionally connected brain areas (Jones et al 2016) and it is tempting to speculate that the described vicious cycle might be one of the underlying mechanisms of this propagation.

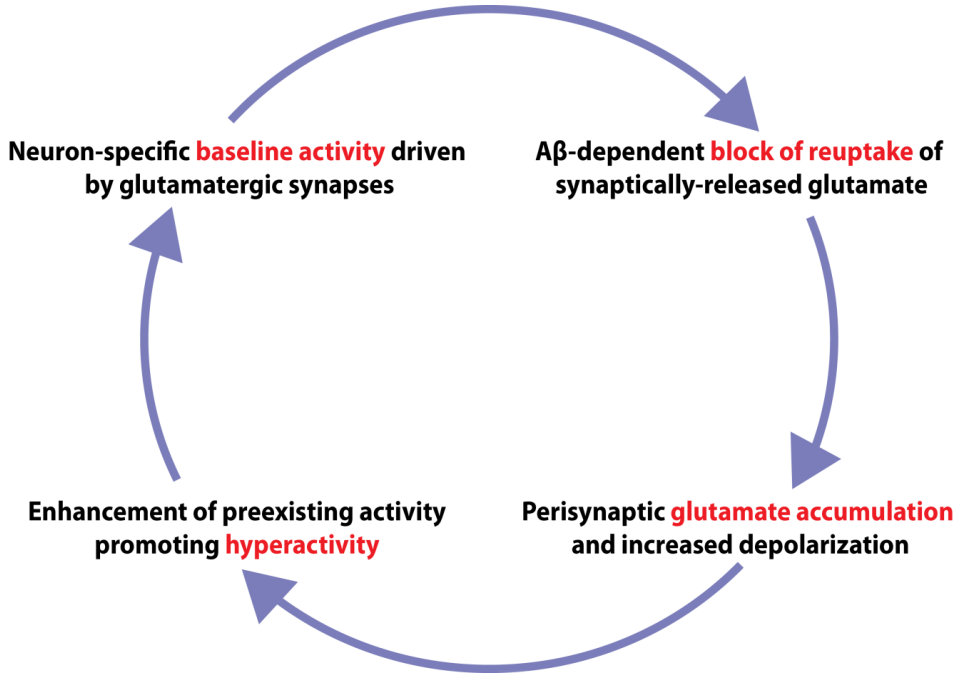

Fig. 47: A vicious cycle of Aβ-dependent neuronal hyperactivation

Implications for the treatment of AD

Disease-modifying drugs against AD could break this vicious cycle at different points. A large variety of drugs that might reduce neuronal activity have been shown to be promising candidates for the symptomatic treatment of AD. The antiepileptic drug levetiracetam, for example, was reported to reduce hippocampal hyperactivity in MCI patients as measured by

fMRI (Bakker et al 2015, Bakker et al 2012). Also, the memory performance of the treated MCI patients was slightly improved. In line with this, levetiracetam also partially restored cognitive functions in rodent models of AD (Koh et al 2010, Sanchez et al 2012). Due to these promising results, levetiracetam is currently undergoing phase 2 clinical testing for treating MCI patients and APOE ε4 carriers (clinicaltrials.gov identifier NCT02002819, NCT03461861). Even though its exact mechanism of action is unclear, levetiracetam was reported to bind to a vesicular protein (Lynch et al 2004) and might decrease glutamate release and, in consequence, postsynaptic neuronal activity (Lee et al 2009, Sanz-Blasco et al 2016).

Another way to prevent the Aβ-induced neuronal hyperactivity might be to enhance the GABAergic inhibitory tone in the brain. This is currently tested by the application of baclofen, sometimes in combination with acamprosate. Both substances lead to a reduced neuronal activation, the GABA-derivate baclofen by a binding to $GABA_B$-receptors (Hill & Bowery 1981) and acamprosate by reportedly preventing excessive glutamate release (Mann et al 2008). The co-application of both drugs prevented Aβ toxicity *in vitro* (Chumakov et al 2015) and has led to slightly beneficial effects in patients with mild AD in an exploratory phase 2 trial (Bennys et al 2016).

One of the central consequences of an Aβ-dependent glutamate accumulation by the impairment of glutamate uptake is the excessive activation of glutamate receptors, such as the NMDAR (**Fig. 36**). In consequence, blocking NMDARs might alleviate some of the toxic effects of Aβ. It was repeatedly observed that pretreating NMDAR expressing cells with diclozilpine (MK-801) could prevent many of the toxic effects of the application of soluble Aβ, including hyperactivation (Alberdi et al 2010, Le et al 1995) and cell death (Domingues et al 2007). However, MK-801 binds to the NMDAR with a very high affinity and, in consequence, MK-801 also blocks its physiological voltage-dependent activation which is instrumental for learning and memory (Frankiewicz et al 1996). These considerations prompted Danysz and

colleagues to develop the uncompetitive NMDA receptor antagonist memantine (Danysz et al 2000), which binds NMDARs with lower affinities and leaves the voltage-dependent unblocking of the receptor largely unaffected. The use of memantine has not only resulted in many beneficial effects both *in vivo* and *in vitro* (Wojciech & Parsons 2012), it is also one of the few drugs that have effectively resulted in a slight improvement of symptoms in AD patients (Reisberg et al 2003) and is routinely used as a disease-modifying drug in patients with early AD.

The most efficient way to break the vicious circle of Aβ-dependent neuronal hyperactivation would be the prevention of the Aβ-induced impairment of glutamate uptake. Even though no specific drugs are available yet, the pharmacological overexpression of GLT-1 was reported to have beneficial effects in mouse models of AD (Hefendehl et al 2016, Takahashi et al 2015, Zumkehr et al 2015). Ceftriaxone, which reportedly increases the transcription of GLT-1 (Lee et al 2008, Rothstein et al 2005), restored glutamate transients (Hefendehl et al 2016) and rescued the cognitive function in mouse models of AD without affecting the plaque pathology (Zumkehr et al 2015). A very potent enhancer of glutamate uptake is LDN/OSU-0212320. This small molecule increases GLT-1 expression by translational upregulation (Colton et al 2010, Kong et al 2014) and had a beneficial effect on synapse survival and behavior in a mouse model of AD (Takahashi et al 2015). Although these results are very promising, it is still too early to know whether ceftriaxone or LDN/OSU will have beneficial effects in AD patients. Moreover, additional research is needed to determine how the application of these drugs affects the neuronal activity in the brain of AD mouse models and patients.

Even though all of these drugs have distinct modes and targets of action, they are all expected to decrease the neuronal activity in the brain, either by an increase in glutamate uptake (ceftriaxone and LDN/OSU-0212320), by a decrease in glutamate release

(levetiracetam, acamprosate), by an increase in GABAergic inhibition (baclofen) or by an inhibition of NMDA receptors (memantine). However, their action on neuronal activity *in vivo* remains to be shown. None of these drugs prevents the interaction of Aβ with glutamate transporters mechanistically or restores the impaired glutamate transport..

4.6 Summary of the main conclusions

In this study, we have identified a cellular mechanism of Aβ-induced neuronal hyperactivity. We have established the *in vivo* hyperactivating effect of Aβ dimers and human AD brain extracts. The key conclusions from this work are: (1) The Aβ-dependent neuronal hyperactivation requires sufficiently strong preceding glutamatergic excitation, as present *in vivo* in some (e.g. hippocampal, cortical layer 5) but not all (e.g. layer 2/3) neurons during spontaneous ongoing activity. (2) The cellular mechanism of Aβ-induced hyperactivity critically depends on the impaired uptake of synaptically released glutamate. (3) These two factors trigger a vicious cycle of Aβ-dependent neuronal hyperactivation in brain areas with high levels of neuronal activity driven by glutamatergic inputs (**Fig. 47**). Our findings clarify why, in AD patients, especially brain areas with high levels of baseline activity are affected by early circuit dysfunctions. Also, our results provide an explanation for the partial success of certain anti-glutamatergic drugs in AD patients and mouse models. Moreover, they encourage the search for targeted treatments to prevent the Aβ-induced impairment of glutamate uptake.

5 Publications in peer-reviewed journals

Zott, B., Simon, M., Chen, H., Unger, F., Hartmann, J., Hong,W., Walsh, D., Sakmann, B., Konnerth, A. (in preparation). A vicious cycle of amyloid β-dependent neuronal hyperactivation

Zott, B., Busche, MA., Sperling, RA., Konnerth, A. 2018. What Happens with the Circuit in Alzheimer's Disease in Mice and Humans? *Annual Review of Neuroscience* 41: 277-97

Focke, C.*, Blume, T.*, Zott, B.*, Shi, Y*., Deussing, M., Peters, F., Schmidt, C., Kleinberger, G., Lindner, S., Gildehaus, F.-J., Beyer, L., Ungern-Sternberg, B., Bartenstein, P., Ozmen, L., Baumann, K., Dorostkar, M., Haass, C., Adelsberger, H., Herms, J., Rominger, A., Brendel, M. 2018. Early and longitudinal microglial activation but not amyloid accumulation predict cognitive outcome in PS2APP mice. *Journal of Nuclear Medicine* 118: 217703
* contributed equally

Keskin, A.D., Kekus, M., Adelsberger, H., Neumann, U., Shimshek, D.R., Song, B., Zott, B., Peng, T., Forstl, H., Staufenbiel, M., Nelken, I., Sakmann, B., Konnerth, A., Busche, MA. 2018. BACE inhibition-dependent repair of Alzheimer's pathophysiology. *Proc Natl Acad Sci U S A* 114: 8631-36

Hartmann, S., Zheng, F., Kyncl, CM., Karch, S., Voelkl, K., Zott, B., D'Avanzo, C., Lomoio, S., Tesco, G. Yeon Kim, D., Alzheimer, C., Huth, T. 2018. β-Secretase BACE1 promotes surface expression and function of Kv3.4 at hippocampal mossy fiber synapses. *The Journal of Neuroscience* 38: 3480-94

Qin, H.*, Fu, L.*, Hu, B.*, Liao, X., Lu, J., He, W., Liang, S., Zhang, K., Li, R., Yao, J., Yan, J., Chen, H., Jia., H, Zott, B., Konnerth, A., Chen, X. 2018. A Visual-Cue-Dependent Memory Circuit for Place Navigation. *Neuron* 99: 47-55.e4
* contributed equally

6 References

Abe K, Misawa M. 2003. The extracellular signal-regulated kinase cascade suppresses amyloid β protein-induced promotion of glutamate clearance in cultured rat cortical astrocytes. *Brain Research* 979: 179-87

Acosta C, Anderson HD, Anderson CM. 2017. Astrocyte dysfunction in Alzheimer disease. *Journal of neuroscience research*

Akerboom J, Carreras Calderón N, Tian L, Wabnig S, Prigge M, et al. 2013. Genetically encoded calcium indicators for multi-color neural activity imaging and combination with optogenetics. *Frontiers in molecular neuroscience* 6: 2

Alberdi E, Sánchez-Gómez MV, Cavaliere F, Pérez-Samartín A, Zugaza JL, et al. 2010. Amyloid β oligomers induce Ca2+ dysregulation and neuronal death through activation of ionotropic glutamate receptors. *Cell Calcium* 47: 264-72

Alzheimer A. 1907. Über eine eigenartige Erkrankung der Hirnrinde. *Allgemeine Zeitschrift für Psychiatrie und psychisch-gerichtliche Medizin* 64(1907): 146-48

Alzheimer A, Stelzmann RA, Schnitzlein HN, Murtagh FR. 1995. An English translation of Alzheimer's 1907 paper, "Uber eine eigenartige Erkankung der Hirnrinde". *Clinical anatomy (New York, N.Y.)* 8: 429–31

Andersen OM, Reiche J, Schmidt V, Gotthardt M, Spoelgen R, et al. 2005. Neuronal sorting protein-related receptor sorLA/LR11 regulates processing of the amyloid precursor protein. *Proceedings of the National Academy of Sciences of the United States of America* 102: 13461-66

Arancio O, Zhang HP, Chen X, Lin C, Trinchese F, et al. 2004. RAGE potentiates Aβ-induced perturbation of neuronal function in transgenic mice. *The EMBO Journal* 23: 4096-105

Arnth-Jensen N, Jabaudon D, Scanziani M. 2002. Cooperation between independent hippocampal synapses is controlled by glutamate uptake. *Nature Neuroscience* 5: 325

Arriagada PV, Growdon JH, Hedley-Whyte ET, Hyman BT. 1992. Neurofibrillary tangles but not senile plaques parallel duration and severity of Alzheimer's disease. *Neurology* 42: 631-31

Avdulov NA, Chochina SV, Igbavboa U, Warden CS, Vassiliev AV, Wood WG. 1997. Lipid Binding to Amyloid β-Peptide Aggregates: Preferential Binding of Cholesterol as Compared with Phosphatidylcholine and Fatty Acids. *Journal of Neurochemistry* 69: 1746-52

Bahmanyar S, Higgins G, Goldgaber D, Lewis D, Morrison J, et al. 1987. Localization of amyloid beta protein messenger RNA in brains from patients with Alzheimer's disease. *Science* 237: 77-80

Bakker A, Albert MS, Krauss G, Speck CL, Gallagher M. 2015. Response of the medial temporal lobe network in amnestic mild cognitive impairment to therapeutic intervention assessed by fMRI and memory task performance. *NeuroImage. Clinical* 7: 688–98

Bakker A, Krauss GL, Albert MS, Speck CL, Jones LR, et al. 2012. Reduction of hippocampal hyperactivity improves cognition in amnestic mild cognitive impairment. *Neuron* 74: 467–74

Bancher C, Brunner C, Lassmann H, Budka H, Jellinger K, et al. 1989. Accumulation of abnormally phosphorylated τ precedes the formation of neurofibrillary tangles in Alzheimer's disease. *Brain Research* 477: 90-99

Bao X, Pal R, Hascup KN, Wang Y, Wang W-T, et al. 2009. Transgenic Expression of *Glud1* (Glutamate Dehydrogenase 1) in Neurons: *In Vivo* Model of Enhanced Glutamate Release, Altered Synaptic Plasticity, and Selective Neuronal Vulnerability. *The Journal of Neuroscience* 29: 13929-44

Barnes CA, Rao G, Shen J. 1997. Age-Related Decrease in the N-Methyl-d-AspartateR-Mediated Excitatory Postsynaptic Potential in Hippocampal Region CA1. *Neurobiology of Aging* 18: 445-52

Barry AE, Klyubin I, Mc Donald JM, Mably AJ, Farrell MA, et al. 2011. Alzheimer's disease brain-derived amyloid-beta-mediated inhibition of LTP in vivo is prevented by immunotargeting cellular prion protein. *J Neurosci* 31: 7259-63

Bateman RJ, Xiong C, Benzinger TLS, Fagan AM, Goate A, et al. 2012. Clinical and biomarker changes in dominantly inherited Alzheimer's disease. *The New England journal of medicine* 367: 795–804

Benilova I, Karran E, De Strooper B. 2012. The toxic Aβ oligomer and Alzheimer's disease: an emperor in need of clothes. *Nature Neuroscience* 15: 349

Bennys K, Haddad R, Gres CS, Schmitt P, Touchon J. 2016. Cognitive event-related potentials used as biomarkers in PLEODIAL-I study: First evidence of a neuropsychological effect of PXT864 in mild Alzheimer's diesease patients. *Alzheimer's & Dementia: The Journal of the Alzheimer's Association* 12: P1061

Bero AW, Yan P, Roh JH, Cirrito JR, Stewart FR, et al. 2011. Neuronal activity regulates the regional vulnerability to amyloid-beta deposition. *Nat Neurosci* 14: 750–56

Berridge MJ, Lipp P, Bootman MD. 2000. The versatility and universality of calcium signalling. *Nature reviews Molecular cell biology* 1: 11

Birkner A, Tischbirek CH, Konnerth A. 2017. Improved deep two-photon calcium imaging in vivo. *Cell Calcium* 64: 29-35

Bishop NA, Lu T, Yankner BA. 2010. Neural mechanisms of ageing and cognitive decline. *Nature* 464: 529-35

Bitan G, Kirkitadze MD, Lomakin A, Vollers SS, Benedek GB, Teplow DB. 2003. Amyloid β-protein (Aβ) assembly: Aβ40 and Aβ42 oligomerize through distinct pathways. *Proceedings of the National Academy of Sciences* 100: 330-35

Bliss T. 2007. *The hippocampus book*. New York, NY, US: Oxford University Press. xx, 832-xx, 32 pp.

Bliss TV, Lømo T. 1973. Long‐lasting potentiation of synaptic transmission in the dentate area of the anaesthetized rabbit following stimulation of the perforant path. *The Journal of physiology* 232: 331-56

Bloom GS. 2014. Amyloid-beta and tau: the trigger and bullet in Alzheimer disease pathogenesis. *JAMA neurology* 71: 505–08

Bobich JA, Zheng Q, Campbell A. 2004. Incubation of nerve endings with a physiological concentration of Aβ 1-42 activates CaV2. 2 (N-Type)-voltage operated calcium channels and acutely increases glutamate and noradrenaline release. *Journal of Alzheimer's Disease* 6: 243-55

Bokvist M, Lindström F, Watts A, Gröbner G. 2004. Two Types of Alzheimer's β-Amyloid (1–40) Peptide Membrane Interactions: Aggregation Preventing Transmembrane Anchoring Versus Accelerated Surface Fibril Formation. *Journal of Molecular Biology* 335: 1039-49

Bookheimer SY, Strojwas MH, Cohen MS, Saunders AM, Pericak-Vance MA, et al. 2000. Patterns of brain activation in people at risk for Alzheimer's disease. *The New England journal of medicine* 343: 450–56

Borlikova GG, Trejo M, Mably AJ, Mc Donald JM, Sala Frigerio C, et al. 2013. Alzheimer brain-derived amyloid β-protein impairs synaptic remodeling and memory consolidation. *Neurobiology of aging* 34: 1315–27

Boudker O, Ryan RM, Yernool D, Shimamoto K, Gouaux E. 2007. Coupling substrate and ion binding to extracellular gate of a sodium-dependent aspartate transporter. *Nature* 445: 387

Braak H, Braak E. 1991. Neuropathological stageing of Alzheimer-related changes. *Acta neuropathologica* 82: 239–59

Brier MR, Thomas JB, Ances BM. 2014. Network dysfunction in Alzheimer's disease: refining the disconnection hypothesis. *Brain connectivity* 4: 299-311

Brorson JR, Bindokas VP, Iwama T, Marcuccilli CJ, Chisholm JC, Miller RJ. 1995. The Ca2+ influx induced by β-amyloid peptide 25–35 in cultured hippocampal neurons results from network excitation. *Journal of Neurobiology* 26: 325-38

Brun VH, Otnæss MK, Molden S, Steffenach H-A, Witter MP, et al. 2002. Place Cells and Place Recognition Maintained by Direct Entorhinal-Hippocampal Circuitry. *Science* 296: 2243-46

Buckner RL, Andrews-Hanna JR, Schacter DL. 2008. The brain's default network: anatomy, function, and relevance to disease. *Annals of the New York Academy of Sciences* 1124: 1–38

Buckner RL, Snyder AZ, Shannon BJ, LaRossa G, Sachs R, et al. 2005. Molecular, structural, and functional characterization of Alzheimer's disease: evidence for a relationship between default activity, amyloid, and memory. *The Journal of neuroscience* 25: 7709–17

Busche MA, Chen X, Henning HA, Reichwald J, Staufenbiel M, et al. 2012. Critical role of soluble amyloid-beta for early hippocampal hyperactivity in a mouse model of Alzheimer's disease. *Proc Natl Acad Sci U S A* 109: 8740-5

Busche MA, Eichhoff G, Adelsberger H, Abramowski D, Wiederhold KH, et al. 2008. Clusters of hyperactive neurons near amyloid plaques in a mouse model of Alzheimer's disease. *Science* 321: 1686-9

Busche MA, Grienberger C, Keskin AD, Song B, Neumann U, et al. 2015a. Decreased amyloid-beta and increased neuronal hyperactivity by immunotherapy in Alzheimer's models. *Nat Neurosci* 18: 1725-27

Busche MA, Kekus M, Adelsberger H, Noda T, Forstl H, et al. 2015b. Rescue of long-range circuit dysfunction in Alzheimer's disease models. *Nat Neurosci* 18: 1623-30

Busche MA, Konnerth A. 2015. Neuronal hyperactivity--A key defect in Alzheimer's disease? *BioEssays : news and reviews in molecular, cellular and developmental biology* 37: 624-32

Busche MA, Konnerth A. 2016. Impairments of neural circuit function in Alzheimer's disease. *Philosophical transactions of the Royal Society of London. Series B, Biological sciences* 371

Cabeza R, Anderson ND, Locantore JK, McIntosh AR. 2002. Aging Gracefully: Compensatory Brain Activity in High-Performing Older Adults. *NeuroImage* 17: 1394-402

Cao Q, Shin WS, Chan H, Vuong CK, Dubois B, et al. 2018. Inhibiting amyloid-β cytotoxicity through its interaction with the cell surface receptor LilrB2 by structure-based design. *Nature Chemistry* 10: 1213-21

Carlo AS, Gustafsen C, Mastrobuoni G, Nielsen MS, Burgert T, et al. 2013. The Pro-Neurotrophin Receptor Sortilin Is a Major Neuronal Apolipoprotein E Receptor for Catabolism of Amyloid-β Peptide in the Brain. *The Journal of Neuroscience* 33: 358-70

Castellano JM, Kim J, Stewart FR, Jiang H, DeMattos RB, et al. 2011. Human apoE Isoforms Differentially Regulate Brain Amyloid-β Peptide Clearance. *Science Translational Medicine* 3: 89ra57

Cerpa W, Farías GG, Godoy JA, Fuenzalida M, Bonansco C, Inestrosa NC. 2010. Wnt-5a occludes Abeta oligomer-induced depression of glutamatergic transmission in hippocampal neurons. *Molecular neurodegeneration* 5: 3

Chapman PF, White GL, Jones MW, Cooper-Blacketer D, Marshall VJ, et al. 1999. Impaired synaptic plasticity and learning in aged amyloid precursor protein transgenic mice. *Nature Neuroscience* 2: 271

Chen JE, Glover GH. 2015. Functional Magnetic Resonance Imaging Methods. *Neuropsychology review* 25: 289-313

Chen T-W, Wardill TJ, Sun Y, Pulver SR, Renninger SL, et al. 2013. Ultrasensitive fluorescent proteins for imaging neuronal activity. *Nature* 499: 295

Chien DT, Szardenings AK, Bahri S, Walsh JC, Mu F, et al. 2014. Early clinical PET imaging results with the novel PHF-tau radioligand F18-T808. *Journal of Alzheimer's disease : JAD* 38: 171–84

Chumakov I, Nabirotchkin S, Cholet N, Milet A, Boucard A, et al. 2015. Combining two repurposed drugs as a promising approach for Alzheimer's disease therapy. *Scientific Reports* 5: 7608

Cirrito JR, Yamada KA, Finn MB, Sloviter RS, Bales KR, et al. 2005. Synaptic activity regulates interstitial fluid amyloid-beta levels in vivo. *Neuron* 48: 913–22

Cissé M, Halabisky B, Harris J, Devidze N, Dubal DB, et al. 2010. Reversing EphB2 depletion rescues cognitive functions in Alzheimer model. *Nature* 469: 47

Cissé M, Sanchez PE, Kim DH, Ho K, Yu G-Q, Mucke L. 2011. Ablation of Cellular Prion Protein Does Not Ameliorate Abnormal Neural Network Activity or Cognitive Dysfunction in the J20 Line of Human Amyloid Precursor Protein Transgenic Mice. *The Journal of Neuroscience* 31: 10427-31

Cleary JP, Walsh DM, Hofmeister JJ, Shankar GM, Kuskowski MA, et al. 2004. Natural oligomers of the amyloid-β protein specifically disrupt cognitive function. *Nature Neuroscience* 8: 79

Clemens Z, Fabó D, Halász P. 2005. Overnight verbal memory retention correlates with the number of sleep spindles. *Neuroscience* 132: 529–35

Clements J, Lester R, Tong G, Jahr C, Westbrook G. 1992. The time course of glutamate in the synaptic cleft. *Science* 258: 1498-501

Collingridge GL, Kehl SJ, McLennan H. 1983. Excitatory amino acids in synaptic transmission in the Schaffer collateral-commissural pathway of the rat hippocampus. *The Journal of Physiology* 334: 33-46

Colton CK, Kong Q, Lai L, Zhu MX, Seyb KI, et al. 2010. Identification of translational activators of glial glutamate transporter EAAT2 through cell-based high-throughput screening: an approach to prevent excitotoxicity. *Journal of biomolecular screening* 15: 653-62

Cornelisse LN, van Elburg RA, Meredith RM, Yuste R, Mansvelder HD. 2007. High speed two-photon imaging of calcium dynamics in dendritic spines: consequences for spine calcium kinetics and buffer capacity. *PloS one* 2: e1073

Cuccaro ML, Carney RM, Zhang Y, Bohm C, Kunkle BW, et al. 2016. SORL1 mutations in early- and late-onset Alzheimer disease. *Neurology. Genetics* 2: e116

Cull-Candy S, Brickley S, Farrant M. 2001. NMDA receptor subunits: diversity, development and disease. *Current opinion in neurobiology* 11: 327-35

Dana H, Mohar B, Sun Y, Narayan S, Gordus A, et al. 2016. Sensitive red protein calcium indicators for imaging neural activity. *Elife* 5: e12727

Dana H, Sun Y, Mohar B, Hulse B, Hasseman JP, et al. 2018. High-performance GFP-based calcium indicators for imaging activity in neuronal populations and microcompartments. *bioRxiv*: 434589

Danbolt NC. 2001. Glutamate uptake. *Progress in Neurobiology* 65: 1-105

Danysz W, Parsons CG, Möbius H-J, Stöffler A, Quack G. 2000. Neuroprotective and symptomatological action of memantine relevant for alzheimer's disease — a unified glutamatergic hypothesis on the mechanism of action. *Neurotoxicity Research* 2: 85-97

Davis KE, Fox S, Gigg J. 2014. Increased hippocampal excitability in the 3xTgAD mouse model for Alzheimer's disease in vivo. *PloS one* 9: e91203-e03

De Bundel D, Schallier A, Loyens E, Fernando R, Miyashita H, et al. 2011. Loss of System xc^- Does Not Induce Oxidative Stress But Decreases Extracellular Glutamate in Hippocampus and Influences Spatial Working Memory and Limbic Seizure Susceptibility. *The Journal of Neuroscience* 31: 5792-803

De Felice FG, Velasco PT, Lambert MP, Viola K, Fernandez SJ, et al. 2007. Aβ Oligomers Induce Neuronal Oxidative Stress through an N-Methyl-D-aspartate Receptor-dependent Mechanism That Is Blocked by the Alzheimer Drug Memantine. *Journal of Biological Chemistry* 282: 11590-601

De Kock CPJ, Bruno RM, Spors H, Sakmann B. 2007. Layer- and cell-type-specific suprathreshold stimulus representation in rat primary somatosensory cortex. *The Journal of physiology* 581: 139-54

De Strooper B, Saftig P, Craessaerts K, Vanderstichele H, Guhde G, et al. 1998. Deficiency of presenilin-1 inhibits the normal cleavage of amyloid precursor protein. *Nature* 391: 387

De Strooper B, Karran E. 2016. The Cellular Phase of Alzheimer's Disease. *Cell* 164: 603-15

Deane R, Du Yan S, Submamaryan RK, LaRue B, Jovanovic S, et al. 2003. RAGE mediates amyloid-β peptide transport across the blood-brain barrier and accumulation in brain. *Nature Medicine* 9: 907

DeKosky ST, Scheff SW, Styren SD. 1996. Structural correlates of cognition in dementia: quantification and assessment of synapse change. *Neurodegeneration : a journal for neurodegenerative disorders, neuroprotection, and neuroregeneration* 5: 417-21

Denk W, Strickler JH, Webb WW. 1990. Two-photon laser scanning fluorescence microscopy. *Science* 248: 73-76

Devanand DP, Pradhaban G, Liu X, Khandji A, De Santi S, et al. 2007. Hippocampal and entorhinal atrophy in mild cognitive impairment. *Prediction of Alzheimer disease* 68: 828-36

Di Scala C, Troadec J-D, Lelièvre C, Garmy N, Fantini J, Chahinian H. 2014. Mechanism of cholesterol-assisted oligomeric channel formation by a short Alzheimer β-amyloid peptide. *Journal of Neurochemistry* 128: 186-95

Dickerson BC, Bakkour A, Salat DH, Feczko E, Pacheco J, et al. 2009. The cortical signature of Alzheimer's disease: regionally specific cortical thinning relates to symptom severity in very mild to mild AD dementia and is detectable in asymptomatic amyloid-positive individuals. *Cerebral cortex (New York, N.Y. : 1991)* 19: 497–510

Dickerson BC, Salat DH, Greve DN, Chua EF, Rand-Giovannetti E, et al. 2005. Increased hippocampal activation in mild cognitive impairment compared to normal aging and AD. *Neurology* 65: 404–11

Dickerson BC, Stoub TR, Shah RC, Sperling RA, Killiany RJ, et al. 2011. Alzheimer-signature MRI biomarker predicts AD dementia in cognitively normal adults. *Neurology* 76: 1395-402

Diekelmann S, Born J. 2010. The memory function of sleep. *Nat Rev Neurosci* 11: 114–26

Dineley KT, Westerman M, Bui D, Bell K, Ashe KH, Sweatt JD. 2001. β-Amyloid Activates the Mitogen-Activated Protein Kinase Cascade via Hippocampal α7 Nicotinic Acetylcholine Receptors: *In Vitro* and *In Vivo* Mechanisms Related to Alzheimer's Disease. *The Journal of Neuroscience* 21: 4125-33

Dohler F, Sepulveda-Falla D, Krasemann S, Altmeppen H, Schlüter H, et al. 2014. High molecular mass assemblies of amyloid-β oligomers bind prion protein in patients with Alzheimer's disease. *Brain* 137: 873-86

Dolev I, Fogel H, Milshtein H, Berdichevsky Y, Lipstein N, et al. 2013. Spike bursts increase amyloid-beta 40/42 ratio by inducing a presenilin-1 conformational change. *Nat Neurosci* 16: 587–95

Dombeck DA, Harvey CD, Tian L, Looger LL, Tank DW. 2010. Functional imaging of hippocampal place cells at cellular resolution during virtual navigation. *Nature Neuroscience* 13: 1433

Domingues A, Almeida S, da Cruz e Silva EF, Oliveira CR, Rego AC. 2007. Toxicity of β-amyloid in HEK293 cells expressing NR1/NR2A or NR1/NR2B N-methyl-d-aspartate receptor subunits. *Neurochemistry International* 50: 872-80

Drzezga A, Becker JA, van Dijk KRA, Sreenivasan A, Talukdar T, et al. 2011. Neuronal dysfunction and disconnection of cortical hubs in non-demented subjects with elevated amyloid burden. *Brain : a journal of neurology* 134: 1635–46

Dubois B, Feldman HH, Jacova C, Hampel H, Molinuevo JL, et al. 2014. Advancing research diagnostic criteria for Alzheimer's disease: The IWG-2 criteria. *The Lancet Neurology* 13: 614–29

Eichenbaum H. 2017. Memory: Organization and Control. *Annual review of psychology* 68: 19–45

Erten-Lyons D, Woltjer RL, Dodge H, Nixon R, Vorobik R, et al. 2009. Factors associated with resistance to dementia despite high Alzheimer disease pathology. *Neurology* 72: 354-60

Esparza TJ, Wildburger NC, Jiang H, Gangolli M, Cairns NJ, et al. 2016. Soluble Amyloid-beta Aggregates from Human Alzheimer's Disease Brains. *Scientific reports* 6: 38187-87

Fernández-Tomé P, Brera B, Arévalo Ma-A, de Ceballos MaL. 2004. β-Amyloid 25-35 inhibits glutamate uptake in cultured neurons and astrocytes: modulation of uptake as a survival mechanism. *Neurobiology of Disease* 15: 580-89

Ferreira JS, Papouin T, Ladépêche L, Yao A, Langlais VC, et al. 2017. Co-agonists differentially tune GluN2B-NMDA receptor trafficking at hippocampal synapses. *eLife* 6: e25492

Ficca G, Lombardo P, Rossi L, Salzarulo P. 2000. Morning recall of verbal material depends on prior sleep organization. *Behavioural brain research* 112: 159–63

Finnema SJ, Nabulsi NB, Eid T, Detyniecki K, Lin S-f, et al. 2016. Imaging synaptic density in the living human brain. *Science Translational Medicine* 8: 348ra96

Fioravante D, Regehr WG. 2011. Short-term forms of presynaptic plasticity. *Current Opinion in Neurobiology* 21: 269-74

Foley D, Ancoli-Israel S, Britz P, Walsh J. 2004. Sleep disturbances and chronic disease in older adults: Results of the 2003 National Sleep Foundation Sleep in America Survey. *Journal of Psychosomatic Research* 56: 497-502

Frankiewicz T, Potier B, Bashir ZI, Collingridge GL, Parsons CG. 1996. Effects of memantine and MK-801 on NMDA-induced currents in cultured neurones and on synaptic transmission and LTP in area CA1 of rat hippocampal slices. *British Journal of Pharmacology* 117: 689-97

Freir DB, Holscher C, Herron CE. 2001. Blockade of long-term potentiation by beta-amyloid peptides in the CA1 region of the rat hippocampus in vivo. *J Neurophysiol* 85: 708-13

Gimbel DA, Nygaard HB, Coffey EE, Gunther EC, Laurén J, et al. 2010. Memory impairment in transgenic Alzheimer mice requires cellular prion protein. *The Journal of neuroscience : the official journal of the Society for Neuroscience* 30: 6367-74

Giuffrida ML, Caraci F, Pignataro B, Cataldo S, De Bona P, et al. 2009. β-amyloid monomers are neuroprotective. *Journal of Neuroscience* 29: 10582-87

Goedert M. 1987. Neuronal localization of amyloid beta protein precursor mRNA in normal human brain and in Alzheimer's disease. *The EMBO Journal* 6: 3627-32

Goedert M, Eisenberg DS, Crowther RA. 2017. Propagation of Tau Aggregates and Neurodegeneration. *Annual Review of Neuroscience* 40: 189-210

Gong Y, Huang C, Li JZ, Grewe BF, Zhang Y, et al. 2015. High-speed recording of neural spikes in awake mice and flies with a fluorescent voltage sensor. *Science (New York, N.Y.)* 350: 1361-66

Göppert-Mayer M. 1931. Über Elementarakte mit zwei Quantensprüngen. *Annalen der Physik* 401: 273-94

Götz J, Bodea L-G, Goedert M. 2018. Rodent models for Alzheimer disease. *Nature Reviews Neuroscience* 19: 583–98

Götz J, Chen F, van Dorpe J, Nitsch RM. 2001. Formation of neurofibrillary tangles in P301L tau transgenic mice induced by Abeta 42 fibrils. *Science (New York, N.Y.)* 293: 1491–95

Gray CM, Maldonado PE, Wilson M, McNaughton B. 1995. Tetrodes markedly improve the reliability and yield of multiple single-unit isolation from multi-unit recordings in cat striate cortex. *Journal of neuroscience methods* 63: 43-54

Grienberger C, Konnerth A. 2012. Imaging Calcium in Neurons. *Neuron* 73: 862-85

Grienberger C, Rochefort NL, Adelsberger H, Henning HA, Hill DN, et al. 2012. Staged decline of neuronal function in vivo in an animal model of Alzheimer's disease. *Nat Commun* 3: 774

Haass C, Hung AY, Schlossmacher MG, Teplow DB, Selkoe DJ. 1993. beta-Amyloid peptide and a 3-kDa fragment are derived by distinct cellular mechanisms. *Journal of Biological Chemistry* 268: 3021-24

Haass C, Lemere CA, Capell A, Citron M, Seubert P, et al. 1995. The Swedish mutation causes early-onset Alzheimer's disease by β-secretase cleavage within the secretory pathway. *Nature medicine* 1: 1291

Hájos N, Ellender TJ, Zemankovics R, Mann EO, Exley R, et al. 2009. Maintaining network activity in submerged hippocampal slices: importance of oxygen supply. *The European journal of neuroscience* 29: 319-27

Hamilton A, Vasefi M, Vander Tuin C, McQuaid Robyn J, Anisman H, Ferguson Stephen SG. 2016. Chronic Pharmacological mGluR5 Inhibition Prevents Cognitive Impairment and Reduces Pathogenesis in an Alzheimer Disease Mouse Model. *Cell reports* 15: 1859-65

Hardy J, Selkoe DJ. 2002. The amyloid hypothesis of Alzheimer's disease: progress and problems on the road to therapeutics. *Science* 297: 353–56

Harris ME, Wang Y, Pedigo NW, Hensley K, Butterfield DA, Carney JM. 1996. Amyloid β Peptide (25–35) Inhibits Na+-Dependent Glutamate Uptake in Rat Hippocampal Astrocyte Cultures. *Journal of Neurochemistry* 67: 277-86

Head E, Powell D, Gold BT, Schmitt FA. 2012. Alzheimer's Disease in Down Syndrome. *European journal of neurodegenerative disease* 1: 353-64

Hefendehl JK, LeDue J, Ko RWY, Mahler J, Murphy TH, MacVicar BA. 2016. Mapping synaptic glutamate transporter dysfunction in vivo to regions surrounding Aβ plaques by iGluSnFR two-photon imaging. *Nature Communications* 7: 13441

Helfrich RF, Mander BA, Jagust WJ, Knight RT, Walker MP. 2018. Old Brains Come Uncoupled in Sleep: Slow Wave-Spindle Synchrony, Brain Atrophy, and Forgetting. *Neuron* 97: 221-30.e4

Helmchen F, Denk W. 2005. Deep tissue two-photon microscopy. *Nature Methods* 2: 932

Helmchen F, Imoto K, Sakmann B. 1996. Ca2+ buffering and action potential-evoked Ca2+ signaling in dendrites of pyramidal neurons. *Biophysical Journal* 70: 1069-81

Herman MA, Jahr CE. 2007. Extracellular Glutamate Concentration in Hippocampal Slice. *The Journal of Neuroscience* 27: 9736-41

Herzig MC, Winkler DT, Burgermeister P, Pfeifer M, Kohler E, et al. 2004. Aβ is targeted to the vasculature in a mouse model of hereditary cerebral hemorrhage with amyloidosis. *Nature Neuroscience* 7: 954

Hestrin S, Sah P, Nicoll RA. 1990. Mechanisms generating the time course of dual component excitatory synaptic currents recorded in hippocampal slices. *Neuron* 5: 247-53

Hill DR, Bowery NG. 1981. 3H-baclofen and 3H-GABA bind to bicuculline-insensitive GABAB sites in rat brain. *Nature* 290: 149

Hita-Yanez E, Atienza M, Gil-Neciga E, Cantero JL. 2012. Disturbed sleep patterns in elders with mild cognitive impairment: the role of memory decline and ApoE epsilon4 genotype. *Current Alzheimer research* 9: 290–97

Hong S, Beja-Glasser VF, Nfonoyim BM, Frouin A, Li S, et al. 2016. Complement and microglia mediate early synapse loss in Alzheimer mouse models. *Science* 352: 712-16

Hong S, Ostaszewski BL, Yang T, O'Malley TT, Jin M, et al. 2014. Soluble Aβ oligomers are rapidly sequestered from brain ISF in vivo and bind GM1 ganglioside on cellular membranes. *Neuron* 82: 308-19

Hong W, Wang Z, Liu W, O'Malley TT, Jin M, et al. 2018. Diffusible, highly bioactive oligomers represent a critical minority of soluble Aβ in Alzheimer's disease brain. *Acta Neuropathologica* 136: 19-40

Hsieh H, Boehm J, Sato C, Iwatsubo T, Tomita T, et al. 2006. AMPAR removal underlies Abeta-induced synaptic depression and dendritic spine loss. *Neuron* 52: 831-43

Hu N-W, Klyubin I, Anwyl R, Rowan MJ. 2009. GluN2B subunit-containing NMDA receptor antagonists prevent Aβ-mediated synaptic plasticity disruption in vivo. *Proceedings of the National Academy of Sciences* 106: 20504-09

Hu N-W, Smith IM, Walsh DM, Rowan MJ. 2008. Soluble amyloid-β peptides potently disrupt hippocampal synaptic plasticity in the absence of cerebrovascular dysfunction in vivo. *Brain* 131: 2414-24

Hudetz AG, Vizuete JA, Pillay S. 2011. Differential effects of isoflurane on high-frequency and low-frequency γ oscillations in the cerebral cortex and hippocampus in freely moving rats. *Anesthesiology* 114: 588-95

Huijbers W, Mormino EC, Schultz AP, Wigman S, Ward AM, et al. 2015. Amyloid-β deposition in mild cognitive impairment is associated with increased hippocampal activity, atrophy and clinical progression. *Brain : a journal of neurology* 138: 1023–35

Hurtado DE, Molina-Porcel L, Iba M, Aboagye AK, Paul SM, et al. 2010. Aβ Accelerates the Spatiotemporal Progression of Tau Pathology and Augments Tau Amyloidosis in an Alzheimer Mouse Model. *The American journal of pathology* 177: 1977–88

Ikonomovic MD, Mizukami K, Warde D, Sheffield R, Hamilton R, et al. 1999. Distribution of Glutamate Receptor Subunit NMDAR1 in the Hippocampus of Normal Elderly and Patients with Alzheimer's Disease. *Experimental neurology* 160: 194-204

Jabaudon D, Shimamoto K, Yasuda-Kamatani Y, Scanziani M, Gähwiler BH, Gerber U. 1999. Inhibition of uptake unmasks rapid extracellular turnover of glutamate of nonvesicular origin. *Proceedings of the National Academy of Sciences of the United States of America* 96: 8733-38

Jack CR, Albert MS, Knopman DS, McKhann GM, Sperling RA, et al. 2011. Introduction to the recommendations from the National Institute on Aging-Alzheimer's Association workgroups on diagnostic guidelines for Alzheimer's disease. *Alzheimer's & dementia : the journal of the Alzheimer's Association* 7: 257–62

Jack CR, Knopman DS, Jagust WJ, Shaw LM, Aisen PS, et al. 2010. Hypothetical model of dynamic biomarkers of the Alzheimer's pathological cascade. *Lancet Neurol* 9: 119-28

Jack CR, Lowe VJ, Weigand SD, Wiste HJ, Senjem ML, et al. 2009. Serial PIB and MRI in normal, mild cognitive impairment and Alzheimer's disease: implications for sequence of pathological events in Alzheimer's disease. *Brain* 132: 1355-65

Jack CR, Petersen RC, Xu YC, O'Brien PC, Smith GE, et al. 1999. Prediction of AD with MRI-based hippocampal volume in mild cognitive impairment. *Neurology* 52: 1397–403

Jacobsen JS, Wu CC, Redwine JM, Comery TA, Arias R, et al. 2006. Early-onset behavioral and synaptic deficits in a mouse model of Alzheimer's disease. *Proc Natl Acad Sci U S A* 103: 5161-6

Jang JH, Surh YJ. 2002. β-Amyloid Induces Oxidative DNA Damage and Cell Death through Activation of c-Jun N Terminal Kinase. *Annals of the New York Academy of Sciences* 973: 228-36

Jankowsky JL, Zheng H. 2017. Practical considerations for choosing a mouse model of Alzheimer's disease. *Molecular neurodegeneration* 12: 89

Jarosz-Griffiths HH, Noble E, Rushworth JV, Hooper NM. 2016. Amyloid-β Receptors: The Good, the Bad, and the Prion Protein. *Journal of Biological Chemistry* 291: 3174-83

Jensen MS, Yaari Y. 1997. Role of Intrinsic Burst Firing, Potassium Accumulation, and Electrical Coupling in the Elevated Potassium Model of Hippocampal Epilepsy. *Journal of Neurophysiology* 77: 1224-33

Jia H, Rochefort NL, Chen X, Konnerth A. 2010. In vivo two-photon imaging of sensory-evoked dendritic calcium signals in cortical neurons. *Nature Protocols* 6: 28

Jin M, O'Nuallain B, Hong W, Boyd J, Lagomarsino VN, et al. 2018. An in vitro paradigm to assess potential anti-Aβ antibodies for Alzheimer's disease. *Nature Communications* 9: 2676

Jin M, Shepardson N, Yang T, Chen G, Walsh D, Selkoe DJ. 2011. Soluble amyloid beta-protein dimers isolated from Alzheimer cortex directly induce Tau hyperphosphorylation and neuritic degeneration. *Proc Natl Acad Sci U S A* 108: 5819–24

Johnson KA, Schultz A, Betensky RA, Becker JA, Sepulcre J, et al. 2016. Tau positron emission tomographic imaging in aging and early Alzheimer disease. *Ann Neurol* 79: 110–19

Jones DT, Knopman DS, Gunter JL, Graff-Radford J, Vemuri P, et al. 2016. Cascading network failure across the Alzheimer's disease spectrum. *Brain : a journal of neurology* 139: 547–62

Jonsson T, Atwal JK, Steinberg S, Snaedal J, Jonsson PV, et al. 2012. A mutation in APP protects against Alzheimer's disease and age-related cognitive decline. *Nature* 488: 96

Kabogo D, Rauw G, Amritraj A, Baker G, Kar S. 2010. β-Amyloid-related peptides potentiate K+-evoked glutamate release from adult rat hippocampal slices. *Neurobiology of Aging* 31: 1164-72

Kadir A, Almkvist O, Forsberg A, Wall A, Engler H, et al. 2012. Dynamic changes in PET amyloid and FDG imaging at different stages of Alzheimer's disease. *Neurobiology of Aging* 33: 198.e1-98.e14

Kadowaki H, Nishitoh H, Urano F, Sadamitsu C, Matsuzawa A, et al. 2004. Amyloid β induces neuronal cell death through ROS-mediated ASK1 activation. *Cell Death And Differentiation* 12: 19

Kam T-I, Song S, Gwon Y, Park H, Yan J-J, et al. 2013. FcγRIIb mediates amyloid-β neurotoxicity and memory impairment in Alzheimer's disease. *The Journal of clinical investigation* 123: 2791-802

Kamenetz F, Tomita T, Hsieh H, Seabrook G, Borchelt D, et al. 2003. APP processing and synaptic function. *Neuron* 37: 925-37

Kamondi A, Acsády L, Wang X-J, Buzsáki G. 1998. Theta oscillations in somata and dendrites of hippocampal pyramidal cells in vivo: Activity-dependent phase-precession of action potentials. *Hippocampus* 8: 244-61

Karch CM, Goate AM. 2015. Alzheimer's disease risk genes and mechanisms of disease pathogenesis. *Biol Psychiatry* 77: 43-51

Kashani A, Lepicard È, Poirel O, Videau C, David JP, et al. 2008. Loss of VGLUT1 and VGLUT2 in the prefrontal cortex is correlated with cognitive decline in Alzheimer disease. *Neurobiology of Aging* 29: 1619-30

Keller BU, Konnerth A, Yaari Y. 1991. Patch clamp analysis of excitatory synaptic currents in granule cells of rat hippocampus. *The Journal of Physiology* 435: 275-93

Kemppainen NM, Scheinin NM, Koivunen J, Johansson J, Toivonen JT, et al. 2014. Five-year follow-up of 11C-PIB uptake in Alzheimer's disease and MCI. *European Journal of Nuclear Medicine and Molecular Imaging* 41: 283-89

Kerr JND, Denk W. 2008. Imaging in vivo: watching the brain in action. *Nature Reviews Neuroscience* 9: 195

Kerr JND, Greenberg D, Helmchen F. 2005. Imaging input and output of neocortical networks *in vivo*. *Proceedings of the National Academy of Sciences of the United States of America* 102: 14063-68

Keskin AD, Kekus M, Adelsberger H, Neumann U, Shimshek DR, et al. 2017. BACE inhibition-dependent repair of Alzheimer's pathophysiology. *Proc Natl Acad Sci U S A* 114: 8631-36

Kessels HW, Nguyen LN, Nabavi S, Malinow R. 2010. The prion protein as a receptor for amyloid-β. *Nature* 466: E3

Kim K, Lee S-G, Kegelman TP, Su Z-Z, Das SK, et al. 2011. Role of excitatory amino acid transporter-2 (EAAT2) and glutamate in neurodegeneration: opportunities for developing novel therapeutics. *Journal of cellular physiology* 226: 2484-93

Kim T, Vidal GS, Djurisic M, William CM, Birnbaum ME, et al. 2013. Human LilrB2 Is a β-Amyloid Receptor and Its Murine Homolog PirB Regulates Synaptic Plasticity in an Alzheimer's Model. *Science* 341: 1399-404

Kirvell SL, Esiri M, Francis PT. 2006. Down-regulation of vesicular glutamate transporters precedes cell loss and pathology in Alzheimer's disease. *Journal of Neurochemistry* 98: 939-50

Klafki H-W, Abramowski D, Swoboda R, Paganetti PA, Staufenbiel M. 1996. The Carboxyl Termini of β-Amyloid Peptides 1-40 and 1-42 Are Generated by Distinct γ-Secretase Activities. *Journal of Biological Chemistry* 271: 28655-59

Klunk WE, Engler H, Nordberg A, Wang Y, Blomqvist G, et al. 2004. Imaging brain amyloid in Alzheimer's disease with Pittsburgh Compound-B. *Ann Neurol* 55: 306–19

Klyubin I, Betts V, Welzel AT, Blennow K, Zetterberg H, et al. 2008. Amyloid beta protein dimer-containing human CSF disrupts synaptic plasticity: prevention by systemic passive immunization. *J Neurosci* 28: 4231-7

Klyubin I, Walsh DM, Lemere CA, Cullen WK, Shankar GM, et al. 2005. Amyloid β protein immunotherapy neutralizes Aβ oligomers that disrupt synaptic plasticity in vivo. *Nature Medicine* 11: 556

Koffie RM, Meyer-Luehmann M, Hashimoto T, Adams KW, Mielke ML, et al. 2009. Oligomeric amyloid beta associates with postsynaptic densities and correlates with excitatory synapse loss near senile plaques. *Proc Natl Acad Sci U S A* 106: 4012-7

Koh MT, Haberman RP, Foti S, McCown TJ, Gallagher M. 2010. Treatment strategies targeting excess hippocampal activity benefit aged rats with cognitive impairment. *Neuropsychopharmacology : official publication of the American College of Neuropsychopharmacology* 35: 1016–25

Kondo M, Kobayashi K, Ohkura M, Nakai J, Matsuzaki M. 2017. Two-photon calcium imaging of the medial prefrontal cortex and hippocampus without cortical invasion. *Elife* 6: e26839

Kong Q, Chang L-C, Takahashi K, Liu Q, Schulte DA, et al. 2014. Small-molecule activator of glutamate transporter EAAT2 translation provides neuroprotection. *The Journal of Clinical Investigation* 124: 1255-67

Kudo W, Lee H-P, Zou W-Q, Wang X, Perry G, et al. 2012. Cellular prion protein is essential for oligomeric amyloid-β-induced neuronal cell death. *Human Molecular Genetics* 21: 1138-44

Kuga N, Sasaki T, Takahara Y, Matsuki N, Ikegaya Y. 2011. Large-scale calcium waves traveling through astrocytic networks in vivo. *Journal of Neuroscience* 31: 2607-14

Kurudenkandy FR, Zilberter M, Biverstål H, Presto J, Honcharenko D, et al. 2014. Amyloid-β-induced action potential desynchronization and degradation of hippocampal gamma oscillations is prevented by interference with peptide conformation change and aggregation. *Journal of Neuroscience* 34: 11416-25

Lacor PN, Buniel MC, Chang L, Fernandez SJ, Gong Y, et al. 2004. Synaptic Targeting by Alzheimer's-Related Amyloid β Oligomers. *The Journal of Neuroscience* 24: 10191-200

Lacor PN, Buniel MC, Furlow PW, Sanz Clemente A, Velasco PT, et al. 2007. Aβ Oligomer-Induced Aberrations in Synapse Composition, Shape, and Density Provide a Molecular Basis for Loss of Connectivity in Alzheimer's Disease. *The Journal of Neuroscience* 27: 796-807

Lahiri DK, Ge Y-W. 2004. Role of the APP Promoter in Alzheimer's Disease: Cell Type-Specific Expression of the β-Amyloid Precursor Protein. *Annals of the New York Academy of Sciences* 1030: 310-16

Lambert J-C, Ibrahim-Verbaas CA, Harold D, Naj AC, Sims R, et al. 2013. Meta-analysis of 74,046 individuals identifies 11 new susceptibility loci for Alzheimer's disease. *Nature Genetics* 45: 1452

Lashuel HA, Hartley D, Petre BM, Walz T, Lansbury Jr PT. 2002. Amyloid pores from pathogenic mutations. *Nature* 418: 291

Laurén J, Gimbel DA, Nygaard HB, Gilbert JW, Strittmatter SM. 2009. Cellular Prion Protein Mediates Impairment of Synaptic Plasticity by Amyloid-β Oligomers. *Nature* 457: 1128-32

Le W-D, Colom LV, Xie W-j, Smith RG, Alexianu M, Appel SH. 1995. Cell death induced by β-amyloid 1–40 in MES 23.5 hybrid clone: the role of nitric oxide and NMDA-gated channel activation leading to apoptosis. *Brain Research* 686: 49-60

Leal SL, Landau SM, Bell RK, Jagust WJ. 2017. Hippocampal activation is associated with longitudinal amyloid accumulation and cognitive decline. *eLife* 6

Lee C-Y, Chen C-C, Liou H-H. 2009. Levetiracetam inhibits glutamate transmission through presynaptic P/Q-type calcium channels on the granule cells of the dentate gyrus. *British journal of pharmacology* 158: 1753-62

Lee SG, Su ZZ, Emdad L, Gupta P, Sarkar D, et al. 2008. Mechanism of ceftriaxone induction of excitatory amino acid transporter-2 expression and glutamate uptake in primary human astrocytes. *The Journal of biological chemistry* 283: 13116-23

Lerdkrai C, Asavapanumas N, Brawek B, Kovalchuk Y, Mojtahedi N, et al. 2018. Intracellular Ca^{2+} stores control in vivo neuronal hyperactivity in a mouse model of Alzheimer's disease. *Proceedings of the National Academy of Sciences* 115: E1279-E88

Lesné S, Koh MT, Kotilinek L, Kayed R, Glabe CG, et al. 2006. A specific amyloid-beta protein assembly in the brain impairs memory. *Nature* 440: 352-7

Lesné S, Kotilinek L, Ashe KH. 2008. Plaque-bearing mice with reduced levels of oligomeric amyloid-β assemblies have intact memory function. *Neuroscience* 151: 745-49

Lester RAJ, Clements JD, Westbrook GL, Jahr CE. 1990. Channel kinetics determine the time course of NMDA receptor-mediated synaptic currents. *Nature* 346: 565

Li S, Hong S, Shepardson NE, Walsh DM, Shankar GM, Selkoe D. 2009. Soluble oligomers of amyloid Beta protein facilitate hippocampal long-term depression by disrupting neuronal glutamate uptake. *Neuron* 62: 788–801

Li S, Jin M, Koeglsperger T, Shepardson NE, Shankar GM, Selkoe DJ. 2011. Soluble Aβ oligomers inhibit long-term potentiation through a mechanism involving excessive activation of

extrasynaptic NR2B-containing NMDA receptors. *The Journal of neuroscience : the official journal of the Society for Neuroscience* 31: 6627–38

Li S, Jin M, Liu L, Dang Y, Ostaszewski BL, Selkoe DJ. 2018. Decoding the synaptic dysfunction of bioactive human AD brain soluble Aβ to inspire novel therapeutic avenues for Alzheimer's disease. *Acta Neuropathologica Communications* 6: 121

Li S, Mallory M, Alford M, Tanaka S, Masliah E. 1997. Glutamate Transporter Alterations in Alzheimer Disease Are Possibly Associated with Abnormal APP Expression. *Journal of Neuropathology & Experimental Neurology* 56: 901-11

Lichtman JW, Conchello J-A. 2005. Fluorescence microscopy. *Nature Methods* 2: 910

Liebscher S, Keller GB, Goltstein PM, Bonhoeffer T, Hubener M. 2016. Selective Persistence of Sensorimotor Mismatch Signals in Visual Cortex of Behaving Alzheimer's Disease Mice. *Current biology : CB* 26: 956-64

Liu P, Reed Miranda N, Kotilinek Linda A, Grant Marianne KO, Forster Colleen L, et al. 2015. Quaternary Structure Defines a Large Class of Amyloid-β Oligomers Neutralized by Sequestration. *Cell reports* 11: 1760-71

Loerch PM, Lu T, Dakin KA, Vann JM, Isaacs A, et al. 2008. Evolution of the aging brain transcriptome and synaptic regulation. *PloS one* 3: e3329

Logothetis NK, Pauls J, Augath M, Trinath T, Oeltermann A. 2001. *Nature* 412: 150–57

Lustig C, Snyder AZ, Bhakta M, O'Brien KC, McAvoy M, et al. 2003. Functional deactivations: change with age and dementia of the Alzheimer type. *Proc Natl Acad Sci U S A* 100: 14504–09

Lynch BA, Lambeng N, Nocka K, Kensel-Hammes P, Bajjalieh SM, et al. 2004. The synaptic vesicle protein SV2A is the binding site for the antiepileptic drug levetiracetam. *Proceedings of the National Academy of Sciences of the United States of America* 101: 9861-66

Malinow R. 2012. New developments on the role of NMDA receptors in Alzheimer's disease. *Current opinion in neurobiology* 22: 559-63

Malthankar-Phatak G, Poplawski S, Toraskar N, Siman R. 2012. Combination therapy prevents amyloid-dependent and -independent structural changes. *Neurobiology of aging* 33: 1273-83

Manabe T, Wyllie DJ, Perkel DJ, Nicoll RA. 1993. Modulation of synaptic transmission and long-term potentiation: effects on paired pulse facilitation and EPSC variance in the CA1 region of the hippocampus. *Journal of Neurophysiology* 70: 1451-59

Mander BA, Marks SM, Vogel JW, Rao V, Lu B, et al. 2015. beta-amyloid disrupts human NREM slow waves and related hippocampus-dependent memory consolidation. *Nat Neurosci* 18: 1051–57

Mann K, Kiefer F, Spanagel R, Littleton J. 2008. Acamprosate: Recent Findings and Future Research Directions. *Alcoholism: Clinical and Experimental Research* 32: 1105-10

Marchetti C, Marie H. 2011. Hippocampal synaptic plasticity in Alzheimer's disease: what have we learned so far from transgenic models? In *Reviews in the Neurosciences*, pp. 373

Marshall L, Helgadóttir H, Mölle M, Born J. 2006. Boosting slow oscillations during sleep potentiates memory. *Nature* 444: 610–13

Martin JJ, Gheuens J, Bruyland M, Cras P, Vandenberghe A, et al. 1991. Early‐onset Alzheimer's disease in 2 large Belgian families. *Neurology* 41: 62-62

Martinez-Losa M, Tracy TE, Ma K, Verret L, Clemente-Perez A, et al. 2018. Nav1.1-Overexpressing Interneuron Transplants Restore Brain Rhythms and Cognition in a Mouse Model of Alzheimer's Disease. *Neuron* 98: 75-89.e5

Marvin JS, Borghuis BG, Tian L, Cichon J, Harnett MT, et al. 2013. An optimized fluorescent probe for visualizing glutamate neurotransmission. *Nature methods* 10: 162-70

Masliah E, Hansen L, Alford M, Deteresa R, Mallory M. 1996. Deficient glutamate tranport is associated with neurodegeneration in Alzheimer's disease. *Annals of Neurology* 40: 759-66

Masliah E, Mallory M, Hansen L, DeTeresa R, Alford M, Terry R. 1994. Synaptic and neuritic alterations during the progression of Alzheimer's disease. *Neuroscience letters* 174: 67-72

McBean GJ, Roberts PJ. 1985. Neurotoxicity of L-Glutamate and DL-Threo-3-Hydroxyaspartate in the Rat Striatum. *Journal of Neurochemistry* 44: 247-54

McDonald JM, Cairns NJ, Taylor-Reinwald L, Holtzman D, Walsh DM. 2012. The levels of water-soluble and triton-soluble Aβ are increased in Alzheimer's disease brain. *Brain research* 1450: 138-47

McKhann GM, Knopman DS, Chertkow H, Hyman BT, Jack CR, et al. 2011. The diagnosis of dementia due to Alzheimer's disease: recommendations from the National Institute on Aging-Alzheimer's Association workgroups on diagnostic guidelines for Alzheimer's disease. *Alzheimer's & dementia : the journal of the Alzheimer's Association* 7: 263–69

McLean CA, Cherny RA, Fraser FW, Fuller SJ, Smith MJ, et al. 1999. Soluble pool of Aβ amyloid as a determinant of severity of neurodegeneration in Alzheimer's disease. *Annals of Neurology* 46: 860-66

Mehlhorn G, Hollborn M, Schliebs R. 2000. Induction of cytokines in glial cells surrounding cortical β-amyloid plaques in transgenic Tg2576 mice with Alzheimer pathology. *International Journal of Developmental Neuroscience* 18: 423-31

Meyer-Luehmann M, Coomaraswamy J, Bolmont T, Kaeser S, Schaefer C, et al. 2006. Exogenous Induction of Cerebral ß-Amyloidogenesis Is Governed by Agent and Host. *Science* 313: 1781-84

Mizrahi A, Crowley JC, Shtoyerman E, Katz LC. 2004. High-Resolution *In Vivo* Imaging of Hippocampal Dendrites and Spines. *The Journal of Neuroscience* 24: 3147-51

Moore BD, Chakrabarty P, Levites Y, Kukar TL, Baine A-M, et al. 2012. Overlapping profiles of Aβ peptides in the Alzheimer's disease and pathological aging brains. *Alzheimer's research & therapy* 4: 18-18

Mormino EC, Brandel MG, Madison CM, Marks S, Baker SL, Jagust WJ. 2012. Aβ Deposition in aging is associated with increases in brain activation during successful memory encoding. *Cerebral cortex (New York, N.Y. : 1991)* 22: 1813–23

Moser EI, Kropff E, Moser M-B. 2008. Place Cells, Grid Cells, and the Brain's Spatial Representation System. *Annual Review of Neuroscience* 31: 69-89

Mullan M, Crawford F, Axelman K, Houlden H, Lilius L, et al. 1992. A pathogenic mutation for probable Alzheimer's disease in the APP gene at the N–terminus of β–amyloid. *Nature Genetics* 1: 345

Müller-Schiffmann A, Herring A, Abdel-Hafiz L, Chepkova AN, Schäble S, et al. 2016. Amyloid-β dimers in the absence of plaque pathology impair learning and synaptic plasticity. *Brain* 139: 509-25

Müller UC, Deller T, Korte M. 2017. Not just amyloid: physiological functions of the amyloid precursor protein family. *Nat Rev Neurosci* 18: 281–98

Murphy-Royal C, Dupuis JP, Varela JA, Panatier A, Pinson B, et al. 2015. Surface diffusion of astrocytic glutamate transporters shapes synaptic transmission. *Nature Neuroscience* 18: 219

Nagarathinam A, Höflinger P, Bühler A, Schäfer C, McGovern G, et al. 2013. Membrane-Anchored Aβ Accelerates Amyloid Formation and Exacerbates Amyloid-Associated Toxicity in Mice. *The Journal of Neuroscience* 33: 19284-94

Nalbantoglu J, Tirado-Santiago G, Lahsaïni A, Poirier J, Goncalves O, et al. 1997. Impaired learning and LTP in mice expressing the carboxy terminus of the Alzheimer amyloid precursor protein. *Nature* 387: 500-05

Ngo H-VV, Martinetz T, Born J, Mölle M. 2013. Auditory closed-loop stimulation of the sleep slow oscillation enhances memory. *Neuron* 78: 545–53

Nicoll RA. 2017. A Brief History of Long-Term Potentiation. *Neuron* 93: 281-90

Nie H, Weng H-R. 2009. Glutamate transporters prevent excessive activation of NMDA receptors and extrasynaptic glutamate spillover in the spinal dorsal horn. *Journal of neurophysiology* 101: 2041-51

Niell CM, Stryker MP. 2008. Highly Selective Receptive Fields in Mouse Visual Cortex. *The Journal of Neuroscience* 28: 7520-36

Nimmerjahn A, Helmchen F. 2012. In Vivo Labeling of Cortical Astrocytes with Sulforhodamine 101 (SR101). *Cold Spring Harbor Protocols* 2012: pdb.prot068155

Nowak LM, Young AB, Macdonald RL. 1982. GABA and bicuculline actions on mouse spinal cord and cortical neurons in cell culture. *Brain REsearch* 244: 155-64

O'Brien JL, O'Keefe KM, LaViolette PS, DeLuca AN, Blacker D, et al. 2010. Longitudinal fMRI in elderly reveals loss of hippocampal activation with clinical decline. *Neurology* 74: 1969–76

O'Brien RJ, Wong PC. 2011. Amyloid Precursor Protein Processing and Alzheimer's Disease. *Annual Review of Neuroscience* 34: 185-204

O'Shea SD, Smith IM, McCabe OM, Cronin MM, Walsh DM, O'Connor WT. 2008. Intracerebroventricular Administration of Amyloid β-protein Oligomers Selectively Increases Dorsal Hippocampal Dialysate Glutamate Levels in the Awake Rat. *Sensors (Basel, Switzerland)* 8: 7428-37

Offe K, Dodson SE, Shoemaker JT, Fritz JJ, Gearing M, et al. 2006. The Lipoprotein Receptor LR11 Regulates Amyloid β Production and Amyloid Precursor Protein Traffic in Endosomal Compartments. *The Journal of Neuroscience* 26: 1596-603

Oheim M, Beaurepaire E, Chaigneau E, Mertz J, Charpak S. 2001. Two-photon microscopy in brain tissue: parameters influencing the imaging depth. *Journal of Neuroscience Methods* 111: 29-37

Ouzounov DG, Wang T, Wang M, Feng DD, Horton NG, et al. 2017. In vivo three-photon imaging of activity of GCaMP6-labeled neurons deep in intact mouse brain. *Nature Methods* 14: 388

Palmqvist S, Schöll M, Strandberg O, Mattsson N, Stomrud E, et al. 2017. Earliest accumulation of β-amyloid occurs within the default-mode network and concurrently affects brain connectivity. *Nature Communications* 8: 1214

Palop JJ, Chin J, Roberson ED, Wang J, Thwin MT, et al. 2007. Aberrant excitatory neuronal activity and compensatory remodeling of inhibitory hippocampal circuits in mouse models of Alzheimer's disease. *Neuron* 55: 697-711

Palop JJ, Mucke L. 2016. Network abnormalities and interneuron dysfunction in Alzheimer disease. *Nat Rev Neurosci* 17: 777-92

Pariente J, Cole S, Henson R, Clare L, Kennedy A, et al. 2005. Alzheimer's patients engage an alternative network during a memory task. *Ann Neurol* 58: 870–79

Park JH, Gimbel DA, GrandPre T, Lee J-K, Kim J-E, et al. 2006a. Alzheimer precursor protein interaction with the Nogo-66 receptor reduces amyloid-beta plaque deposition. *The Journal of neuroscience : the official journal of the Society for Neuroscience* 26: 1386-95

Park JH, Widi GA, Gimbel DA, Harel NY, Lee DHS, Strittmatter SM. 2006b. Subcutaneous Nogo receptor removes brain amyloid-beta and improves spatial memory in Alzheimer's

transgenic mice. *The Journal of neuroscience : the official journal of the Society for Neuroscience* 26: 13279-86

Parpura-Gill A, Beitz D, Uemura E. 1997. The inhibitory effects of β-amyloid on glutamate and glucose uptakes by cultured astrocytes. *Brain Research* 754: 65-71

Paxinos G, Franklin K. 2012. *Paxinos and Franklin's the Mouse Brain in Stereotaxic Coordinates, Fourth Edition*. Academic Press.

Peigneux P, Laureys S, Fuchs S, Collette F, Perrin F, et al. 2004. Are spatial memories strengthened in the human hippocampus during slow wave sleep? *Neuron* 44: 535–45

Perea G, Navarrete M, Araque A. 2009. Tripartite synapses: astrocytes process and control synaptic information. *Trends in Neurosciences* 32: 421-31

Podlisny MB, Ostaszewski BL, Squazzo SL, Koo EH, Rydell RE, et al. 1995. Aggregation of Secreted Amyloid -Protein into Sodium Dodecyl Sulfate-stable Oligomers in Cell Culture. *Journal of Biological Chemistry* 270: 9564-70

Prasher VP, Farrer MJ, Kessling AM, Fisher EMC, West RJ, et al. 2004. Molecular mapping of alzheimer-type dementia in Down's syndrome. *Annals of Neurology* 43: 380-83

Prince M, Wimo A, Guerchet M, Ali G, Wu Y, Prina M. 2015. World Alzheimer Report 2015. The Global Impact of Dementia. Alzheimer's Disease International. *Alzheimer's Disease International (ADI), London*

Pujol-Pina R, Vilaprinyó-Pascual S, Mazzucato R, Arcella A, Vilaseca M, et al. 2015. SDS-PAGE analysis of Aβ oligomers is disserving research into Alzheimer´s disease: appealing for ESI-IM-MS. *Scientific Reports* 5: 14809

Puzzo D, Gulisano W, Arancio O, Palmeri A. 2015. The keystone of Alzheimer pathogenesis might be sought in Aβ physiology. *Neuroscience* 307: 26-36

Puzzo D, Privitera L, Leznik E, Fa M, Staniszewski A, et al. 2008. Picomolar amyloid-beta positively modulates synaptic plasticity and memory in hippocampus. *J Neurosci* 28: 14537-45

Quiroz YT, Budson AE, Celone K, Ruiz A, Newmark R, et al. 2010. Hippocampal hyperactivation in presymptomatic familial Alzheimer's disease. *Ann Neurol* 68: 865–75

Quist A, Doudevski I, Lin H, Azimova R, Ng D, et al. 2005. Amyloid ion channels: A common structural link for protein-misfolding disease. *Proceedings of the National Academy of Sciences of the United States of America* 102: 10427-32

Raichle ME, MacLeod AM, Snyder AZ, Powers WJ, Gusnard DA, Shulman GL. 2001. A default mode of brain function. *Proc Natl Acad Sci U S A* 98: 676–82

Rammes G, Hasenjäger A, Sroka-Saidi K, Deussing JM, Parsons CG. 2011. Therapeutic significance of NR2B-containing NMDA receptors and mGluR5 metabotropic glutamate receptors in mediating the synaptotoxic effects of β-amyloid oligomers on long-term potentiation (LTP) in murine hippocampal slices. *Neuropharmacology* 60: 982-90

Ramsden M, Kotilinek L, Forster C, Paulson J, McGowan E, et al. 2005. Age-Dependent Neurofibrillary Tangle Formation, Neuron Loss, and Memory Impairment in a Mouse Model of Human Tauopathy (P301L). *The Journal of Neuroscience* 25: 10637-47

Reisberg B, Doody R, Stöffler A, Schmitt F, Ferris S, Möbius HJ. 2003. Memantine in Moderate-to-Severe Alzheimer's Disease. *New England Journal of Medicine* 348: 1333-41

Renner M, Lacor PN, Velasco PT, Xu J, Contractor A, et al. 2010. Deleterious effects of amyloid beta oligomers acting as an extracellular scaffold for mGluR5. *Neuron* 66: 739-54

Resch-Genger U, Grabolle M, Cavaliere-Jaricot S, Nitschke R, Nann T. 2008. Quantum dots versus organic dyes as fluorescent labels. *Nature Methods* 5: 763

Resenberger UK, Harmeier A, Woerner AC, Goodman JL, Müller V, et al. 2011. The cellular prion protein mediates neurotoxic signalling of β-sheet-rich conformers independent of prion replication. *The EMBO Journal* 30: 2057-70

Roberson ED, Scearce-Levie K, Palop JJ, Yan F, Cheng IH, et al. 2007. Reducing endogenous tau ameliorates amyloid beta-induced deficits in an Alzheimer's disease mouse model. *Science (New York, N.Y.)* 316: 750–54

Rochefort NL, Garaschuk O, Milos R-I, Narushima M, Marandi N, et al. 2009. Sparsification of neuronal activity in the visual cortex at eye-opening. *Proceedings of the National Academy of Sciences* 106: 15049-54

Rochefort NL, Jia H, Konnerth A. 2008. Calcium imaging in the living brain: prospects for molecular medicine. *Trends in Molecular Medicine* 14: 389-99

Rodriguez-Kern A, Gegelashvili M, Schousboe A, Zhang J, Sung L, Gegelashvili G. 2003. Beta-amyloid and brain-derived neurotrophic factor, BDNF, up-regulate the expression of glutamate transporter GLT-1/EAAT2 via different signaling pathways utilizing transcription factor NF-κB. *Neurochemistry International* 43: 363-70

Rogers J, Cooper NR, Webster S, Schultz J, McGeer PL, et al. 1992. Complement activation by beta-amyloid in Alzheimer disease. *Proceedings of the National Academy of Sciences of the United States of America* 89: 10016-20

Rönicke R, Mikhaylova M, Rönicke S, Meinhardt J, Schröder UH, et al. 2011. Early neuronal dysfunction by amyloid β oligomers depends on activation of NR2B-containing NMDA receptors. *Neurobiology of Aging* 32: 2219-28

Rose T, Goltstein PM, Portugues R, Griesbeck O. 2014. Putting a finishing touch on GECIs. *Frontiers in molecular neuroscience* 7: 88

Rothstein JD, Dykes-Hoberg M, Pardo CA, Bristol LA, Jin L, et al. 1996. Knockout of Glutamate Transporters Reveals a Major Role for Astroglial Transport in Excitotoxicity and Clearance of Glutamate. *Neuron* 16: 675-86

Rothstein JD, Patel S, Regan MR, Haenggeli C, Huang YH, et al. 2005. Beta-lactam antibiotics offer neuroprotection by increasing glutamate transporter expression. *Nature* 433: 73–77

Rudinskiy N, Hawkes JM, Betensky RA, Eguchi M, Yamaguchi S, et al. 2012. Orchestrated experience-driven Arc responses are disrupted in a mouse model of Alzheimer's disease. *Nat Neurosci* 15: 1422-9

Rushworth JV, Hooper NM. 2011. Lipid Rafts: Linking Alzheimer's Amyloid-β Production, Aggregation, and Toxicity at Neuronal Membranes. *International Journal of Alzheimer's Disease* 2011: 603052

Sanchez PE, Zhu L, Verret L, Vossel KA, Orr AG, et al. 2012. Levetiracetam suppresses neuronal network dysfunction and reverses synaptic and cognitive deficits in an Alzheimer's disease model. *Proc Natl Acad Sci U S A* 109: E2895-903

Santacruz K, Lewis J, Spires T, Paulson J, Kotilinek L, et al. 2005. Tau suppression in a neurodegenerative mouse model improves memory function. *Science (New York, N.Y.)* 309: 476-81

Sanz-Blasco S, Piña-Crespo JC, Zhang X, McKercher SR, Lipton SA. 2016. Levetiracetam inhibits oligomeric Aβ-induced glutamate release from human astrocytes. *Neuroreport* 27: 705-09

Scala F, Fusco S, Ripoli C, Piacentini R, Li Puma DD, et al. 2015. Intraneuronal Abeta accumulation induces hippocampal neuron hyperexcitability through A-type K(+) current inhibition mediated by activation of caspases and GSK-3. *Neurobiol Aging* 36: 886-900

Schallier A, Smolders I, Van Dam D, Loyens E, De Deyn PP, et al. 2011. Region- and age-specific changes in glutamate transport in the APP23 mouse model for Alzheimer's disease. *Journal of Alzheimer's disease : JAD* 24.2: 287-300

Scheuner D, Eckman C, Jensen M, Song X, Citron M, et al. 1996. Secreted amyloid β–protein similar to that in the senile plaques of Alzheimer's disease is increased in vivo by the

presenilin 1 and 2 and APP mutations linked to familial Alzheimer's disease. *Nature Medicine* 2: 864

Schmid AW, Freir DB, Herron CE. 2008. Inhibition of LTP in vivo by beta-amyloid peptide in different conformational states. *Brain Research* 1197: 135-42

Schmid Lena C, Mittag M, Poll S, Steffen J, Wagner J, et al. 2016. Dysfunction of Somatostatin-Positive Interneurons Associated with Memory Deficits in an Alzheimer's Disease Model. *Neuron* 92: 114-25

Schreiner A, Rose C. 2012. Quantitative imaging of intracellular so dium. *Current Microscopy Contributions to Advances in Science and Technology (Méndez-Vilas A, ed)*: 119-29

Scimemi A, Meabon JS, Woltjer RL, Sullivan JM, Diamond JS, Cook DG. 2013. Amyloid-β1-42 slows clearance of synaptically released glutamate by mislocalizing astrocytic GLT-1. *The Journal of neuroscience : the official journal of the Society for Neuroscience* 33: 5312-18

Scott HA, Gebhardt FM, Mitrovic AD, Vandenberg RJ, Dodd PR. 2011. Glutamate transporter variants reduce glutamate uptake in Alzheimer's disease. *Neurobiology of Aging* 32: 553.e1-53.e11

Scoville WB, Milner B. 1957. Loss of recent memory after bilateral hippocampal lesions. *Journal of neurology, neurosurgery, and psychiatry* 20: 11

Selkoe DJ. 2002. Alzheimer's disease is a synaptic failure. *Science* 298: 789-91

Selkoe DJ. 2008. Soluble Oligomers of the Amyloid β-Protein Impair Synaptic Plasticity and Behavior. *Behavioural brain research* 192: 106-13

Selkoe DJ, Hardy J. 2016. The amyloid hypothesis of Alzheimer's disease at 25 years. *EMBO molecular medicine* 8: 595–608

Sengupta U, Nilson AN, Kayed R. 2016. The Role of Amyloid-β Oligomers in Toxicity, Propagation, and Immunotherapy. *EBioMedicine* 6: 42-49

Serrano-Pozo A, Frosch MP, Masliah E, Hyman BT. 2011a. Neuropathological alterations in Alzheimer disease. *Cold Spring Harbor perspectives in medicine* 1: a006189

Serrano-Pozo A, Mielke ML, Gómez-Isla T, Betensky RA, Growdon JH, et al. 2011b. Reactive glia not only associates with plaques but also parallels tangles in Alzheimer's disease. *The American journal of pathology* 179: 1373-84

Shankar GM, Bloodgood BL, Townsend M, Walsh DM, Selkoe DJ, Sabatini BL. 2007. Natural oligomers of the Alzheimer amyloid-beta protein induce reversible synapse loss by modulating an NMDA-type glutamate receptor-dependent signaling pathway. *J Neurosci* 27: 2866-75

Shankar GM, Li S, Mehta TH, Garcia-Munoz A, Shepardson NE, et al. 2008. Amyloid-beta protein dimers isolated directly from Alzheimer's brains impair synaptic plasticity and memory. *Nat Med* 14: 837–42

Shoham S, O'Connor DH, Segev R. 2006. How silent is the brain: is there a "dark matter" problem in neuroscience? *Journal of Comparative Physiology A* 192: 777-84

Shoji M, Kanai M. 2001. Cerebrospinal fluid Aβ40 and Aβ42: natural course and clinical usefulness. *Journal of Alzheimer's Disease* 3: 313-21

Simon AM, de Maturana RL, Ricobaraza A, Escribano L, Schiapparelli L, et al. 2009. Early changes in hippocampal Eph receptors precede the onset of memory decline in mouse models of Alzheimer's disease. *J Alzheimers Dis* 17: 773-86

Siskova Z, Justus D, Kaneko H, Friedrichs D, Henneberg N, et al. 2014. Dendritic structural degeneration is functionally linked to cellular hyperexcitability in a mouse model of Alzheimer's disease. *Neuron* 84: 1023-33

Somjen GG. 1979. Extracellular Potassium in the Mammalian Central Nervous System. *Annual Review of Physiology* 41: 159-77

Sperling RA, Aisen PS, Beckett LA, Bennett DA, Craft S, et al. 2011. Toward defining the preclinical stages of Alzheimer's disease: recommendations from the National Institute on Aging-Alzheimer's Association workgroups on diagnostic guidelines for Alzheimer's disease. *Alzheimer's & dementia : the journal of the Alzheimer's Association* 7: 280–92

Sperling RA, Dickerson BC, Pihlajamaki M, Vannini P, LaViolette PS, et al. 2010. Functional alterations in memory networks in early Alzheimer's disease. *Neuromolecular medicine* 12: 27–43

Sperling RA, Laviolette PS, O'Keefe K, O'Brien J, Rentz DM, et al. 2009. Amyloid deposition is associated with impaired default network function in older persons without dementia. *Neuron* 63: 178–88

Spira AP, Gamaldo AA, An Y, Wu MN, Simonsick EM, et al. 2013. Self-reported sleep and β-amyloid deposition in community-dwelling older adults. *JAMA neurology* 70: 1537–43

Spires TL, Meyer-Luehmann M, Stern EA, McLean PJ, Skoch J, et al. 2005. Dendritic spine abnormalities in amyloid precursor protein transgenic mice demonstrated by gene transfer and intravital multiphoton microscopy. *J Neurosci* 25: 7278-87

Spires TL, Orne JD, SantaCruz K, Pitstick R, Carlson GA, et al. 2006. Region-specific dissociation of neuronal loss and neurofibrillary pathology in a mouse model of tauopathy. *The American journal of pathology* 168: 1598-607

Spoelgen R, von Arnim CAF, Thomas AV, Peltan ID, Koker M, et al. 2006. Interaction of the Cytosolic Domains of sorLA/LR11 with the Amyloid Precursor Protein (APP) and β-Secretase β-Site APP-Cleaving Enzyme. *The Journal of Neuroscience* 26: 418-28

Sprecher KE, Koscik RL, Carlsson CM, Zetterberg H, Blennow K, et al. 2017. Poor sleep is associated with CSF biomarkers of amyloid pathology in cognitively normal adults. *Neurology* 89: 445-53

Spruston N. 2008. Pyramidal neurons: dendritic structure and synaptic integration. *Nature Reviews Neuroscience* 9: 206

Staresina BP, Bergmann TO, Bonnefond M, van der Meij R, Jensen O, et al. 2015. Hierarchical nesting of slow oscillations, spindles and ripples in the human hippocampus during sleep. *Nat Neurosci* 18: 1679–86

Stargardt A, Swaab DF, Bossers K. 2015. The storm before the quiet: neuronal hyperactivity and Aβ in the presymptomatic stages of Alzheimer's disease. *Neurobiology of Aging* 36: 1-11

Stéphan A, Laroche S, Davis S. 2001. Generation of Aggregated β-Amyloid in the Rat Hippocampus Impairs Synaptic Transmission and Plasticity and Causes Memory Deficits. *The Journal of Neuroscience* 21: 5703-14

Steriade M. 2006. Grouping of brain rhythms in corticothalamic systems. *Neuroscience* 137: 1087–106

Steriade M, Nunez A, Amzica F. 1993. A novel slow (< 1 Hz) oscillation of neocortical neurons in vivo: depolarizing and hyperpolarizing components. *Journal of Neuroscience* 13: 3252–65

Stine WB, Jungbauer L, Yu C, LaDu MJ. 2011. Preparing Synthetic Aβ in Different Aggregation States. *Methods in molecular biology (Clifton, N.J.)* 670: 13-32

Stocca G, Vicini S. 1998. Increased contribution of NR2A subunit to synaptic NMDA receptors in developing rat cortical neurons. *The Journal of physiology* 507: 13-24

Stosiek C, Garaschuk O, Holthoff K, Konnerth A. 2003. In vivo two-photon calcium imaging of neuronal networks. *Proceedings of the National Academy of Sciences* 100: 7319

Sturchler-Pierrat C, Abramowski D, Duke M, Wiederhold KH, Mistl C, et al. 1997. Two amyloid precursor protein transgenic mouse models with Alzheimer disease-like pathology. *Proceedings of the National Academy of Sciences of the United States of America* 94: 13287-92

Svoboda K, Block SM. 1994. Biological applications of optical forces. *Annual review of biophysics and biomolecular structure* 23: 247-85

Tada M, Takeuchi A, Hashizume M, Kitamura K, Kano M. 2014. A highly sensitive fluorescent indicator dye for calcium imaging of neural activity in vitro and in vivo. *European Journal of Neuroscience* 39: 1720-28

Takahashi K, Kong Q, Lin Y, Stouffer N, Schulte DA, et al. 2015. Restored glial glutamate transporter EAAT2 function as a potential therapeutic approach for Alzheimer's disease. *The Journal of experimental medicine* 212: 319-32

Talantova M, Sanz-Blasco S, Zhang X, Xia P, Akhtar MW, et al. 2013. Aβ induces astrocytic glutamate release, extrasynaptic NMDA receptor activation, and synaptic loss. *Proceedings of the National Academy of Sciences* 110: E2518-E27

Tanaka K, Watase K, Manabe T, Yamada K, Watanabe M, et al. 1997. Epilepsy and Exacerbation of Brain Injury in Mice Lacking the Glutamate Transporter GLT-1. *Science* 276: 1699-702

Tanzi RE. 2012. The Genetics of Alzheimer Disease. *Cold Spring Harbor Perspectives in Medicine*: a006296

Terry RD, Masliah E, Salmon DP, Butters N, DeTeresa R, et al. 1991. Physical basis of cognitive alterations in Alzheimer's disease: synapse loss is the major correlate of cognitive impairment. *Ann Neurol* 30: 572-80

Thal DR, Rub U, Orantes M, Braak H. 2002. Phases of A beta-deposition in the human brain and its relevance for the development of AD. *Neurology* 58: 1791–800

Theer P, Hasan MT, Denk W. 2003. Two-photon imaging to a depth of 1000 µm in living brains by use of a Ti:Al_2O_3 regenerative amplifier. *Optics letters* 28: 1022-24

Thomson AM. 2000. Facilitation, augmentation and potentiation at central synapses. *Trends in Neurosciences* 23: 305-12

Tian L, Hires SA, Looger LL. 2012. Imaging Neuronal Activity with Genetically Encoded Calcium Indicators. *Cold Spring Harbor Protocols* 2012: pdb.top069609

Tischbirek C, Birkner A, Jia H, Sakmann B, Konnerth A. 2015. Deep two-photon brain imaging with a red-shifted fluorometric Ca^{2+} indicator. *Proceedings of the National Academy of Sciences* 112: 11377-82

Tischbirek CH, Birkner A, Konnerth A. 2017. In vivo deep two-photon imaging of neural circuits with the fluorescent Ca2+ indicator Cal-590. *The Journal of Physiology* 595: 3097-105

Traynelis SF, Dingledine R. 1988. Potassium-induced spontaneous electrographic seizures in the rat hippocampal slice. *Journal of neurophysiology* 59: 259-76

Tsai J, Grutzendler J, Duff K, Gan W-B. 2004. Fibrillar amyloid deposition leads to local synaptic abnormalities and breakage of neuronal branches. *Nature Neuroscience* 7: 1181

Tsien RY. 1981. A non-disruptive technique for loading calcium buffers and indicators into cells. *Nature* 290: 527-8

Ulrich JD, Finn MB, Wang Y, Shen A, Mahan TE, et al. 2014. Altered microglial response to Aβ plaques in APPPS1-21 mice heterozygous for TREM2. *Molecular Neurodegeneration* 9: 20

Um Ji W, Kaufman Adam C, Kostylev M, Heiss Jacqueline K, Stagi M, et al. 2013. Metabotropic Glutamate Receptor 5 Is a Coreceptor for Alzheimer Aβ Oligomer Bound to Cellular Prion Protein. *Neuron* 79: 887-902

Um JW, Nygaard HB, Heiss JK, Kostylev MA, Stagi M, et al. 2012. Alzheimer amyloid-β oligomer bound to postsynaptic prion protein activates Fyn to impair neurons. *Nature Neuroscience* 15: 1227

Utevsky AV, Smith DV, Huettel SA. 2014. Precuneus is a functional core of the default-mode network. *The Journal of neuroscience* 34: 932–40

Vargha-Khadem F, Gadian DG, Watkins KE, Connelly A, Van Paesschen W, Mishkin M. 1997. Differential Effects of Early Hippocampal Pathology on Episodic and Semantic Memory. *Science* 277: 376-80

Vázquez de la Torre A, Gay M, Vilaprinyó-Pascual S, Mazzucato R, Serra-Batiste M, et al. 2018. Direct Evidence of the Presence of Cross-Linked Aβ Dimers in the Brains of Alzheimer's Disease Patients. *Analytical Chemistry* 90: 4552-60

Verret L, Mann EO, Hang GB, Barth AM, Cobos I, et al. 2012. Inhibitory interneuron deficit links altered network activity and cognitive dysfunction in Alzheimer model. *Cell* 149: 708-21

Walsh DM, Klyubin I, Fadeeva JV, Cullen WK, Anwyl R, et al. 2002. Naturally secreted oligomers of amyloid beta protein potently inhibit hippocampal long-term potentiation in vivo. *Nature* 416: 535-9

Wang H-Y, Lee DHS, Davis CB, Shank RP. 2000. Amyloid Peptide Aβ1-42 Binds Selectively and with Picomolar Affinity to α7 Nicotinic Acetylcholine Receptors. *Journal of Neurochemistry* 75: 1155-61

Wang Z, Jackson RJ, Hong W, Taylor WM, Corbett GT, et al. 2017. Human Brain-Derived Aβ Oligomers Bind to Synapses and Disrupt Synaptic Activity in a Manner That Requires APP. *The Journal of neuroscience : the official journal of the Society for Neuroscience* 37: 11947-66

Watase K, Hashimoto K, Kano M, Yamada K, Watanabe M, et al. 1998. Motor discoordination and increased susceptibility to cerebellar injury in GLAST mutant mice. *European Journal of Neuroscience* 10: 976-88

Watt AD, Perez KA, Rembach A, Sherrat NA, Hung LW, et al. 2013. Oligomers, fact or artefact? SDS-PAGE induces dimerization of beta-amyloid in human brain samples. *Acta Neuropathol* 125: 549-64

Wei W, Nguyen LN, Kessels HW, Hagiwara H, Sisodia S, Malinow R. 2010. Amyloid beta from axons and dendrites reduces local spine number and plasticity. *Nat Neurosci* 13: 190-6

Welzel AT, Maggio JE, Shankar GM, Walker DE, Ostaszewski BL, et al. 2014. Secreted amyloid β-proteins in a cell culture model include N-terminally extended peptides that impair synaptic plasticity. *Biochemistry* 53: 3908-21

Westerberg CE, Lundgren EM, Florczak SM, Mesulam M-M, Weintraub S, et al. 2010. Sleep influences the severity of memory disruption in amnestic mild cognitive impairment: results from sleep self-assessment and continuous activity monitoring. *Alzheimer disease and associated disorders* 24: 325–33

Willem M, Tahirovic S, Busche MA, Ovsepian SV, Chafai M, et al. 2015. eta-Secretase processing of APP inhibits neuronal activity in the hippocampus. *Nature* 526: 443-7

Williamson R, Wheal H. 1992. The contribution of AMPA and NMDA receptors to graded bursting activity in the hippocampal CA1 region in an acute in vitro model of epilepsy. *Epilepsy research* 12: 179-88

Wilson IA, Ikonen S, Gallagher M, Eichenbaum H, Tanila H. 2005. Age-associated alterations of hippocampal place cells are subregion specific. *J Neurosci* 25: 6877-86

Wilson MA, McNaughton BL. 1994. Reactivation of hippocampal ensemble memories during sleep. *Science* 265: 676–79

Wojciech D, Parsons C. 2012. Alzheimer's disease, β - amyloid, glutamate, NMDA receptors and memantine – searching for the connections. *British Journal of Pharmacology* 167: 324-52

Wolfe MS, Xia W, Ostaszewski BL, Diehl TS, Kimberly WT, Selkoe DJ. 1999. Two transmembrane aspartates in presenilin-1 required for presenilin endoproteolysis and γ-secretase activity. *Nature* 398: 513

Wu L, Saggau P. 1994. Presynaptic calcium is increased during normal synaptic transmission and paired-pulse facilitation, but not in long-term potentiation in area CA1 of hippocampus. *Journal of Neuroscience* 14: 645-54

Xie H, Hou S, Jiang J, Sekutowicz M, Kelly J, Bacskai BJ. 2013. Rapid cell death is preceded by amyloid plaque-mediated oxidative stress. *Proceedings of the National Academy of Sciences*: 201217938

Xu W, Fitzgerald S, Nixon RA, Levy E, Wilson DA. 2015. Early hyperactivity in lateral entorhinal cortex is associated with elevated levels of AβPP metabolites in the Tg2576 mouse model of Alzheimer's disease. *Experimental neurology* 264: 82-91

Yamamoto K, Tanei Z-i, Hashimoto T, Wakabayashi T, Okuno H, et al. 2015. Chronic Optogenetic Activation Augments Aβ Pathology in a Mouse Model of Alzheimer Disease. *Cell reports* 11: 859-65

Yan SD, Chen X, Fu J, Chen M, Zhu H, et al. 1996. RAGE and amyloid-β peptide neurotoxicity in Alzheimer's disease. *Nature* 382: 685

Yanagisawa K, Odaka A, Suzuki N, Ihara Y. 1995. GM1 ganglioside-bound amyloid beta-protein (A beta): a possible form of preamyloid in Alzheimer's disease. *Nat Med* 1: 1062-6

Yang T, Li S, Xu H, Walsh DM, Selkoe DJ. 2016. Large soluble oligomers of amyloid β-protein from Alzheimer brain are far less neuroactive than the smaller oligomers to which they dissociate. *The Journal of Neuroscience*: 1698-16

Yang T, Li S, Xu H, Walsh DM, Selkoe DJ. 2017. Large Soluble Oligomers of Amyloid beta-Protein from Alzheimer Brain Are Far Less Neuroactive Than the Smaller Oligomers to Which They Dissociate. *J Neurosci* 37: 152-63

Yang W, Yuste R. 2017. In vivo imaging of neural activity. *Nature methods* 14: 349-59

Yassa MA, Lacy JW, Stark SM, Albert MS, Gallagher M, Stark CEL. 2011. Pattern separation deficits associated with increased hippocampal CA3 and dentate gyrus activity in nondemented older adults. *Hippocampus* 21: 968–79

Yuan P, Grutzendler J. 2016. Attenuation of beta-Amyloid Deposition and Neurotoxicity by Chemogenetic Modulation of Neural Activity. *J Neurosci* 36: 632-41

Yuste R, MacLean J, Vogelstein J, Paninski L. 2011. Imaging Action Potentials with Calcium Indicators. *Cold Spring Harbor Protocols* 2011: pdb.prot5650

Zhao J, Li A, Rajsombath M, Dang Y, Selkoe DJ, Li S. 2018. Soluble Aβ Oligomers Impair Dipolar Heterodendritic Plasticity by Activation of mGluR in the Hippocampal CA1 Region. *iScience* 6: 138-50

Zhou Y, Danbolt NC. 2014. Glutamate as a neurotransmitter in the healthy brain. *Journal of neural transmission (Vienna, Austria : 1996)* 121: 799-817

Zott B, Busche MA, Sperling RA, Konnerth A. 2018. What Happens with the Circuit in Alzheimer's Disease in Mice and Humans? *Annual Review of Neuroscience* 41: 277-97

Zucker RS, Regehr WG. 2002. Short-Term Synaptic Plasticity. *Annual Review of Physiology* 64: 355-405

Zumkehr J, Rodriguez-Ortiz CJ, Cheng D, Kieu Z, Wai T, et al. 2015. Ceftriaxone ameliorates tau pathology and cognitive decline via restoration of glial glutamate transporter in a mouse model of Alzheimer's disease. *Neurobiology of aging* 36: 2260–71